Composite Hydrogel Scaffolds with Eggshell Particles as a Novel Bone Regeneration Material

Nick Calvert

Thesis submitted to the
Faculty of Graduate and Postdoctoral Studies
in partial fulfillment of the requirements for
the Master of Science degree in
Cellular and Molecular Medicine

Department of Cellular and Molecular Medicine
Faculty of Medicine
University of Ottawa

uOttawa

L'Université canadienne
Canada's university

Table of Contents:

List of Figures:

List of Tables:

List of Abbreviations:

AA	Ascorbic acid
ALP	Alkaline phosphatase
ANOVA	Analysis of variance
AS	Alginate solution
BGP	β-glycerophosphate
BMP	Bone morphogenic protein
CGM	Cellular growth media
CM	Compressive modulus
CS	Chitosan solution
DMEM	Dulbecco's modified eagle medium
DTT	Dithiothreitol
ECM	Extracellular matrix
EDS	Energy dispersive X-ray spectroscopy
EDTA	Ethylenediaminetetraacetic acid
EHA	Eggshell-derived hydroxyapatite
ES	Eggshell
FBS	Fetal bovine serum
FTIR	Fourier-transform infrared spectroscopy
FZD	Frizzled Protein
GAPDH	Glyceraldehyde-3-phosphate dehydrogenase
HA	Hydroxyapatite
IBMX	3-isobutyl-1-methylxanthine
MEPE	Matrix extracellular phosphoglycoprotein
MSC	Mesenchymal stem cell
NTES	Nanotextured eggshell
OPN	Osteopontin
PA	Phosphoric acid
PBS	Phosphate buffered saline

PDMS	Polydimethylsiloxane
PLGA	Poly-lactic-co-glycolic acid
P_i	Inorganic Phosphate
PP_i	Inorganic pyrophosphate
PVDF	Polyvinylidene fluoride
RUNX2	Runt-related transcription factor 2
SDS	Sodium dodecyl sulfate
SDS-PAGE	Sodium dodecyl sulfate – gel electrophoresis
SEM	Scanning electron micrograph
SGM	Scaffold growth media
SHA	Synthetic hydroxyapatite
TCA	Trichloroacetic acid
TPBS	Tween20 – phosphate buffered saline
UTM	Universal testing machine
αMEM	Alpha minimum essential media

Abstract:

The development of bone regeneration materials to support new bone formation is an active field of research. This report describes the development and characterization of a novel composite scaffold made of a chitosan-alginate co-polymer hydrogel matrix and eggshell (ES) particles. Scaffolds with ES particles or with nanotextured ES (NTES) particles following treatment with phosphoric acid were compared to scaffolds without particles. The scaffolds with particles exhibited a higher porosity and a larger median pore size. Their mechanical strength remained low, but both scaffold types were more resistant to deformation following compression than the scaffolds without particles. The osteogenic potential of the scaffolds was then evaluated with human bone-marrow derived mesenchymal stem cells (MSCs) from four different donors. Results showed that the inclusion of ES or NTES particles significantly increased MSC adherence and viability, as well as alkaline phosphatase activity in the scaffolds. A change of cell morphology and a small, although not statistically significant, increase of osteogenic protein expression (RUNX2 and osteopontin) were also observed at later time points (days 14 and 21). Overall, this research highlights the potential of ES for bone regeneration applications, opening the door for a high-value repurposing of a current industrial waste product.

Acknowledgements:

I would first and foremost like to thank my supervisors Dr. Isabelle Catelas and Dr. Maxwell Hincke for not only affording me this extraordinary learning experience and the opportunity to develop and prove myself throughout the course of this project, but also for their continual guidance and support. You have both provided exceptional mentorship to my personal growth and in developing my skills as a scientist, and I truly appreciate it.

I would also like to thank my advisory committee members Dr. Erik Suuronen and Dr. Andrew Pelling for their constructive feedback and guidance throughout the course of my research. The experience and counsel that you were both able to impart will always be valued.

To the relationships that I have been fostered with members of both the Hincke and the Catelas labs, you have all become very close and dear friends and helped to make some of the most daunting days of graduate studies a lot more fun. I appreciate your support and friendship. I would like to make special mention to Dr. Eric A. Lehoux, who always fostered and aided in my problem solving with the many unique problems I encountered through my work.

Most importantly, I want to thank all of my close friends and family for their continued support throughout the entire course of my academic career. Though the distance between us has made it difficult to spend as much time together as we would like, you have all made great efforts to maintain our relationships and I truly appreciate that. I would especially like to thank both my mom and my dad for always supporting and believing in me. I could not have asked for two better parents. I would also like to personally thank my girlfriend, Gen, who stood by my side and supported me through the good times and the bad, and who always believed in me and tried to make every day special.

Copyrighted Content:

All figures reproduced from other journals that were used in this monograph fall under the Creative Commons License (CC-BY 2.0), with the exception of Figure 6, which reproduction authorization was obtained from the original publishing journal.

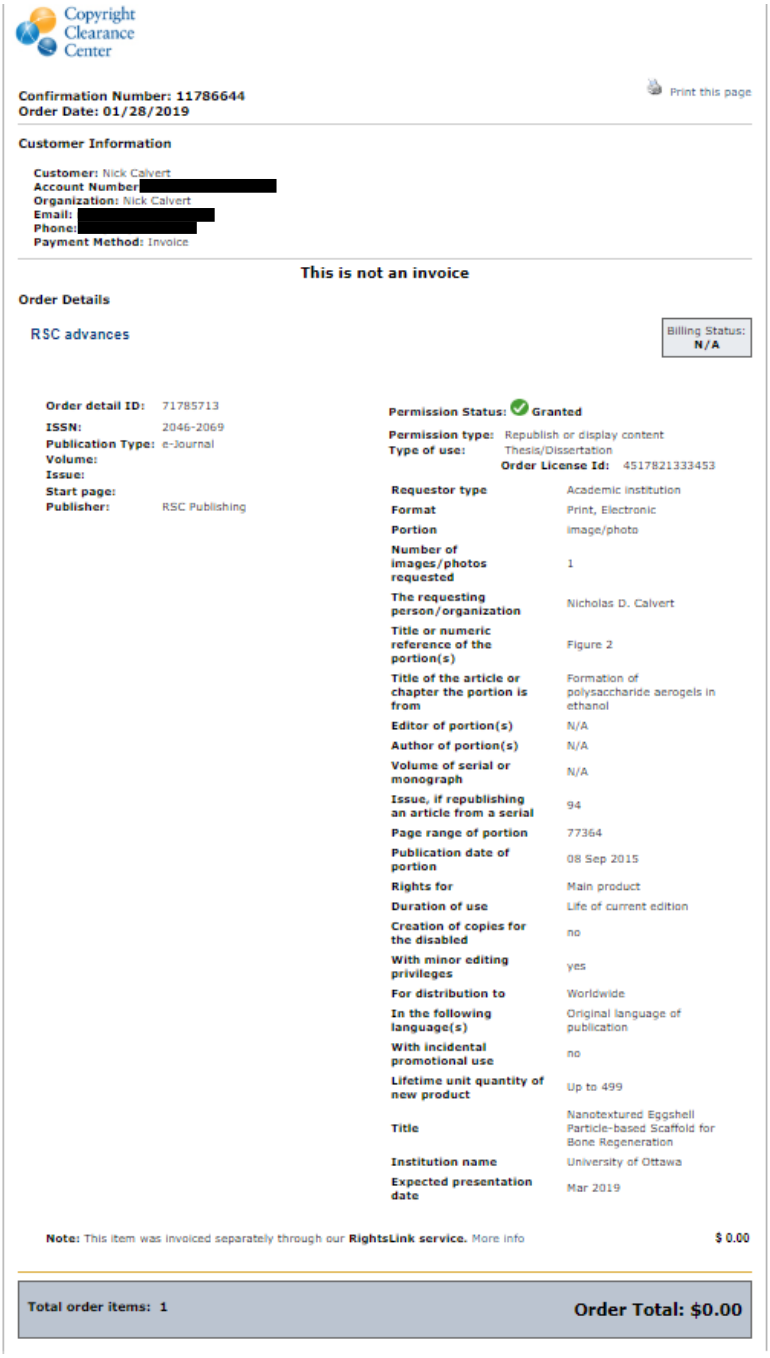

Copyright Clearance Center

Print this page

Confirmation Number: 11786644
Order Date: 01/28/2019

Customer Information

Customer: Nick Calvert
Account Number: [redacted]
Organization: Nick Calvert
Email: [redacted]
Phone: [redacted]
Payment Method: Invoice

This is not an invoice

Order Details

RSC advances

Billing Status: **N/A**

Order detail ID:	71785713
ISSN:	2046-2069
Publication Type:	e-Journal
Volume:	
Issue:	
Start page:	
Publisher:	RSC Publishing

Permission Status: Granted

Permission type: Republish or display content
Type of use: Thesis/Dissertation
Order License Id: 4517821333453

Requestor type	Academic institution
Format	Print, Electronic
Portion	image/photo
Number of images/photos requested	1
The requesting person/organization	Nicholas D. Calvert
Title or numeric reference of the portion(s)	Figure 2
Title of the article or chapter the portion is from	Formation of polysaccharide aerogels in ethanol
Editor of portion(s)	N/A
Author of portion(s)	N/A
Volume of serial or monograph	N/A
Issue, if republishing an article from a serial	94
Page range of portion	77364
Publication date of portion	08 Sep 2015
Rights for	Main product
Duration of use	Life of current edition
Creation of copies for the disabled	no
With minor editing privileges	yes
For distribution to	Worldwide
In the following language(s)	Original language of publication
With incidental promotional use	no
Lifetime unit quantity of new product	Up to 499
Title	Nanotextured Eggshell Particle-based Scaffold for Bone Regeneration
Institution name	University of Ottawa
Expected presentation date	Mar 2019

Note: This item was invoiced separately through our **RightsLink service.** More info $ 0.00

Total order items: 1 **Order Total: $0.00**

1.0 Background:

1.1 Current State of Treatments for Bone Regeneration:

Bone defects and loss of healthy bone mass as a result of disease, fracture, or aging are a worldwide problem. After blood, bone is the second most commonly transplanted tissue (Campana et al., 2014a). The worldwide incidence of bone defects and bone disease continues to increase from year to year. This has been attributed to an aging population, as well as environmental factors such as chemical pollutants in the air (Amini et al., 2012; US Department of Health and Human Services, 2004). The autograft procedure, which is the most common procedure for treatment of bone defects, was performed worldwide more than 2.2 million times in 2008 (Neighbour, 2008), and is currently the gold standard for treatment of bone defects. It involves harvesting healthy bone from a different area in the affected patient, and grafting it to the defective area (Campana et al., 2014b; Oppenheim et al., 2002). While the autograft procedure represents the most successful method for treatment of bone defects, there is limited access to healthy bone and it is associated with a high degree of pain and discomfort for the patient (Oppenheim et al., 2002). The lengthy surgical time required for the autograft procedure also makes it very expensive in comparison to the allograft procedure and other non-grafting treatment options (Cooper & Kaeding, 2010).

An alternative is the allograft procedure, which involves harvesting healthy bone tissue from a donor or from a cadaver to graft it to the site of defect in the affected patient (Tuchman et al., 2016). Allografts present a reduced risk of hyperacute rejection compared to xenografts, which come from different species. However, graft rejection is still a possibility (Aro & Aho,

1993) and bone removal can also lead to donor-site morbidity for the donating patient (Hilborne, 1998).

Due to the increasing incidence of bone defects and drawbacks associated with the procedures described above, the development of bone substitutes using different biomaterials has become a very active area of research (Christman, 2019). A biomaterial is an exogeneous material that is implanted to repair, replace or mimic a tissue or organ (Winkler et al., 2018). The following literature review evaluates the factors associated with an effective bone regeneration biomaterial by examining bone mechanobiology and biochemistry of existing bone regeneration biomaterials, in order to predict the features of a superior biomaterial.

1.2 Biochemistry and Mechanobiology of Bone Growth and Regeneration:

1.2.1 Basics of Bone Biology:

An important strategy for the development of a new tissue engineering construct is to examine all features of the tissue that is to be replicated or repaired. Therefore, in the context of bone tissue engineering, the basics of bone mechanobiology and biochemistry for normal growth and regulation must be thoroughly understood. Bone is a composite tissue characterized by two distinctly different regions: the cortical (hard, dense shell) exterior region and the cancellous (spongy, porous) interior region (Buck & Dumanian, 2012a). The highly porous cancellous region contains both large and small pore sizes in order to allow for cellular movement and neovascularization, respectively. Vascularization of this region is necessary for nutrient diffusion, waste removal and growth factor migration, in order to sustain cellular

viability (Rowe, 2008). Cells within this region include mesenchymal stem cells (MSCs) and hematopoietic stem cells (HSCs), which terminally differentiate into either bone-secreting osteoblasts or bone-resorbing osteoclasts, respectively (Buck & Dumanian, 2012b). Osteoblasts produce bone extracellular matrix (ECM) by first secreting collagen fibres which help to create the cancellous bone porous matrix (Buck & Dumanian, 2012b; Rowe, 2008). Within this matrix, osteoblasts deposit calcium phosphate, encasing themselves within the mineralized matrix while secreting additional ECM proteins. This process, known as osteogenesis, produces apatite, the main mineral component of bone (Buck & Dumanian, 2012b; Rowe, 2008). It is important to mention that while bone mineral is commonly referred to as hydroxyapatite (HA), pure HA consists of only calcium, phosphate, and a hydroxyl counterion. Due to the ionic complexity of the surrounding environment, bone mineral is more correctly defined as poorly crystalline carbonated apatite, typically containing many cationic and anionic substitutions (e.g., Na^{2+}, Mg^{2+}, F^{-}, Cl^{-}) (Cacciotti, 2016). The MSCs are almost always the cells of choice for *in vitro* investigation of biomaterial osteoconductivity, osteoinductivity, or osteogenicity, since they are the precursors to the mineral-secreting osteoblasts, as well as many other cell types (Buck & Dumanian, 2012a).

The mechanical properties of bone are also important to understand when designing a new bone regeneration biomaterial. Since bone is load-bearing in many instances, it is usually necessary to create a material that will have the appropriate mechanical properties. This feature can provide durability of the material and ensure that cells remain viable by preventing mechanical failure (Tozzi et al., 2016). There are a variety of mechanical factors that are important for osteogenesis which will be discussed later in this literature review.

The properties of cancellous bone vary depending on a variety of factors, such as the type of bone, as well as the age and the activity level of the person (Currey et al., 2007). The cancellous region of bone has an average porosity between 70% - 80%, with a median pore size between 100 µm – 500 µm (Cowin & Telega, 2003). There are also many pores smaller than 70 µm in diameter, which are important for vascularization (Karageorgiou & Kaplan, 2005). Cancellous bone is often reported to have a compressive modulus (CM) in the high MPa to low GPa range (Cowin & Telega, 2003). Overall, a bone regeneration biomaterial must not only be physically and mechanically similar to bone, but must also support MSC differentiation into osteoblasts.

1.2.2 Factors Involved in Osteogenic Differentiation:

MSCs have a large number of potential downstream lineages (Figure 1). Therefore, the ability of a biomaterial to either directly induce or promote MSC differentiation into a specific lineage based on the intended application is critical to its effectiveness. The process mediating osteogenic differentiation is governed by a variety of chemical signaling pathways, growth factors, chemotactic interactions, and physical cues (Figure 2).

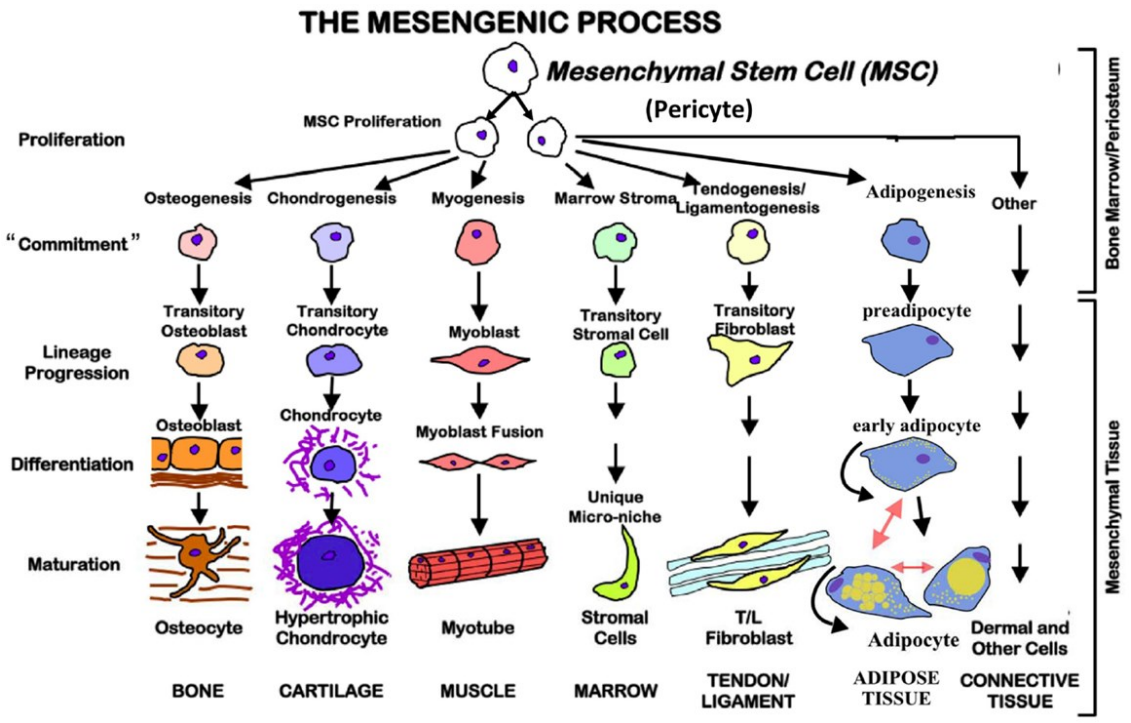

Figure 1. The mesengenic process. Mesenchymal stem cells are multipotent and possess the ability to proliferate and commit to different cell types based on the environmental conditions. They also may be redirected from one lineage to another. The figure and legend are from Dimarino et al., 2013.

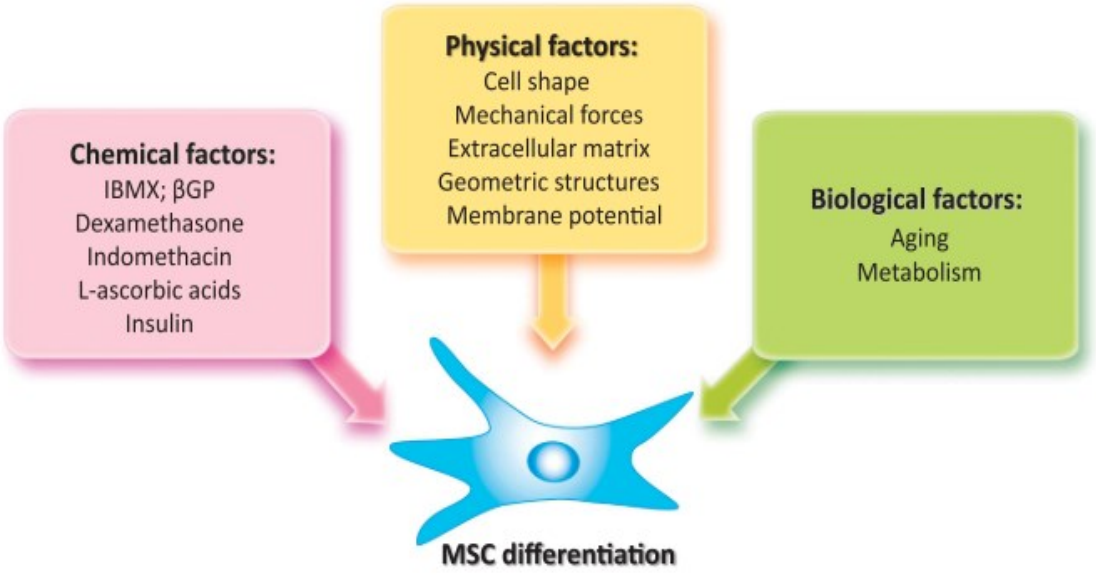

Figure 2. Multiple factors control mesenchymal stem cell (MSC) differentiation. The lineage commitment of MSCs can be regulated by three major cues, including chemical, physical, and biological factors. Chemical factors have been proven to be important in directing adipogenesis and osteogenesis of MSCs *in vitro* through regulating key transcription factors during MSC differentiation. *In vivo*, the differentiation of MSCs can also be altered by physical factors in the stem cell niche. Investigations into the regulation of MSC differentiation commitment by cell shape, external mechanical forces, extracellular matrix or geometric structures have provided very useful information for stem cell-based bone tissue regeneration/ engineering. Meanwhile, tilted differentiation balance of MSCs is also observed during aging or other pathological processes, arguing for the roles of biological factors in lineage commitment of MSCs. Taken together, these three types of factors likely work closely and cooperate with each other to regulate MSC differentiation. IBMX, isobutylmethylxanthine; βGP, β-glycerophosphate. The figure and legend are from Chen et al., 2016.

Intracellular Signaling Pathways:

There are multiple signaling pathways that not only promote MSC differentiation towards osteoblastic lineage, but also prevent their differentiation into the many other available MSC lineages (Figure 3). The canonical Wnt signaling pathway is one of the primary drivers for osteoblastic differentiation of MSCs, as it is responsible for activation of the osteoblast differentiation "master switch", Runt-related transcription factor 2 (RUNX2) (Komori, 2010). Wnt is also responsible for supressing transcription factors responsible for MSC differentiation into non-osteoblastic lineages. Moreover, RUNX2 is responsible for the activation of another transcription factor, Osterix (OSX), while also supressing pathways that lead to differentiation to other lineages (Nakashima et al., 2002). These two transcription factors are responsible for the activation and up-regulation of many osteogenic specific protein transcripts (Chen et al., 2016). Almost all of these proteins are transcription factors or are involved in creating the ECM. Some of these critical proteins include:

- Bone morphogenic proteins (BMP-2, BMP-4): transcription factors responsible for up-regulation of osteogenic proteins (Luu et al., 2007)
- Bone-specific alkaline phosphatase (ALP): an enzyme responsible for the creation of phosphate via inorganic pyrophosphate to inorganic phosphate ($PP_i \rightarrow P_i$) reaction. This P_i also acts as a promoter of osteopontin through a glucocorticoid response element in the OPN gene (Fatherazi et al., 2009; Golub & Boesze-Battaglia, 2007)

- Osteopontin (OPN): a membrane-targeted protein (also present in pre-osteoblastic MSCs) which acts as a structural protein for the organic matrix. OPN is also involved in osteoclast activity and the bone response to external stress (Noda & Denhardt, 2008; Singh et al., 2018).

Patient age, metabolic rate, and disease state are very important factors that influence osteogenic potential. Indeed, this potential is reduced with increasing age and slowing metabolism, due to dysregulation of the Wnt signaling pathway caused by age-associated radical oxygen species (ROS) damage to critical, as well as due to the diminishing pool of endogenous MSCs (Infante & Rodríguez, 2018).

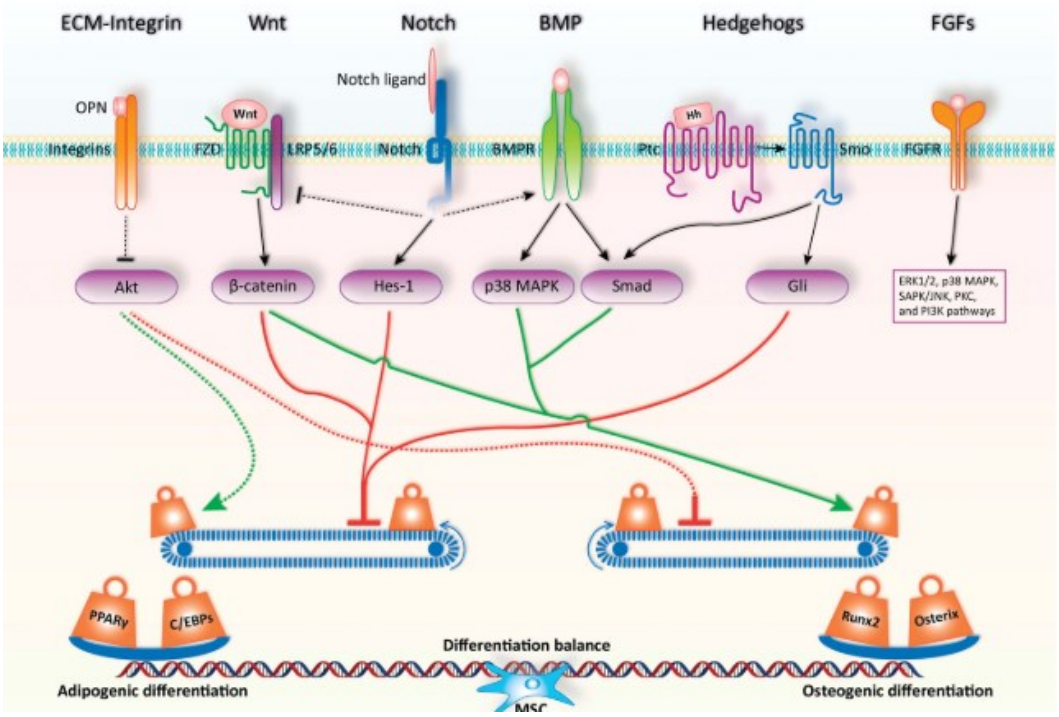

Figure 3. Signaling pathways and key transcription factors in regulating the adipo-osteogenic differentiation of mesenchymal stem cells (MSCs). The fine balance of adipogenic and osteogenic differentiation of MSCs is achieved by the actions of critical signaling pathways and key transcription factors. MSCs exist in specific microenvironments or niches, which is composed of various extracellular matrix components, growth factors, cytokines, and chemokines. Upon interaction with MSCs, these components activate or inhibit the lineage commitment of MSCs. In addition, the initiated cellular signaling pathways can also interfere with each other to form a fine regulatory network. Ultimately, this signaling network maintains a delicate differentiation balance through regulating key transcription factors such as PPARγ and C/EBPs or Runx2 and Osterix for adipogenesis or osteogenesis, respectively. OPN, osteopontin; FZD, Frizzled receptor; Hh, Hedgehog; Ptc, Patched; Smo, Smoothened. The figure and legend are from Chen et al., 2016.

Adding to the complexity of the osteoblast differentiation pathways are extracellular factors that strongly induce osteoblast differentiation via interaction with some of the endogenous pathways previously discussed.

Chemical signals:

The most widely studied components inducing osteogenic differentiation are dexamethasone (Dex), ascorbic acid (AA), and β-glycerophosphate (BGP). Dex is a corticosteroid that induces transcription of four and a half Lin11, Isl-1, and Mec-3 domains protein 2 (FHL-2), which potentiates β-catenin transport to the nucleus, leading to transcription of RUNX2 and ultimately osteogenic differentiation (Langenbach & Handschel, 2013). AA has two functions in osteogenic differentiation: it facilitates the proper protein folding of collagen fibres required for collagen matrix crosslinking (Langenbach & Handschel, 2013), and it acts as a transcription factor for ALP (Leboy et al., 1989). Finally, AA, in conjunction with BGP, which acts as an organic phosphate source for ALP, leads to an increase in downstream transcription of OPN (Langenbach & Handschel, 2013). Dex, AA and BGP are often used as *in vitro* cell culture additives when evaluating the osteogenicity of a biomaterial. Finally, in addition to being a primary mineral component of bone, calcium phosphate has also been shown to act as a differentiating factor due to the available phosphate source being able to act as an inductor of differentiation (Li et al., 2017). Other factors that induce osteogenic differentiation include osteoblast-specific proteins (e.g., OPN, BMPs). Many of the osteogenic proteins are also transcription factors for other osteogenic proteins through protein-receptor interactions. Therefore, the addition of these proteins directly to cell cultures or biomaterials can often act as differentiating factors (Elashoff et al., 2015).

Mechanical signals:

One of the most important and complex stimuli leading to differentiation of MSCs is mechanical stimulation (Figure 4). As described earlier, Wnt-activated RUNX2 leads to MSC osteogenic differentiation. However, a preliminary signal must also exist to induce *in vivo* osteogenic differentiation since the MSCs have such a wide variety of potential terminally differentiated lineages. One of these precursory signals is mechanical stimulation. Much research effort has gone into understanding MSC mechanobiology, and the nature of mechanical factors that induce osteogenesis. One factor is the surface to which MSC adhere. MSCs are more favorably adherent to rough rather than smooth surfaces (Boyan et al., 1996). In fact, some rough surfaces are sufficient to induce MSC differentiation into osteoblasts (Boyan et al., 2016). The uneven distribution of the cytoskeleton generates tension on the actin-myosin complex, which acts as a differentiating signal. Dynamic compressive stimulation of MSCs (cyclical loading and unloading of the cells) will strongly induce chondrocyte or osteoblast differentiation, again through actin-myosin mediated tension (Michalopoulos et al., 2012; Tran et al., 2011). The common factor is the application of a compressive or stretching force to the MSC cytoskeleton (Müller et al., 2013).

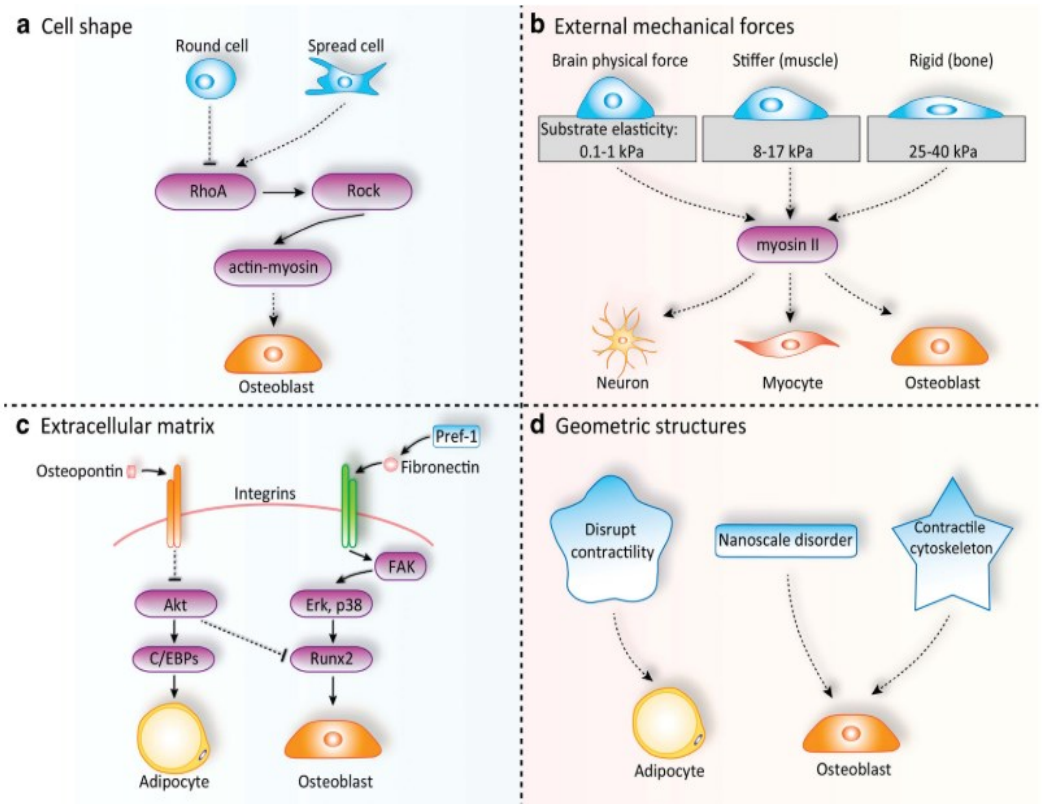

Figure 4. Physical factors regulating lineage commitment of mesenchymal stem cells (MSCs). MSCs physically interact with various components in the tissue microenvironment *in vivo*. The physical factors including cell shape, external mechanical forces, extracellular matrix, and geometric structures are involved in stem cell fate decision. By regulating RhoA-ROCK signaling pathway, spread cells tend to differentiate into osteoblasts while round cells tend to become adipocytes (a). Different physical forces can also direct MSCs to differentiate into different lineages via controlling myosin II activity (b). Meanwhile, components of extracellular matrix, such as osteopontin and fibronectin, can regulate the adipo-osteogenic balance of MSCs through binding to integrin receptors (c). In addition, geometric cues such as nanoscale changes can also effectively dictate the differentiation of MSCs (d). The figure and legend are from Chen et al., 2016.

Nanotexture:

Nanotexture is defined as a topographical feature at the nanometer scale, and has various effects, such as influencing cellular adhesion, proliferation, and orientation in many cell types (Gogolides et al., 2006; Islam et al., 2015). For example, a rough, disorderly patterned nanotexture can strongly induce osteoblastic differentiation in MSCs (Khang et al., 2012). This has been attributed to stretching of the MSC cytoskeleton (Lim & Donahue, 2007). Since a rough and disordered nanotexture induces small increments of stretching across the entire MSC cytoplasm, the degree of stretching necessary to induce differentiation is greatly reduced. For example, an uneven nanopit array that allows MSC cytoskeleton to spread on large surface area showed the greatest stimulation of OPN protein synthesis (Dalby et al., 2007).

In summary, the differentiation of MSCs into osteoblasts can be mediated through a variety of chemical, mechanical, and physical factors.

1.3 Bone Regeneration Materials:

A variety of bone regeneration materials have been designed and tested. One common property is that they provide a three-dimensional (3D) cellular environment. Cellular behavior in two dimensions (2D) is extremely different than in 3D, due to dimensional changes affecting cell-to-cell communication, nutrient diffusion, and cellular mechanics (Duval et al., 2017). In addition, synthetic implantable biomaterials designed to replace endogenous bone should mimic some or all mechanical properties of endogenous human bone (Polo-Corrales et al., 2014).

1.3.1 Bone Fillers:

Bone regeneration has been studied for almost a century. Some of the earliest bone graft substitutes are known as bone fillers (Goldberg, 1992). These were hard-drying cements composed of HA, calcium phosphate, or other calcium-based components (Kirkpatrick et al., 2010), easily shaped to the contours of the defective site to fill a void. While there are only a few successful examples of these fillers, they are still a viable option for sealing bone fractures with minimal loss of bone tissue (Nusselt et al., 2014). Much of the reasoning behind the use of these cements was their mechanical and compositional similarity to bone. However, the major downside of most of the early bone filler cements was that they were either entirely non-porous or did not have an adequate porosity or range of pore sizes (Kenny & Buggy, 2003). The lack of porosity creates a very brittle and easily fractured material due to the high Young's modulus and prevents infiltration by endogenous MSCs. These materials would therefore not support the bone remodelling process by both mineral-secreting osteoblasts and mineral-resorbing osteoclasts. In addition, because of the crystallinity of the mineral in most cement fillers, osteoclasts have a reduced ability to resorb the mineral, preventing the repair of microfractures by bone homeostasis (Touaitahuata et al., 2014). Finally, the high mechanical strength of bone fillers relative to the strength of endogenous bone can also lead to stress shielding. Stress shielding is the reduction in bone density via osteoclast activity, caused by a reduction in mechanical stress on endogenous bone by an implant (Weinans & Huiskes, 2015). Therefore, porosity in bone regeneration biomaterials is critical for both cellular viability and preservation of surrounding endogenous bone (Karageorgiou & Kaplan, 2005).

1.3.2 Porous Biomaterials:

Porous biomaterials represent the majority of the biomaterials that have been developed. There are three generic classes of porous biomaterials: ceramics, metals and alloys, and polymers. These biomaterials can also be combined to form composites. Porous biomaterials have become widely used because they allow for nutrient diffusion and cellular invasion. As well, the scaffold-like porous matrices present a biomimetic 3D environment that allows for cellular growth and interactions.

Ceramics:

Modern porous ceramics have overcome the shortcomings of their predecessors due to their inherent porosity. Many of these modern ceramics are injected or molded to the site of defect, and release a gas (often CO_2) during the hardening process which acts as a porogen (Xu et al., 2006). They can also include growth factors or chemicals within the mineral that allows for better interaction between endogenous proteins and the ceramic material (Combes & Rey, 2010). Porous ceramics, often composed of calcium carbonate or calcium phosphate, have been used with some success in the medical field (i.e. Geistlich Bio-Oss®, Biocoral®) (Baghban et al., 2009; Mangano et al., 2011; Piattelli et al., 1997). However, the main issue with these materials, again, is that they are often very stiff and brittle, which can lead to fracture following implantation (Kenny & Buggy, 2003). Finally, Bioglass 45S5, which bonds chemically to bone and helps facilitate the growth of new bone tissue, has also been used in a clinical setting in particle form or as a sintered scaffold (Fiume et al., 2018). Though very successful in regenerating smaller bones, such as those in the inner ear, it has been less successful for large defects in

weight-bearing bones due to its brittle mechanical properties (Jones et al., 2016; Baino et al., 2018).

Metals and Alloys:

Porous metal biomaterials are often made of either Fe, Cr, Co, Ni, Ti, Ta, Mo, or W alloys (Ivanova et al., 2014). Most of these metals are non-cytotoxic at low concentrations (Nakada et al., 2008). These types of biomaterials are favored mostly due to their very strong mechanical properties, which increase implant durability (Ivanova et al., 2014). Many titanium porous scaffolds have been used as bone regeneration materials, due to their very strong mechanical properties and controllable pore size and porosity (Prasad et al., 2017). Such scaffolds are created through sintering or thermal-molding of titanium alloys and other alloy metals (Torres-Sanchez et al., 2017). Metal alloy implants do not degrade due to their compositions. However, these materials can potentially lead to an inflammatory response, as research has shown that metal ions (i.e., Co^{2+}, Cr^{3+}) released from metal implants can be potentially cytotoxic (Salloum et al., 2018). Also, these materials do not swell. Swelling can facilitate the material to pull fluid into the core of an implanted material, allowing for fluid equilibrium. Therefore, the absence of swelling can cause the core (3D center) of the material to have low concentrations of nutrients and growth factors, leading to cell death (Zhao et al., 2015).

Polymers:

Polymers for tissue engineering applications are either natural or synthetic. While there are numerous sub-types of polymer scaffolds, the most widely used in bone tissue engineering

are hydrogel-based scaffolds. Hydrogel scaffolds are formed using hydrophilic polymers that are crosslinked covalently or non-covalently. The hydrophilicity of these types of scaffolds causes the biomaterial to swell in aqueous environments, allowing the material to reach ionic/osmotic equilibrium and better prevent/minimize the development of a necrotic core observed in metallic biomaterials (Holback et al., 2011). However, necrotic core can still be an issue in hydrogels. Some commonly used polymers include chitosan, alginate, collagen, polyvinylpyrrolidone, polycaprolactone, and poly-lactic-co-glycolic acid (PLGA).

Hydrogels are extremely versatile materials because they permit a high degree of "tailoring"; almost all of the properties of the hydrogels can be designed specifically to fit the need of the material (Chai et al., 2017). The first level of selection is the type of polymer. Polymers are chosen to exhibit mechanical properties similar to bone, while also degrading after an appropriate amount of time for replacement by endogenous tissue. Injectable polymers are preferred to minimize invasiveness of the implantation procedure. Chemically modified polymers, or mixtures of multiple types of polymers can create scaffolds with different physicochemical properties (Engelberg & Kohn, 1991). Moreover, the method of producing the hydrogel (thermal molding, compression molding, chemical crosslinking, porogen leeching, freeze-drying, 3D printing, etc.) will modify their physicochemical properties (Davidenko et al., 2015). Hydrogels can encapsulate drugs, growth factors, cells, or other chemicals, while still acting as a porous matrix (Peppas, 1997; Silva et al., 2009; Yuan et al., 2017). Proteins and peptide sequences can be coupled to polymers to act as signaling molecules (Park et al., 2004). Finally, hydrogel scaffolds are often easily degraded by endogenous proteases, and can be designed to degrade and disappear once endogenous ECM is deposited (Pangburn et al., 1982).

Nevertheless, the greatest shortcoming of hydrogel biomaterials as bone regeneration materials is that they are often mechanically very weak, especially compared to ceramics or metals (Anseth et al., 1996). Hydrogel scaffolds in bone tissue engineering are commonly utilized as a component of composite materials. Bone fillers and metal alloy materials often have great mechanical properties but lack important cellular viability properties, such as pore size and porosity. Composite materials made of a hydrogel and ceramic, or hydrogel and metal, possess a combination of favorable mechanical properties, with tailorable pore size and porosity (Siddiqui et al., 2018). Because of this, composite materials with hydrogels have been considered as some of the best bone regeneration materials.

1.4 Hydrogel Design:

As described in the preceding section, hydrogel scaffolds have a high degree of customization, aside from those inherent to the polymer being used. This section will evaluate some of the methods used to generate hydrogels with respect to modulation of the physicochemical properties of the resulting material.

1.4.1 Pore Size and Porosity:

A variety of different methods can produce different pore sizes, porosities, and pore structures in the biomaterial. Four of the most commonly used methods for pore generation are gas foaming, porogen leeching, freeze-gelation, and freeze-drying.

Gas Foaming:

Gas foaming is one of the simplest methods of pore production within a scaffold. In this method, the pores are generated by in-gassing the polymer solution (Dehghani & Annabi, 2011), thereby creating bubbles within the gel solution. After crosslinking of the polymer, pores remain at the site of the gas bubbles. Porosity and pore size can be controlled by varying the type of gas, the length of in-gassing time, and the pressure at which the gas is introduced into the gel solution (Sun et al., 2016). Gas foaming can also be performed chemically by acid-base reaction with the gel solution to produce a gas prior to or during crosslinking. An example of this would be the addition of sodium bicarbonate to an acidic chitosan solution (CS), which induces both crosslinking due to neutralization, and gas formation due to CO_2 release from the bicarbonate (Shen et al., 2007). Another approach is through the use of surfactants to induce air bubbles by modifying the surface tension between air and the solution (Eiselt et al., 2000).

Porogen Leeching:

Porogen leeching is a pore-forming method where the polymer gel is loaded with a porogen, followed by freezing or crosslinking, and then leeching to remove the porogen (Liao et al., 2002; Figure 5). A porogen is any particle of a specific geometric shape and size that is packed into the material. The porogen is soluble in a solvent in which the polymer is not, so that only the porogen is dissolved while the polymer remains intact. A notable example of this is the use of generated paraffin spheres as porogen (Ma et al., 2003). Briefly, melted paraffin wax in a gelatin solution can be poured over swirling ice water to generate very small paraffin wax spheres. These spheres can be sieved to a specific size, and varying amounts can be loaded

into the material. Paraffin wax is soluble in most organic solvents (i.e., chloroform, hexanes), which may not react with certain polymers, and can leech the spheres out of the scaffold to leave spherical pores in their place. Other common porogen-solvent combinations include sodium chloride-water, or glucose-water (Smith et al., 2017; Tran et al., 2011).

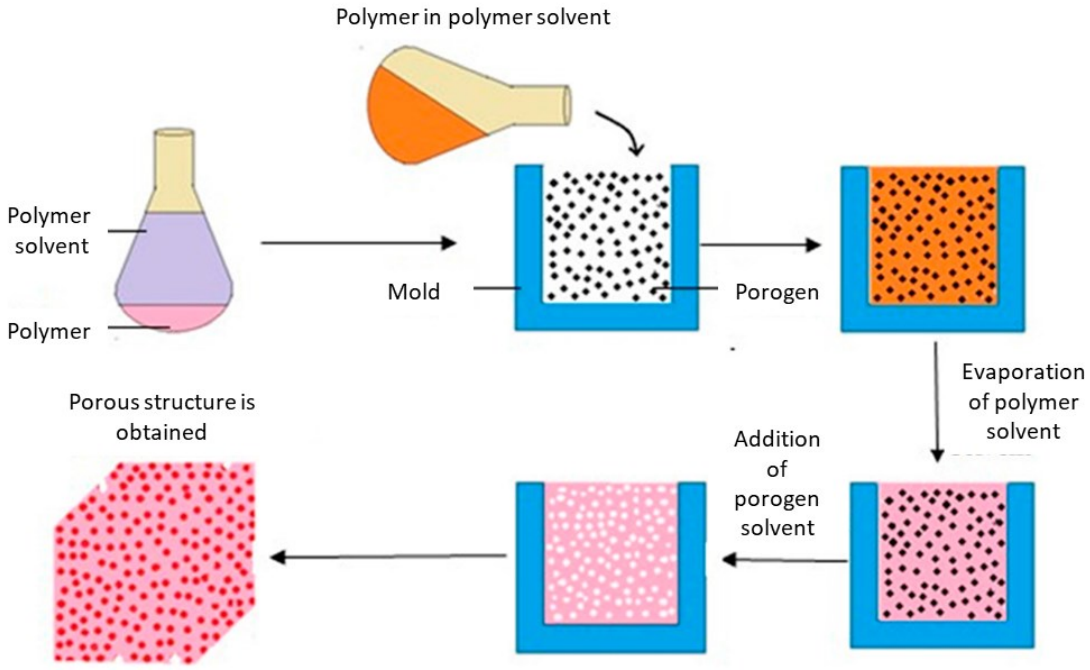

Figure 5. Schematic diagram of solvent casting and particulate leaching technique. Adapted from Sampath et al. (2016). This schematic diagram depicts the different stages of the solvent casting and particulate leaching technique. The polymer material is dissolved in a solvent system that dissolves only the polymer, and then is cast into a mold containing a porogen. The solvent is evaporated to obtain a dry, porogen-loaded material, which is dissolved in a solvent system that dissolves only the porogen. The structure is finally dried again to obtain a porous scaffold.

Freeze-Gelation and Freeze-Drying:

Both freeze-gelation (Figure 6) and freeze-drying (Figure 7) are based on ice-crystal nucleation and growth to generate pores; however, these two methods differ in how the final scaffold pore structure is produced when the ice crystals are eliminated. When water freezes, ice crystals nucleate and grow away from the direction to which the cold temperature is applied. If this occurs in a freezer, the freezing will start at the surfaces of the material and proceed towards the centre. However, hydrogel scaffolds are often frozen in a unidirectional manner, i.e., the freezing origin is applied to one surface of the material, while the other surfaces are insulated. This forces the ice crystals to grow in only one direction, which creates a well-organized pore system. The more multi-directionally the freezing temperature is applied, the less homogeneous is the resulting crystal nucleation (Pawelec et al., 2015). Moreover, the temperature at which the solution is frozen will greatly affect the resulting pore sizes generated within the scaffold. Lower temperatures will result in smaller pore sizes, since this temperature directly affects the rate of ice crystal nucleation and growth (O'Brien et al., 2004; Pawelec et al., 2014).

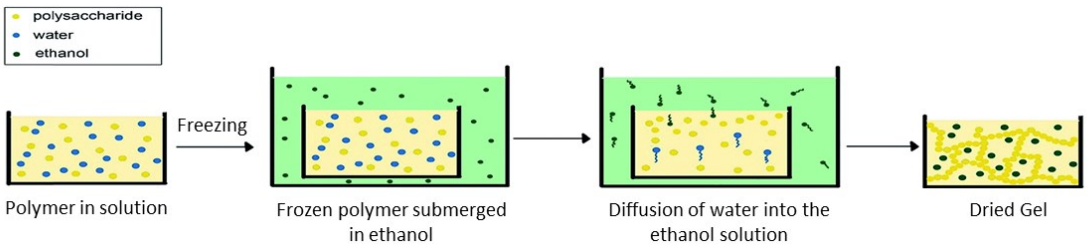

Figure 6. Schematic illustration of freeze-gelation. The polymer solution is frozen and submerged in ice-cold ethanol, where freezing point depression facilitates the diffusion of the frozen water molecules from the polymer. The resulting scaffold is air dried to obtain a porous, dry scaffold. The figure is reproduced, with modification, from Tkalec et al. with permission of The Royal Society of Chemistry (RSC). The original RSC article is available online: http://dx.doi.org/10.1039/10.1039/C5RA14140K (Tkalec, Knez, & Novak, 2015).

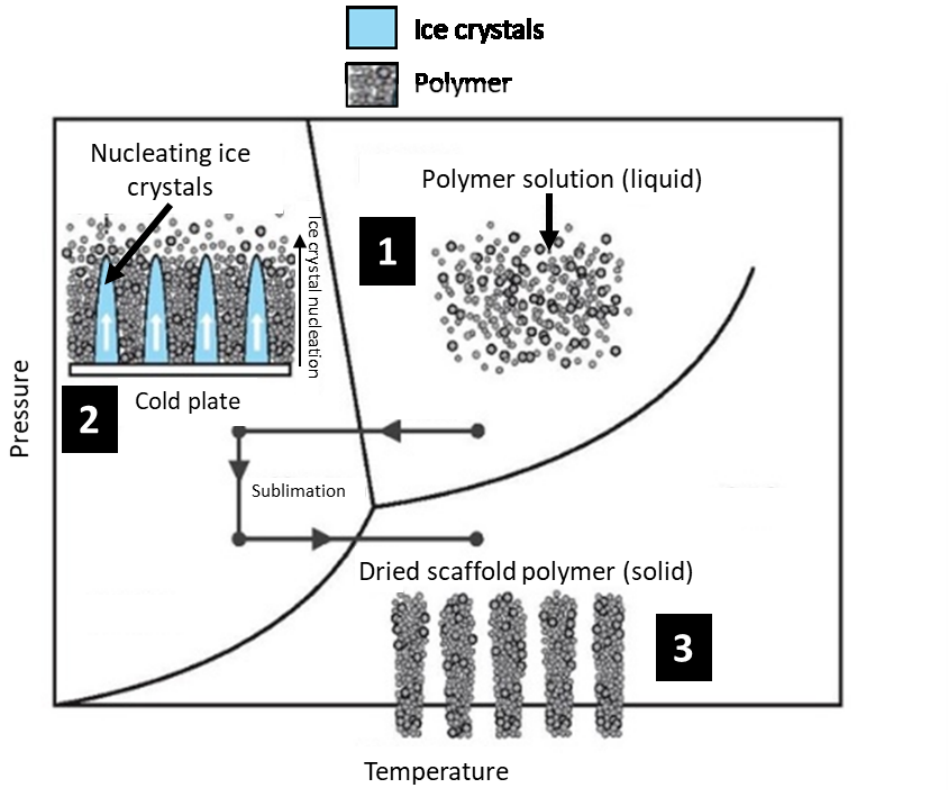

Figure 7. Scaffold formation by freeze-drying. A polymer in solution is frozen by applying cold to only one side of the solution, inducing directional ice crystal nucleation growth. Sublimation of the resultant ice crystals by freeze-drying removes the ice crystals without thawing, leaving pores within the dry polymer. The figure was adapted from Wikimedia Commons.

Freeze-gelation is the process of eliminating ice crystals, through the addition of a water-miscible solvent that remains in liquid state at the freezing temperature of the ice crystals. It is believed that this solvent modifies the freezing temperature of the water, and dissolves the ice crystals while maintaining the frozen state of the scaffold (Hsieh et al., 2007). The most commonly used solvent for freeze gelation is an ethanol solution, which can produce

porous scaffolds that are comparable to those from other methods such as freeze-drying (Ho et al., 2004).

Freeze-drying (lyophilisation) is a different process to eliminate ice crystals from the hydrogel by sublimation (Pikal & Shah, 1990). The interior of the lyophilizer is maintained at a temperature lower than that of the material, such that when vacuum is applied, sublimation of water molecules from ice crystals within the hydrogel occurs. For example, ice crystal nucleation followed by lyophilization has been used to produce a dry, porous chitosan-sodium hyaluronate scaffold (Ma et al., 2014).

1.4.2 Mechanical Strength:

The mechanical strength of a hydrogel is a characteristic of the polymer which it is made of. However, choice of production method will modify the mechanical strength of the resulting hydrogel, and will often lead to changes in other hydrogel characteristics, such as pore size and porosity. Moreover, the inherent porosity and pore size of a polymer will also affect the hydrogel mechanical strength (Bi & Liang, 2016). A simple example of this principle would be the addition of a chemical crosslinker. Once the solvent is removed, the hydrogel structure is based on a combination of hydrogen and covalent bonds between the polymer constituents. However, this bonding is often incomplete since there are reactive groups which remain available for crosslinking (Van Tomme et al., 2008; Wong et al., 2015). Reaction with a chemical crosslinker (such as formaldehyde, glutaraldehyde or genipin) will mechanically strengthen the material by crosslinking these groups further. Ionic solutions can also create non-covalent crosslinkages that increase polymer mechanical strength. A good example of this would be the

addition of calcium chloride to an alginate solution (AS), which crosslinks via coordinate bonding between the alginate carboxylate groups and divalent Ca^{2+} ions (Nokhodchi & Tailor, 2004).

The mechanical strength of a hydrogel can also be modified by the addition of another material or polymer, to produce a composite material (as discussed earlier). An inherently weak hydrogel scaffold can be reinforced with a second polymer (forming a co-polymer system) or a ceramic/metallic component to increase the overall mechanical strength (Gong et al., 2003). Examples include calcium phosphate-alginate hydrogel scaffolds, and chitosan-alginate co-polymer scaffolds (Li & Zhang, 2005; Zhao et al., 2015). Both of these have significantly higher mechanical strength than their constituent hydrogel components alone.

1.4.3 Degradation:

Hydrogel degradation is an extremely important feature, and is critical for the purpose of a biomaterial. Once endogenous tissue has been deposited, there is no further need for the scaffold (Lyu et al., 2007). Aside from the material breakdown inherent to the type of polymer, there are two major factors that modify the kinetics of material degradation: chemical crosslinking and material plasticization. Degradation of a material in cell culture often occurs through hydrolysis of chemical bonds within the hydrogel; on the other hand, *in situ* degradation of an implanted scaffold involves more complex mechanisms. The most common form of *in situ* degradation with carbohydrate polymers can be lysosomal (Xu & Ren, 2015) or lysozyme-induced degradation (Hakkarainen & Albertsson, 2008; Pangburn et al., 1982).

Chemical crosslinking and plasticization reduce the rate of material degradation by blocking reactive groups on the polymer backbone, such as amine and carboxyl groups (Bartnikowski et al., 2015), and reduces rates of hydrolysis or lysozyme degradation (Makadia & Siegel, 2011; Yoshimura et al., 1988). Plasticization has a similar outcome, but without modifying other material properties. Plasticization adds non-reactive hydrocarbons or different reactive groups to either reduce or increase degradation, respectively (Sanyang et al., 2016; Vieira et al., 2011). There are many plasticizers available, but one of the most widely utilized is glycerol, which reduces degradation by blocking exposed functional groups (Epure et al., 2011).

1.5 Eggshell as a Bone Regeneration Material:

The common point of many of the biomaterials discussed previously is that they aim to mimic the physical and mechanical properties of the type of tissue being regenerated, a strategy often referred to as biomimetic. Attempts to use chicken eggshell (ES) as a bone regeneration material can be described as both bioinspired and biomimetic. Researchers may have initially been drawn by superficial parallels between the hard, calcium-based minerals that form both ES (calcite) and human bone (HA).

1.5.1 Use of Eggshells as a Bone Regeneration Material:

Earlier research examining ES as a possible biomaterial utilized fragments of ES or ES particles in a variety of ways. For example, multiple studies examined the implantation of ES particle powders in skull bones or teeth in animal models (Baliga et al., 1998; Dupoirieux et al., 1995; Dupoirieux et al., 2000). ES particles (400-600 μm) have been evaluated as grafts in

induced bone defects in both rat mandible and rabbit calvaria (Dupoirieux et al., 1995). However, after two months of implantation within a defect, only fibrous tissue was observed surrounding the ES particles in both animal models. No immune response was observed in either case, and therefore ES was proposed for use as a suitable secondary component of bone regeneration material (Dupoirieux et al., 1995). Chicken ES particles sandwiched between sheets of polytetrafluoroethylene membrane were subsequently evaluated to serve as a guide for cells external to the defect (Laurent Dupoirieux et al., 2000). Again, only fibrous tissue was observed in the defect zone. The lack of porosity was underlined as a reason for the absence of significant bone regeneration in the induced defects.

Chicken ES can serve as a precursor for synthetic calcium phosphate or HA, the latter being the main mineral component of bone, since calcite can be chemically converted into HA. A number of studies have examined methods for producing ES-derived HA (EHA) (Demirel & Aksakal, 2016; Padmanabhan et al., 2015; Ramesh et al., 2016), and the bone regeneration effects of EHA have been compared to synthetically-derived HA (SHA) (Kattimani et al., 2016). Human patients between the ages of 20 to 45 years requiring maxillofacial cystectomy or apicoectomy participated in a study where their graft was packed with either EHA or SHA material. Again, the researchers noted the biocompatibility of the EHA, with no adverse immune response being observed. Some bone regeneration occurred with either EHA or SHA, shown by radiological evaluation of bone density, but with very little difference between the two groups (Kattimani et al., 2016). In agreement with previous work, the possibility of coupling ES with a porous matrix or growth factors to improve the outcome was proposed (Dupoirieux et al., 2000; Kattimani et al., 2016).

ES has also been used to reinforce polymer hydrogel scaffolds to form composite mineral-hydrogel biomaterials (Dadhich et al., 2016). An ES slurry was created using acetic and phosphoric acids, and combined with chitosan to create a printable solution. This suspension was used to create a 3D scaffolds in an ethanol coagulation bath, followed by further sintering of the resulting scaffold. These scaffolds were first evaluated with human MSCs from Wharton's jelly, and osteogenic differentiation was observed through an increase in ALP activity over 7 days. This scaffold was also evaluated in a rabbit model through subcutaneous implantation. Histological evaluation showed some markers of bone formation at 15 and 30 days, such as increases in collagen and OPN. These markers at both time points were consistently higher in the ES-coated chitosan scaffold than in both the calcium phosphate-coated chitosan scaffold and the tricalcium phosphate scaffold, which was indicative of a greater degree of osteogenic differentiation (Dadhich et al., 2016).

Finally, ES has been utilized as a template, rather than as a direct bone regeneration material. The surface of ES was treated with hydrochloric and sulfuric acids to produce a surface nanotexture, which was then imprinted using polydimethylsiloxane (PDMS) to create a nanotextured PDMS membrane (Asghar et al., 2012). Human fibroblasts were cultured on the surface of these PDMS templates, and an increase in fibroblast adherence and proliferation on the membrane surface was found to be associated with the nanotexturing.

1.5.2 Biology:

Much of the research described in the previous section (Section 1.5.1) either used the ES directly or utilized the ground ES for a reinforcing cement. The following sections (Sections

1.5.2 and 1.5.3) will discuss the biology of the ES and why ES particles are a promising hydrogel scaffold component.

The primary purpose of the avian ES is to protect the embryo growing within the egg until it is fully matured and ready to hatch. The ES is inherently non-porous, likely due to its function of providing mechanical protection, and being a barrier to bacterial contamination of the content. While there is a small number of respiratory pores on the surface, the small number and size of these pores (<20 μm) are inadequate for cellular invasion (Riley et al., 2014).

The avian ES is formed predominantly of calcium carbonate in the form of calcite (Murakami et al., 2007; Hincke et al., 2012). ES mineralization occurs upon a collagen-based fibrous meshwork (ES membranes). Following nucleation, the growth of elongated calcite crystals towards the ultimate ES surface occurs in an acellular uterine fluid with elevated calcium and bicarbonate ions (Nys et al., 2004). A large number of ES matrix proteins have been identified, with some orthologs to non-collagenous constituents of bone, such as OPN and matrix extracellular phosphoglycoprotein (MEPE) (Hincke et al., 1999; Hincke et al., 2008; Hincke et al., 2012).

1.5.3 Future Considerations for Eggshell as a Bone Regeneration Material:

This introductory chapter has discussed the importance of porosity in bone regeneration biomaterials, while also addressing the shortcomings of previous studies with ES as a bone regeneration biomaterial. The poor performance of ES as a packing material for bone regeneration has been attributed to its inherent non-porosity. While some researchers have

used ES as a calcium source for coating of scaffolds, no research with ES particles embedded into hydrogel scaffolds has been reported. The benefit of this approach is that ES matrix proteins, such as collagens and OPN, are available as osteogenic factors to induce differentiation. We predict that ES particles embedded in a hydrogel scaffold will allow cellular interaction with these exposed proteins, and stimulate an osteogenic response. In addition, it has been established that a nanotexture can be generated on the surface of ES particles. Thus, ES particles can be acid-treated to introduce a surface nanotexture with exposed proteins. Both of these factors could promote osteogenesis.

Overall, a composite scaffold made of ES particles embedded in a hydrogel matrix may provide an environment for MSC differentiation in a novel bone regeneration biomaterial.

2.0 Hypotheses and Objectives:

2.1 Hypotheses:

The hypotheses of this Master's thesis were:

1. The addition of ES particles into a porous composite hydrogel matrix produces a scaffold that induces more osteogenic differentiation of MSCs than the composite hydrogel scaffold without particles;

2. ES particles with a nanotextured surface have a stronger osteogenic effect than ES particles without a nanotextured surface.

2.2 Objectives:

The objectives of this Master's thesis were two-fold:

1. Develop porous composite hydrogel scaffolds containing ES particles (with or without a nanotextured surface) to mimic the physicochemical properties of bone;
2. Analyze the osteogenic potential of these scaffolds *in vitro*.

3.0 Materials and Methods:

3.1 Preparation and Characterization of Particles:

3.1.1 Removal of Eggshell Cuticle and Membranes:

Whole white eggs from Lohmann White Leghorn hens (Burnbrae Farms, Lyn, ON) were opened at the narrow end using a Dremel tool. The content was discarded and the interior was washed thoroughly with Milli-Q water and Dulbecco's phosphate-buffered saline without magnesium and calcium (PBS; ThermoFisher Scientific, Waltham, MA). The washed shell was cut in half and placed in 0.268M sodium hypochlorite (40^{o}C, 15 min, under stirring) in order to remove the surface cuticle and protein membrane of the ES halves. The shell halves were then washed thoroughly with Milli-Q water and PBS. After drying overnight, the halves were manually crushed for 60 s using a mortar and pestle. This powder was sieved (Keck Sieve Shaker Kit; Cole-Parmer, Montreal, QC) to obtain particles sized between 229 µmand 381 µm. This size range was based on the pore size of the meshes inherent to the shaker kit. These ES particles were stored at 4^{o}C until used.

3.1.2 Preparation of Nanotextured Eggshell Particles:

ES particles underwent a nanotexturing treatment in order to produce the nanotextured ES (NTES) particles. Particles (5 mg) were suspended in 1 ml of 0.250 M phosphoric acid (PA) for 10min at room temperature. The resulting NTES particles were collected through vacuum filtration on Whatman qualitative filter discs (11 µm pore size; Millipore-Sigma, Burlington, MA) and washed thoroughly with PBS and Milli-Q water before air-drying overnight and storage at 4^{o}C.

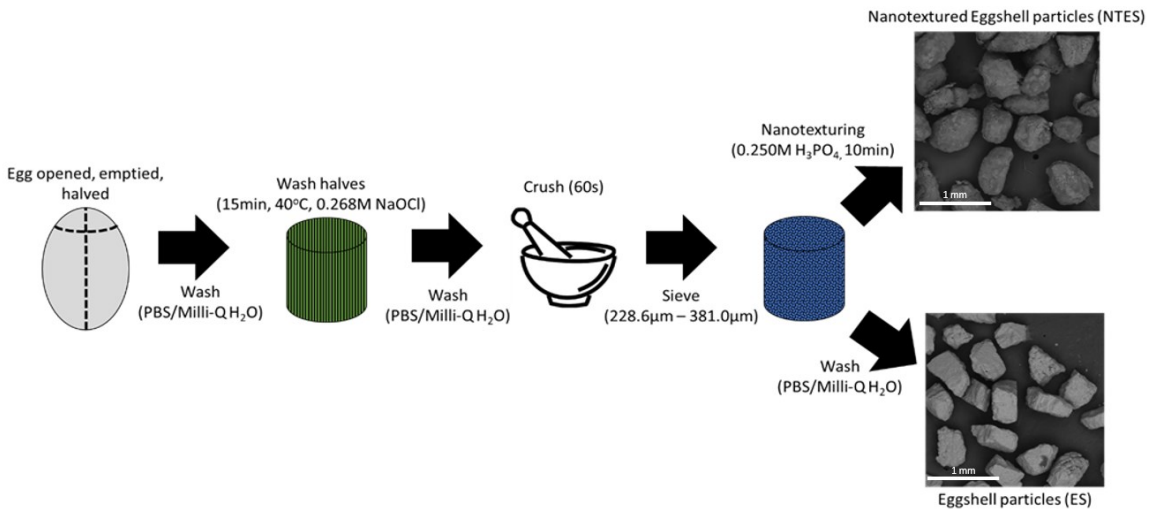

Figure 8. Schematic depicting eggshell (ES) and nanotextured eggshell (NTES) particle preparation.

3.1.3 Surface Topography and Elemental Analysis of Particles:

The surface topography of both ES and NTES particles was evaluated using images obtained by scanning electron microscopy (SEM; TeScan Vega-II XMU SEM, Brno, Czech Republic) at a voltage of 20.0 kV after gold sputter-coating (5 min, under vacuum). SEM micrographs were analyzed visually to discern morphological differences between the two types of particles. Energy dispersive X-ray spectroscopy (EDS) was performed on samples after acquiring the SEM micrographs using the INCA EDS detection system (Oxford Instruments, Abingdon, United Kingdom) to determine the composition of particle surface elements. Elemental weight percentages were calculated from the weight of the detected element relative to the weight of all elements in the sample.

3.1.4 Fourier-Transform Infrared Spectroscopy of Particles:

Fourier-transform infrared (FTIR) attenuated total reflection (ATR) spectroscopy was performed on ES and NTES particles using an FTIR spectrometer at wave numbers from 0 to 4000 cm^{-1} (Model 6200, JASCO Analytical Instruments, Japan). FTIR was used as a complement to EDS analysis, in order to identify chemical bonds.

3.2 Preparation of Scaffolds:

Sodium alginate (AS; alginic acid from brown seaweed, M_w = 120 kDa – 190 kDa; Millipore-Sigma) was dissolved in Milli-Q water to prepare a final solution of 2% w/v and chitosan (CS; >75% deacetylated; M_w = 310 kDa – 375 kDa; Millipore-Sigma) was dissolved in acetic acid (3% v/v) to prepare a 2% w/v solution. AS (750 µl) was aliquoted into a Peel-A-Way® histology mold (22 mm squared, 20mm deep; Ted Pella Incorporated, Redding, CA). Particles (ES or NTES; 20% w/v) were added to the AS solution and mixed manually with a metal stir-stick until a homogeneous suspension was achieved. This concentration of particles was determined to be the highest that would not affect the pore structure of the final scaffold (data not shown). CS (750 µl) was then added to this suspension and mixed manually with the same flat-edged tool until homogenously distributed. Finally, glutaraldehyde (0.03% v/v final concentration) was added to this suspension and mixed thoroughly to initiate crosslinking. Scaffolds without particles (blank) were generated following the same steps, without particles. These scaffold samples were placed on a directional freezing apparatus (custom-made) and held at a temperature of -20°C for 24 h. Only the bottom surface of the scaffolds was in contact with the

cold plate in order to facilitate unidirectional ice crystal-nucleated pore formation. The frozen scaffolds were then placed in a freeze-drying flask (Labconco, Kansas City, MO) and kept for 24 h in a Styrofoam box containing dry ice and frozen gel packs. The freeze-dried scaffolds were stored in a desiccator until used. Overall, 3 types of scaffolds were generated for evaluation: ES particle-based scaffolds, NTES particle-based scaffolds, and blank scaffolds (without particles).

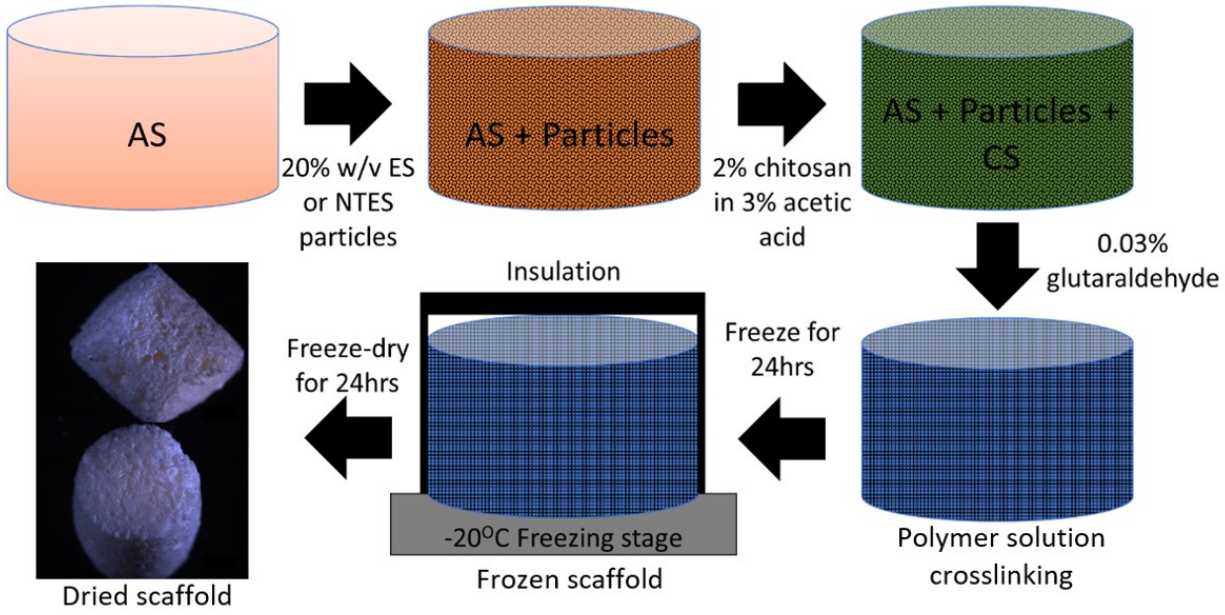

Figure 9. Schematic depicting the fabrication of scaffolds containing ES, NTES or no particles.

3.3 Scaffold Physicochemical Characterization:

3.3.1 Scaffold Microstructure Analysis and Pore Size Measurements:

Dried scaffolds (three of each type of preparation) were sectioned using a scalpel in either parallel or perpendicular planes to the Z-axis. These cross-sectional surfaces were gold sputter-coated as previously described (Section 3.1.3) and analyzed using scanning electron microscopy (TeScan Vega-II XMU SEM, 20.0 kV). The morphology of the scaffold microstructure was evaluated qualitatively by visual examination of SEM micrographs (two for each scaffold replicate). The size of twenty-five randomly selected pores on each cross-sectional image was measured using image analysis software (FIJI, NIH). Data from both cross-sectional images were pooled for statistical analysis.

3.3.2 Porosity Measurements:

The porosity of all scaffold types was evaluated using a fluid swelling test. After recording their dry weight, the scaffolds were placed in warm (37^{o}C) PBS and incubated under cell culture conditions (37^{o}C, 5% CO_2, 95% humidity) for 30 min. Excess fluid on the scaffold surface was removed by dabbing the surface with absorbent paper. The weight of the fluid-filled scaffold was recorded and the scaffold final volume was measured using digital calipers (Traceable® S/N 140408171; ThermoFisher Scientific). The percent porosity was determined based on the change in the scaffold mass and total volume, using the following formula:

$$\text{Porosity (\%)} = \frac{\left(\frac{\rho_{PBS}}{\Delta W_S}\right)}{V_S} \text{x } 100,$$

where the density of the PBS solution (ρ_{PBS}) divided by the change in scaffold mass (ΔWs), then divided by the volume of the wet scaffold (Vs), represents the empty pores that are filled with PBS.

3.3.3 Mechanical Strength Analysis:

The stiffness and CM of the scaffolds were determined using a protocol adapted from Bas et al. (Bas et al., 2017). Dried scaffolds were first equilibrated in PBS (37^{o}C) for 30 min before testing. All testing was performed on scaffolds submerged in PBS. Temperature (37^{o}C) was maintained during testing by using a heating plate. Scaffolds were submitted to an unconfined compression test by applying a compressive load to achieve 70% of the scaffold original height at a displacement rate of 0.01 mm/s using a 5N load cell in a universal testing machine (UTM; MTS Sintech 1G; MTS Systems Corporation, Eden Prairie, MN). The stiffness and the CM of the scaffolds were calculated from the linear regression of the load-displacement curve and from the slope of the stress-strain plot generated by the UTM software, respectively. The scaffold height was measured before and immediately after testing using digital calipers (Traceable® S/N 140408171; ThermoFisher Scientific) to determine any damage to the scaffold microstructure.

3.3.4 Scaffold Stability and Hydrolytic Resistance:

Scaffolds were submerged in PBS (37^{o}C) and placed in an incubator under cell culture conditions for 21 days. Scaffolds were taken out of the incubator every 7 days, patted dry to remove excess fluid and placed in a 96-well plate (Corning, Tewksbury, MA). Optical density at 590 nm was read using a microplate reader (BioTek Eon; BioTek, Winooski, VT). Decreases in

optical density of the scaffold compared to day 0 were attributed to loss of scaffold microstructure due to degradation. The scaffold dimensions at day 0 and day 21 were measured using digital calipers (Traceable® S/N 140408171) to correlate degradation with loss in scaffold physical volume.

3.3.5 Analysis of Particle Distribution in Scaffolds:

Distribution of either ES or NTES particles in their respective scaffolds was quantitatively evaluated using a homogeneity model developed for a micro-computed tomography scanner (µCT; SkyScan 1174v2; SkyScan, Belgium). Scaffolds were imaged using the µCT scanner with an unfiltered X-ray source (37 kV, 648 µA). Images were acquired every 0.7^{o} over a 180^{o} rotation. An upper and lower frame of the image was drawn, and the integrated density of each frame was determined. Integrated density was used to visualize the three-dimensionality of the particles in the image. The integrated density values of the upper and lower frames were blanked and subtracted from one another and the absolute value was recorded. This was repeated for each rotation of the scaffold and all the data were presented as a distribution. The integrated density of the blank scaffold (without particles) was used as a control. In this model, subtraction of the upper and lower frame integrated density values would generate a theoretical value of zero for perfectly homogeneous material.

3.4 Seeding of Human Bone Marrow-derived Mesenchymal Stem Cells into Scaffolds:

3.4.1 Pre-Seeding Cell Culture:

Human MSCs (first passage) were thawed and grown to approximately 85% confluency in a 150 cm^2 cell culture flask (Corning), using an initial seeding density of 5000 cells/cm^2. Flasks were filled with 30 ml of cellular growth media (CGM) prepared from α minimum essential media (αMEM; Life Technologies, Carlsbad, CA) supplemented with 10% heat-inactivated fetal bovine serum (FBS; Millipore-Sigma, Burlington, MA). Once confluent, cells were detached with 0.25% trypsin-EDTA (Life Technologies). Trypsin was inactivated with the addition of fresh CGM, and the cell suspension was centrifuged at 500 x g for 5 min. Cells were resuspended in fresh CGM and seeded into new 150 cm^2 cell culture flasks at a seeding density of 5000 cells/cm^2 in 30 ml of CGM. This was repeated until MSCs were in their fifth passage, at which point cells were seeded in the scaffolds. MSCs from four different donors (i.e., cells from 4 different lots: 3 from ATCC [PCS-500-012 Lot #64430737, Lot #70011721, Lot #70011720] and 1 from CET [HMSC-BM-500 Lot #102]) were cultured for scaffold seeding. Data were generated for each lot number.

3.4.2 Scaffold Sterilization and Preparation Prior to Seeding:

Dried scaffolds were submerged in 70% ethanol and placed in an incubator overnight under cell culture conditions. The scaffolds were then washed with PBS (37^{o}C), submerged in scaffold growth media (SGM) prepared from CGM supplemented with 10 nM Dex (Millipore-Sigma), 20 µM AA (Millipore-Sigma), 50 mM BGP (Millipore-Sigma) and 1% penicillin-streptomycin (Life Technologies), and placed in an incubator overnight under cell culture

conditions. After the overnight incubation, the scaffolds were used immediately for cell seeding.

3.4.3 Scaffold Seeding and Culture:

MSCs in their fifth passage were pelleted and resuspended in SGM at 8334 cells/μl so that a total of 250,000 cells would be seeded in each scaffold after pipetting 2.5 μl of cell suspension 6 times on each scaffold. More specifically, 2.5 μl of MSC suspension were first pipetted onto the scaffolds in two random spots, followed by a 30-min incubation. All incubations occurred under cell culture conditions. After repeating this seeding step three times, the scaffolds were incubated for 1 h, flipped 180^{o}, and the entire procedure was repeated on this other side. Finally, the scaffolds were incubated for 1.5h after the addition of a few drops of SGM, were placed in a 48-well plate (Corning), covered gently with SGM, and incubated overnight under cell culture conditions.

The scaffolds were then transferred into cell culture inserts (0.4 μm pore size; ThermoFisher Scientific) placed in a 24-well plate (Corning) to help nutrient diffusion (Sekine & Haraguchi, 2011). Both the interior and exterior of the cell culture inserts were filled with SGM until the scaffold was submerged. Scaffolds were cultured for up to 21 days. SGM was replenished every 2 days. The final experimental design (Figure 10) consisted of 3 scaffold types (blank, ES particles, and NTES particles), each with 3 technical replicates for each of the 4 time points analyzed (days 0, 7, 14, and 21).

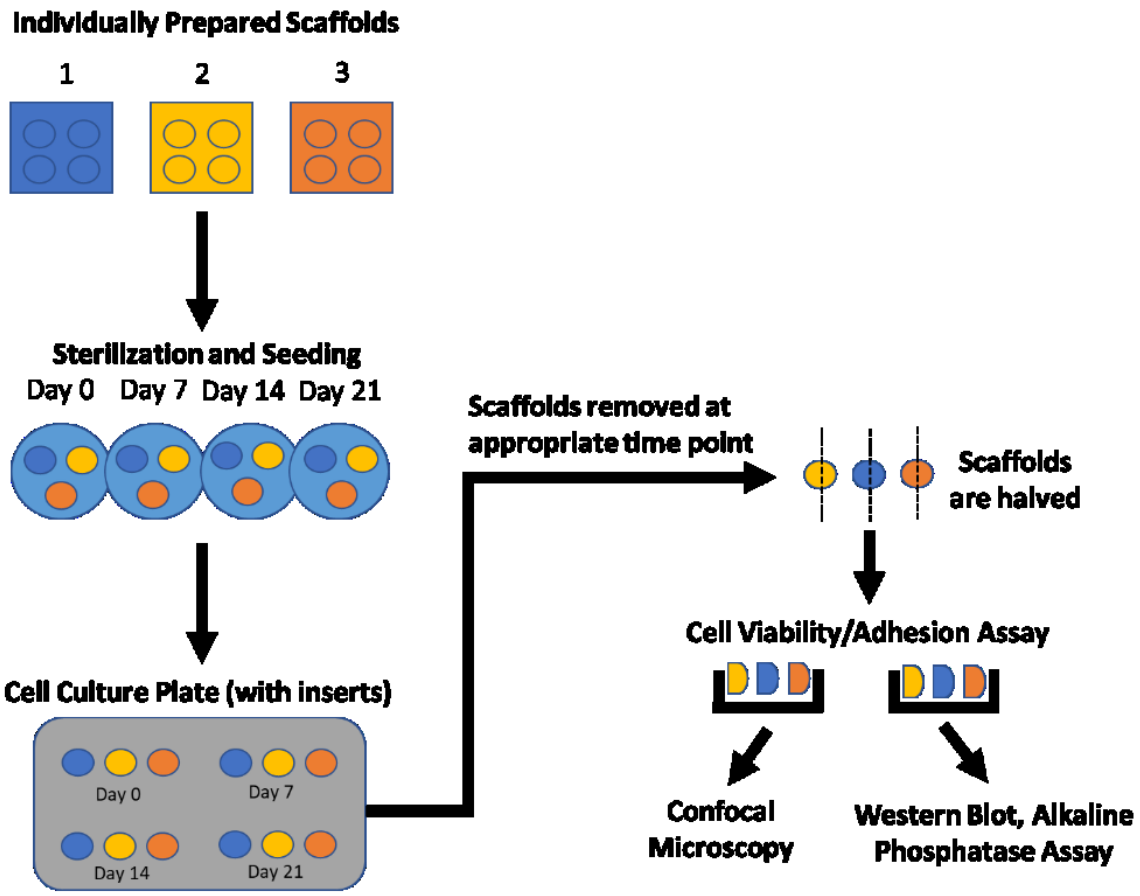

Figure 10. Schematic depicting the cell culture workflow for all scaffold types.

3.5 Cell Retention and Viability:

3.5.1 Evaluation of Mesenchymal Stem Cell Retention in Scaffolds:

The retention of MSCs in the different scaffolds was evaluated using the AlamarBlue® assay. Scaffolds at the day 0 were washed thoroughly with SGM (37°C) to dislodge any poorly adherent or dead cells. They were then bisected with a scalpel and both halves were incubated for 3 h under cell culture conditions in SGM supplemented with 10% AlamarBlue® reagent

(ThermoFisher Scientific). At the end of the incubation, a 100 µl aliquot was added to a 96-well plate (Corning) and fluorescence was determined at an excitation/emission wavelength of 530 nm/590 nm (BioTek Eon, BioTek). The number of cells in the scaffolds was then determined using a standard curve generated with known numbers of MSC. The numbers of cells from each half of the scaffold were summed and compared to the number of cells initially seeded in each scaffold (250,000) to determine the percentage of cells retained.

3.5.2 Evaluation of Mesenchymal Stem Cell Viability in Scaffolds:

The viability MSCs in the different scaffolds was evaluated using the AlamarBlue® assay. Scaffolds at days 7, 14, and 21 were washed thoroughly with SGM. They were then bisected with a scalpel and both halves were incubated for 3 h under cell culture conditions in SGM supplemented with 10% AlamarBlue® reagent (ThermoFisher Scientific). At the end of the incubation, 100 µl aliquot was added to a 96-well plate (Corning) and fluorescence was determined at an excitation/emission wavelength of 530 nm/590 nm (BioTek Eon, BioTek). The number of cells in the scaffolds was then determined using a standard curve generated with known numbers of MSC. The numbers of cells from each half of the scaffolds were summed to obtain the total number of cells in the whole scaffolds.

3.6 Osteogenic Differentiation of Mesenchymal Stem Cells in Scaffolds:

3.6.1 Lysis of Mesenchymal Stem Cells in Scaffolds:

Following the AlamarBlue® assay at each time point, one of the scaffold halves was washed with 1 ml of ice-cold PBS that was then aspirated, and incubated in 150 µl of ice-cold lysis buffer (10% cOmplete protease inhibitor cocktail without EDTA (Roche, Basel, Switzerland) and 90% CytoBuster™ (Millipore-Sigma)) for 30 min on ice. The scaffold in lysis solution was then agitated on an agitator (5 min, 4°C). Following agitation, the scaffold in lysis solution was centrifuged (16,500 x g, 25 min, 4°C) to pellet any scaffold and cellular debris. Supernatants were transferred into new 1.5 ml Eppendorf tubes. An aliquot (50 µl) of each sample was pipetted out and kept on ice (for ALP assay), while the remaining volume was stored at -80°C for further use (for Western blot analysis).

3.6.2 Analysis of Alkaline Phosphatase Activity in Scaffolds:

The 50 µl aliquots of the fresh cell lysates on ice were added to a 96-well plate (Corning). One hundred microlitres of previously prepared ALP assay buffer containing 100mM diethanolamine (Millipore-Sigma), 0.5mM $MgCl_2$ (Millipore-Sigma), and 2mM para-nitrophenylphosphate (pNPP) (ThermoFisher Scientific), adjusted to pH 9.8 with HCl, were added to each sample in the plate. The plate was incubated for 1 h at room temperature, and protected from light. ALP present in the cell lysates catalysed the cleavage of pNPP to produce the chromophore *p*-nitrophenol. After the incubation, 50 µl of 2M NaOH were added to each sample to stop the reaction. Absorbances at 405 nm were read using a plate reader (BioTek Eon, BioTek). The activity of ALP in the lysates was determined by correlating the values

obtained to an ALP standard curve, prepared with known ALP enzyme concentrations (Worthington Biochemical Corp, Lakewood, NJ). ALP activity was normalized to the number of metabolically active cells in the scaffold. The number of cells (determined using AlamarBlue®) was used for normalization due to the unreliability of protein concentration, since medium FBS is retained by the scaffolds. Importantly, a corrective factor was applied to the number of cells counted at day 14 and day 21, by dividing the number by 1.6. Indeed, the cell counts of MSCs grown in differentiating media increased at days 14 and 21 by a 1.6 fold, which was determined in the literature to be caused by a change in metabolic rate in the differentiation pathway for MSCs (Shum et al., 2016). This led to a change in the rate of mitochondrial-mediated reduction of the AlamarBlue® reagent, necessitating the need for the corrective factor.

3.6.3 Analysis of Osteogenic Proteins RUNX2 and Osteopontin in Scaffolds:

Cell lysates (100 μL) were thawed on ice vortex-mixed with cold (4°C), freshly-prepared deoxycholic acid (0.5%, 10 μl; Millipore-Sigma), and incubated at room temperature for 10 min. Room temperature 72% trichloroacetic acid (TCA) (10 μL) was added to each sample. Samples were then vortexed, incubated on ice for 10 min, and centrifuged (16,500 x g, 4°C, 10 min) to obtain a protein pellet. The supernatants were discarded while the pellets were vortex-mixed with 100 μL ice-cold acetone, and incubated on ice for 15 min. After another centrifugation (16,500 x g, 4°C, 15min), the supernatants were discarded and the protein pellets were air-dried at room temperature for 1 h.

The protein pellets were re-solubilized in 100 mM NaOH / CytoBuster™ (25 μl, room temperature) for sodium dodecyl sulfate polyacrylamide gel electrophoresis (SDS-PAGE).

Samples were mixed in a 1:1 ratio with loading buffer solution (2X LI-COR loading buffer (LI-COR Biosciences, Lincoln, NE) containing 200 mM dithiothreitol (DTT) (Millipore-Sigma)), heated (95^{o}C, 5 min) and then vortexed. An aliquot of each sample (20 µl) was then loaded on a precast gel (4% - 12% Novex® Bis-Tris, ThermoFisher Scientific). Samples were organized such that each gel contained the cell supernatants for all time points of 1 technical replicate for 1 MSC donor from both ES and NTES scaffolds. SDS-PAGE was performed using a Novex® gel box (ThermoFisher Scientific) on ice at 110V for 120 min. Following separation, gels were washed with Western blot transfer buffer (25 mM Tris, 192 mM glycine, 20% methanol). A Western blot transfer stack consisting of a low fluorescence polyvinylidene difluoride (PVDF) membrane (0.4 µm pore size; Bio-Rad, Hercules, CA) and the SDS-PAGE gel was placed between blotting paper and sponges, loaded into a cassette and placed in a wet-transfer tank (Bio-Rad) for electro-transfer on ice (105 V, 80 min). Following transfer, the PVDF membrane was dried overnight on filter paper. The membrane was then re-hydrated with 100% methanol, washed with Milli-Q water and incubated in 0.1% Tween-20 in PBS (TPBS; ThermoFisher Scientific) for 5 min. The membrane was then incubated with REVERT™ Total Protein Stain (LI-COR Biosciences) for 5 min on a shaker at low speed and protected from light. After discarding the stain, a de-staining solution provided with the REVERT™ kit was used to wash the membrane twice. Finally, the membrane was air-dried for 2 h and imaged at 700 nm using the LI-COR Odyssey (LI-COR Biosciences) instrument.

In order to perform Western blotting, each membrane was re-hydrated with 100% methanol, washed with water and TPBS, and blocked for 1h at room temperature in LI-COR PBS blocking buffer (LI-COR Biosciences). It was then washed with TPBS for 10 min on a shaker at

low speed, and incubated with monoclonal mouse anti-human RUNX2 antibody (ZR002, 3 μg/ml [ThermoFisher Scientific] in LI-COR PBS blocking buffer) at 4°C overnight in a black Western blot incubation box (LI-COR Biosciences). Following the incubation, the primary antibody was retained and stored at -20°C for re-use. The membrane was then rinsed 3 times with TPBS in the black Western blot incubation box, washed with TPBS on a shaker (10 min, low speed), then rinsed 3 more times with TPBS in black Western blot incubation box before incubation with goat anti-mouse IRDye® 800CW secondary antibody (LI-COR Biosciences) in LI-COR PBS blocking buffer for 1 h at room temperature. After the incubation, the membrane was washed 3 times with TPBS, dried overnight (at room temperature, protected from light), and imaged on the LI-COR Odyssey at 700 nm and 800 nm. Finally, the membrane was re-hydrated as before, and the primary and secondary antibody procedures were repeated for OPN (7C5H12, 1:500 [ThermoFisher Scientific] in LI-COR PBS blocking buffer), and GAPDH (AM4300, 2 μg/ml [ThermoFisher Scientific] in LI-COR PBS blocking buffer). Changes in protein expression were quantified from the acquired images using ImageStudio software (LI-COR Biosciences). GAPDH was used as a loading control.

3.6.4 Analysis of Mesenchymal Stem Cell Morphology in Scaffolds:

MSC morphology was visualized directly on scaffolds using a LIVE/DEAD Cell Viability stain (Invitrogen Molecular Probes, 2005) according to the manufacturer's protocol. Scaffolds from culture at each time point were washed with PBS (37°C) and incubated with 1 ml of dye solution (2 μM calcein-AM [ThermoFisher Scientific], 4 μM ethidium homodimer-1 [ThermoFisher Scientific], and 160 μM of Hoechst 33342 [ThermoFisher Scientific] in PBS) for 25 min under cell culture conditions. Calcein-AM stains green the cytoplasm of living cells,

ethidium homodimer-1 stains red the nucleus of dead cells and Hoechst 33342 stains blue the nucleus of living cells. After the incubation with the dye, scaffolds were washed once with warm (37^{o}C) PBS and then mounted on glass slides with PBS under coverslips that had built-in 1mm spacers (Imaging Spacers 70327-20S; Electron Microscopy Sciences, Hatfield, PA). Images of MSCs on scaffolds were acquired using the LSM 880 with Airyscan confocal microscope (Zeiss, Oberkochen, Germany), using tile-scanning and Z-scanning parameters to form large, 3-dimensional images. Images were displayed using Imaris software (Bitplane, Zurich, Switzerland).

3.7 Statistical Analysis:

3.7.1 Statistical Analysis for Physicochemical Characterizations of Scaffolds:

Statistical analysis was performed using SPSS v25 (IBM, Armonk, NY). Normality was assumed for all data except for pore size and particle homogeneity analyses. Levene's test was used to determine if the assumption of homogeneity of variance was met. Porosity and mechanical strength measurements were analyzed using a one-way analysis of variance (ANOVA), followed by Tukey post-hoc tests. Pore size distribution and particle homogeneity were analyzed using Kruskal-Wallis. Scaffold degradation was analyzed using a two-way ANOVA with scaffold type and time as factors, and was followed by Tukey post-hoc tests. $p<0.05$ was considered significant in all data. Data are presented as means ± standard deviation (SD) or medians with interquartile range, where appropriate.

3.7.2 Statistical Analysis of Adhesion, Viability, and Differentiation of Mesenchymal Stem Cells in Scaffolds:

Levene's statistic and visual analysis of quantile-quantile plots were performed for all data sets. All statistical analyses were performed using a mixed linear model constructed in R (version 3.5.2) with cell donor used as a random factor and scaffold and/or timepoint used as fixed factor(s). Pairwise comparisons were performed using Tukey post-hoc tests with a single-step adjustment. All data are presented as the mean ± standard error of the mean (S.E.M.).

4.0 Results:

4.1 Characterization of ES and NTES Particles:

ES and NTES particles were prepared as described in Sections 3.1.1 – 3.1.2.

4.1.1 Surface Topography:

The particle surface before and after the nanotexturing treatment was visualized through SEM (Figure 11), in order to assess the morphology of the unaltered ES surface, as well as to evaluate the effects of the phosphoric acid treatment. The surface of the unaltered ES particles showed interspersed bumps, pores and fine striations at high magnification (Figure 11A, B). After the nanotexturing treatment, the surface of the NTES particles showed cuboidal deposits (Figure 11C) and displayed a distinctly different surface morphology, with randomly distributed pattern of grooves, ridges, and pores (Figure 11D).

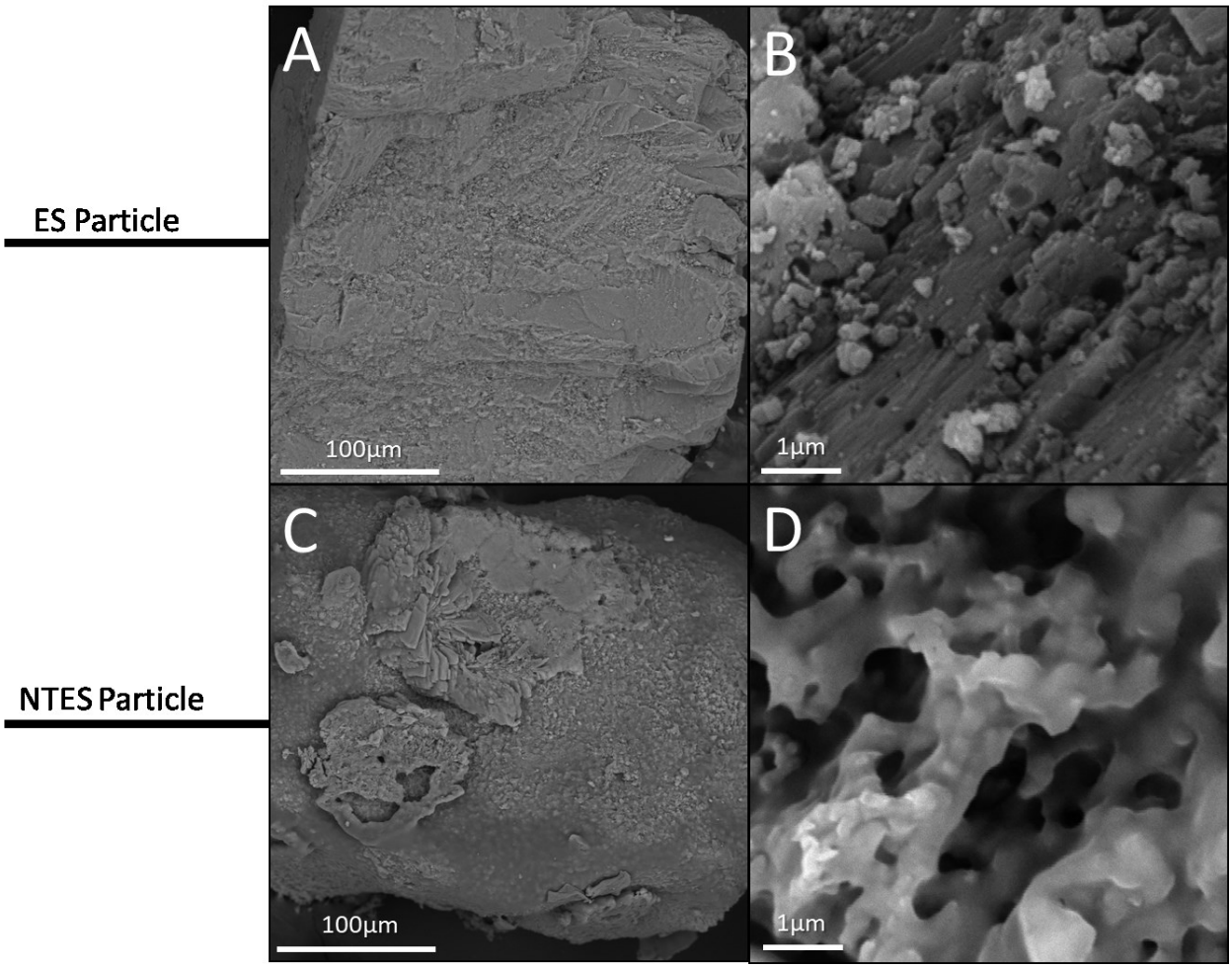

Figure 11. Representative scanning electron microscopy (SEM) micrographs of eggshell (ES) particles before (A, B) and after nanotexturing (C, D). In order to produce nanotexturing, particles were treated with 0.250 M phosphoric acid for 10 min under stirring. Magnification: 100x (A, C) and 3000x (B, D).

4.1.2 Chemical Analysis of Particles by EDS and FTIR:

EDS analysis was performed to detect changes in the elemental composition of the particle surface associated with nanotexturing (data not shown). The elemental composition of ES and NTES particles was similar, including mainly oxygen, calcium, and carbon, as well as traces of magnesium. Phosphorus was only present on the surface of the NTES particles.

FTIR was performed in order to gain insight into the identity of the phosphorous-containing compound(s) (Figure 12). The spectral profile was similar for both ES and NTES particles, with the exceptions of new peaks (approximately 500 cm^{-1}, 1000 cm^{-1}, 1600 cm^{-1} and 2800 cm^{-1} to 3500 cm^{-1}) appearing in the NTES particle spectrum. According to FTIR database guides, these peaks could be due to phosphate and protonated phosphate ions (PO_4^{3-}, 500 cm^{-1} and 1000 cm^{-1}; HPO_4^{2-} 1600 cm^{-1}), while the broad peak was likely associated with the protein amide bonds (Coates, 2006; Jastrzbski et al., 2011).

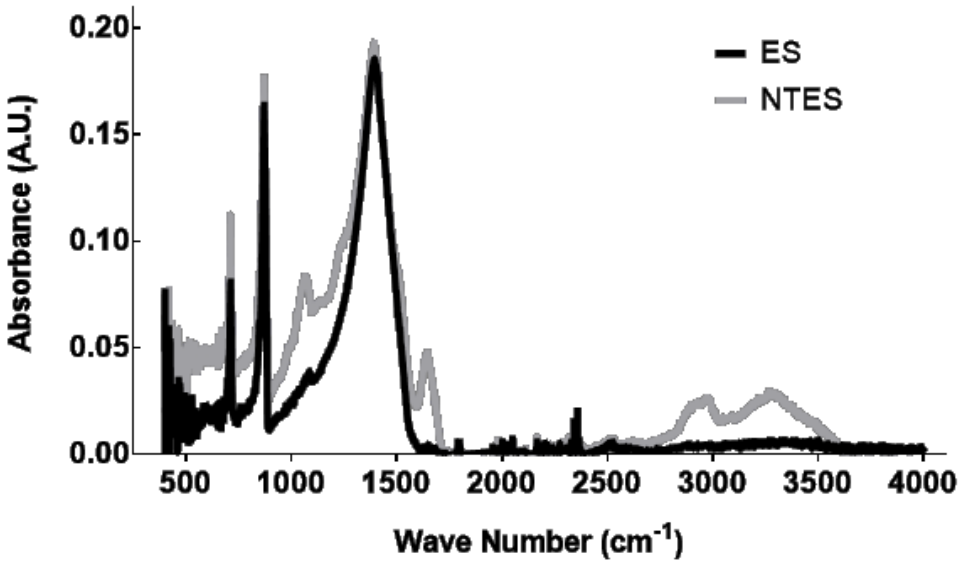

Figure 12. Fourier-transform infrared spectroscopy (FTIR) of eggshell (ES) and nanotextured eggshell (NTES) particles. FTIR analysis was performed to determine the surface constituents on ES before (black) and after (grey) nanotexturing treatment with 0.250 M phosphoric acid. Peaks are attributed to PO_4^{3-} at 500 cm^{-1} and 1000 cm^{-1}, protonated phosphate at 1600 cm^{-1}, and amide peptide bonds between 2800 cm^{-1} to 3500 cm^{-1}.

4.2 Preparation and Characterization of Scaffolds:

Different methods for preparation of porous hydrogel scaffolds were initially compared in order to determine the method that resulted in the most homogeneous ES particle distribution without a reduction of scaffold porosity and pore size. Three preparation methods were evaluated for pure 2% chitosan scaffolds: freeze-gelation, freeze-drying, and paraffin-sphere porogen leeching.

4.2.1 Scaffold Preparation

The freeze-gelation method produced scaffolds that were unstable due to inadequate drying. Porogen leeching and freeze-drying approaches both reliably produced 2% chitosan / 2% alginate co-polymer scaffolds with a homogeneous particle distribution. However, porogen leeching produced scaffolds that were mechanically weak. Overall, the freeze-drying method led to the most promising results (Table 1) after a few optimization steps to prevent resorption of the scaffold polymer into the frozen solvent. A Styrofoam box packed with ice packs and dry ice was used to maintain the low temperature of the scaffold during freeze-drying, which prevented the frozen solvent from thawing while still maintaining a temperature differential appropriate for sublimation. Other optimizations included the order of addition of the polymers, as well as the amount of crosslinking glutaraldehyde to use; both of which led to a more homogeneous distribution of ES or NTES particles. The final scaffold preparation method is described in details in Materials and Methods (Section 3.2.0).

Table 1. Comparison of the different methods to produce chitosan scaffolds (without particles).

Scaffold Preparation Method	Result
Freeze-Gelation	- Consistently collapsed during drying, no further testing
Porogen Leeching	- Excellent pore size and porosity - Tedious preparation method - Inconsistent physicochemical properties in resulting scaffold - Mechanically very weak and easy degradation in solution
Freeze-Drying	- Excellent pore size and porosity - Mechanically strong - Consistent physicochemical properties in resulting scaffold - Easy and simple preparation method - No observed degradation in solution

4.2.2 Microstructure:

The microstructure of the three scaffold types (containing no particles, ES particles, or NTES particles) was qualitatively evaluated using SEM to compare the scaffold morphologies and to observe how the particles were integrated into the pore walls (Figure 13). Ice crystal growth occurred in the Z direction (the X-Y plane of the scaffold was in contact with the freezing block). Two different planes (perpendicular and parallel sections) were examined for each scaffold to evaluate the continuity of the pores in 3D. The morphology of the scaffold walls appeared very smooth in the absence of either particle type (blank scaffolds, Figure 13A, B). The walls appeared rougher with the inclusion of either ES or NTES particles (Figure 13C, D, and Figure 13E, F, respectively). The microstructure of the scaffolds without particles consisted

of well-ordered, consistently spaced pores. The inclusion of either ES or NTES particles resulted in a loss of this morphology, and scaffolds with ES and NTES particles had a much more disordered and randomly distributed pore structure than the scaffolds without particles. Notably, ES or NTES particles in their respective scaffolds appeared to contribute to the pore walls.

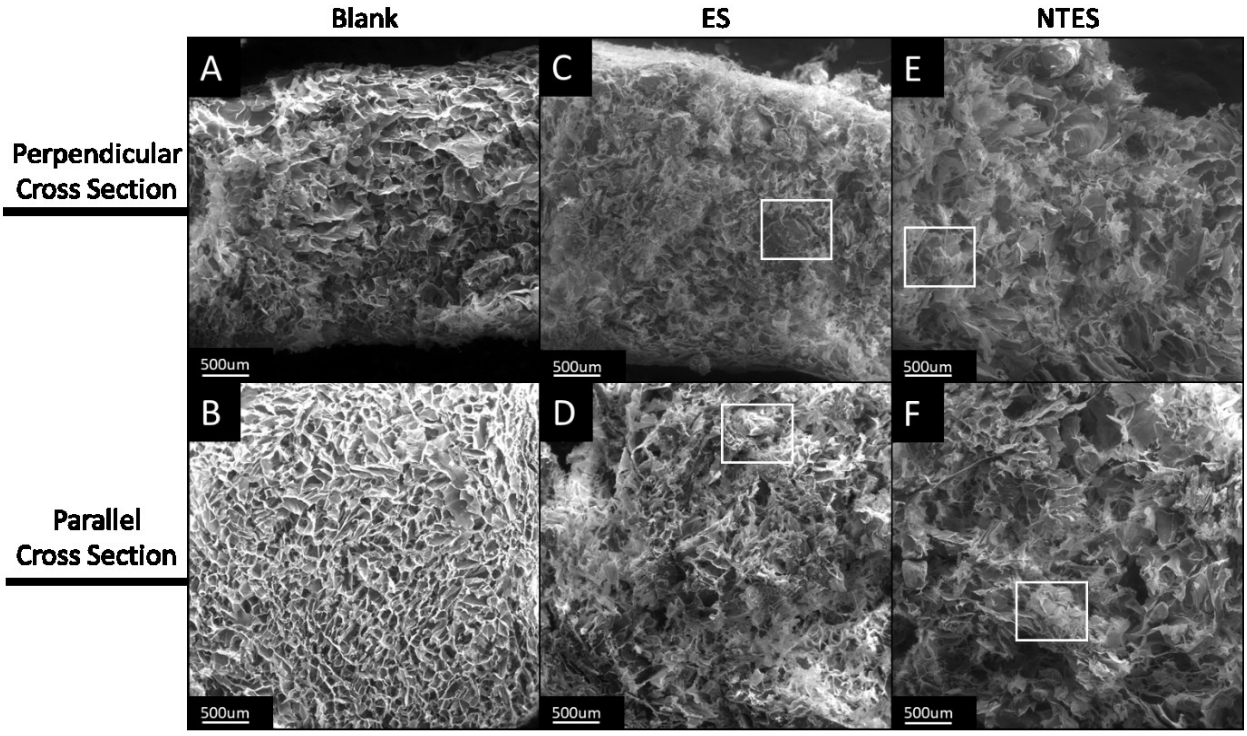

Figure 13. Representative scanning electron microscopy (SEM) micrographs of scaffolds. SEM analysis was performed on scaffolds without particles (A, B), or with ES (C, D) or NTES (E, F) particles. Scaffolds were cut either perpendicular or parallel to the Z axis (parallel to direction of ice crystal nucleation) and imaged to observe their morphology. White boxes indicate examples of visible ES or NTES particles.

4.2.3 Pore Size Distribution:

Image analysis of SEM micrographs described in the previous section was performed to determine the distribution of pore sizes in the different scaffolds (Figure 14), in order to predict the suitability of the scaffolds for bone regeneration, as well as to determine differences due to the inclusion of either ES or NTES particles. All scaffolds depicted pore size distributions that were non-gaussian, and had a similar number of pores between 50 µm to 300 µm diameter (Figure 14A – 14C). Comparison of the median pore size of scaffolds (Figure 14D) revealed that scaffolds containing NTES particles had a greater median pore size (113 µm [interquartile range: 88 µm – 140 µm]) than scaffolds with either ES particles and or no particles (94 µm [interquartile range: 75 µm – µm 112] and 99 µm [interquartile range: 74 µm – 135 µm], respectively) (p=0.011 and p<0.001, respectively).

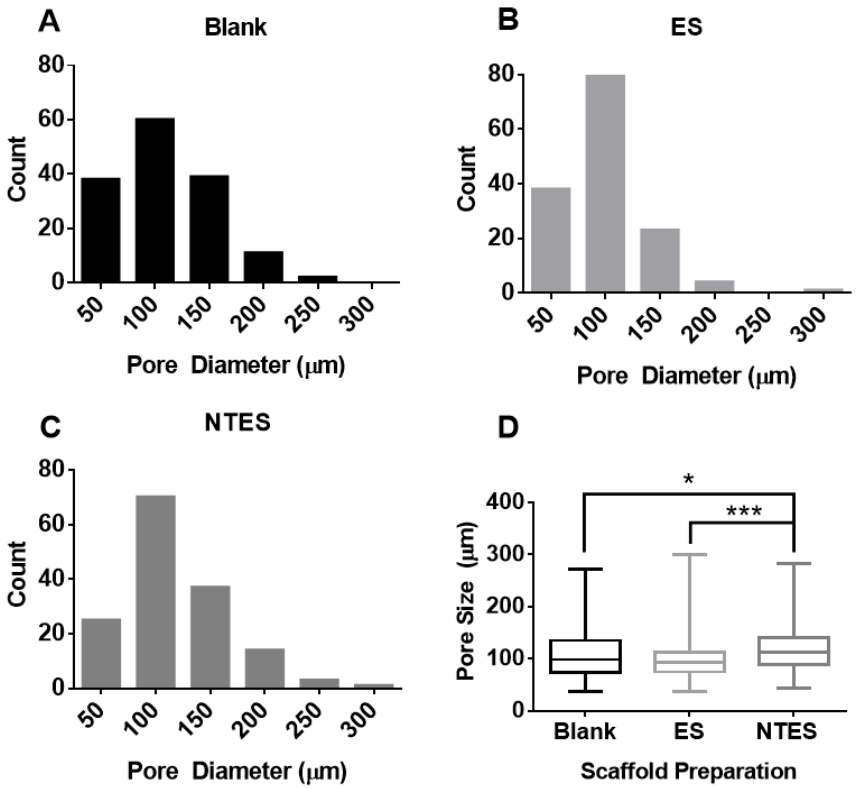

Figure 14. Distributions of the scaffold pore sizes. (A) Scaffolds without particles; (B) Scaffolds with ES particles; (C) Scaffolds with NTES particles; (D) Comparison of the pore size distributions. Pore sizes were measured as described in Materials and Methods (Section 3.3.2) for three individually prepared samples of each scaffold type. Data are presented as binned pore size distributions (A-C) and box-and-whisker plots (D) with median (horizontal line), interquartile range (top and bottom of boxes), and minimum/maximum range (tails) of three independent scaffolds for each type (50 measurements for each scaffold). Statistical analysis was performed using Kruskal-Wallis followed by Dunn's post-hoc tests with Benjamini-Hochberg correction for multiple comparisons. An asterisk (*) and a triple asterisk (***) indicate a significant difference with $p<0.05$ and $p<0.001$, respectively.

4.2.4 Porosity:

The porosity of the different scaffolds was measured to determine if the scaffolds depicted a suitable porosity for bone regeneration applications, as well as to observe any changes after inclusion of either ES or NTES particles (Figure 15). Results showed that the inclusion of ES or NTES particles significantly increased the scaffold porosity (81 ± 4% and 89 ± 5%, respectively), compared to the scaffolds without particles (59 ± 5%) (p<0.01 in both cases).

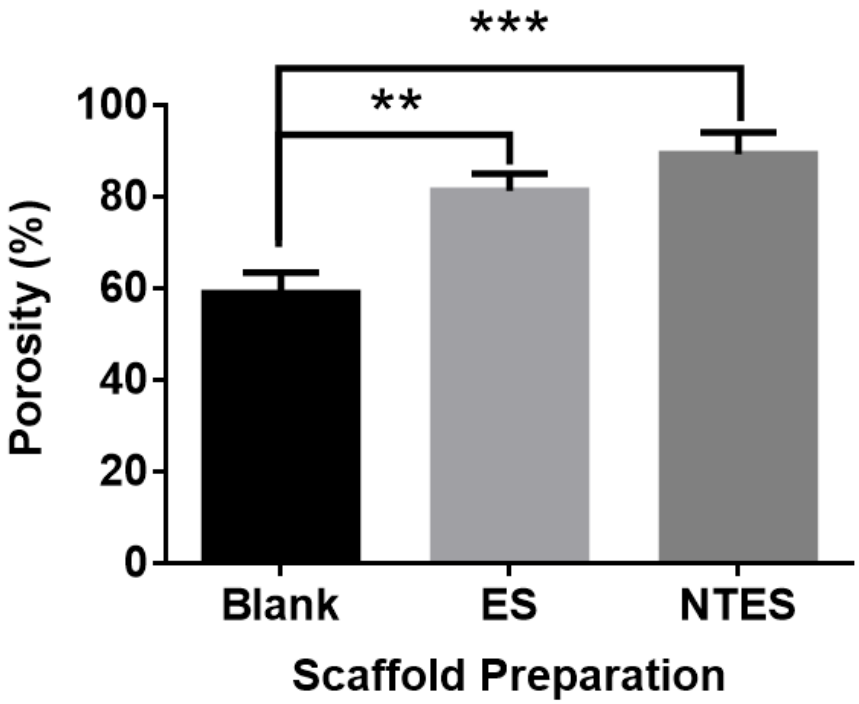

Figure 15. Porosity of scaffolds. Dry scaffolds were submerged in phosphate buffered saline (PBS) under cell culture conditions (37^{O}C, 5% CO_2, humidified atmosphere) for 30 min. Scaffold mass and volume were measured before and after the incubation to determine the porosity based on the correlated changes of those properties (see Section 3.3.1). Data are presented as means ± standard deviation of three independently prepared scaffolds of each type. Statistical analysis was performed using a one-way ANOVA followed by Tukey post-hoc tests. A double asterisk (**) and a triple asterisk (***) indicate a significant difference between a given scaffold type and the scaffolds without particles, with $p<0.01$ and $p<0.001$, respectively.

4.2.5 Mechanical Strength:

The overall mechanical strength of scaffolds was assessed by measuring their stiffness (Figure 16A) and CM (Figure 16B). The scaffolds with either ES or NTES particles had a slightly larger stiffness than the scaffolds without particles (0.026 ± 0.006 N/mm and 0.022 ± 0.003 N/mm for the scaffolds with ES and NTES particles, respectively, vs. 0.017 ± 0.001 N/mm for the scaffolds without particles), although the difference was marginally significant and only between the scaffolds with ES particles and the scaffolds without particles (p=0.048). Similarly, the scaffolds with either ES or NTES particles had a slightly larger CM than the scaffolds without particles (3.69 ± 0.70 kPa and 3.14 ± 0.62 kPa for the scaffolds with ES and NTES particles, respectively, vs. 2.03 ± 0.39 kPa for scaffolds without particles), but the difference was only significant between the scaffolds with ES particles and the scaffolds without particles (p=0.031).

The height of the scaffolds before and after testing was also measured as an evaluation of scaffold resiliency, with any permanent change in height from compression reflecting test-induced damage to the scaffold microstructure (Figure 16C). The height recovery of the scaffolds with either ES or NTES particles was significantly greater than that of the scaffolds without particles (97 ± 1% and 97 ± 1% for the scaffolds with ES and NTES particles, respectively, vs. 94 ± 1% for the scaffolds without particles) (p=0.015 and p=0.022, respectively).

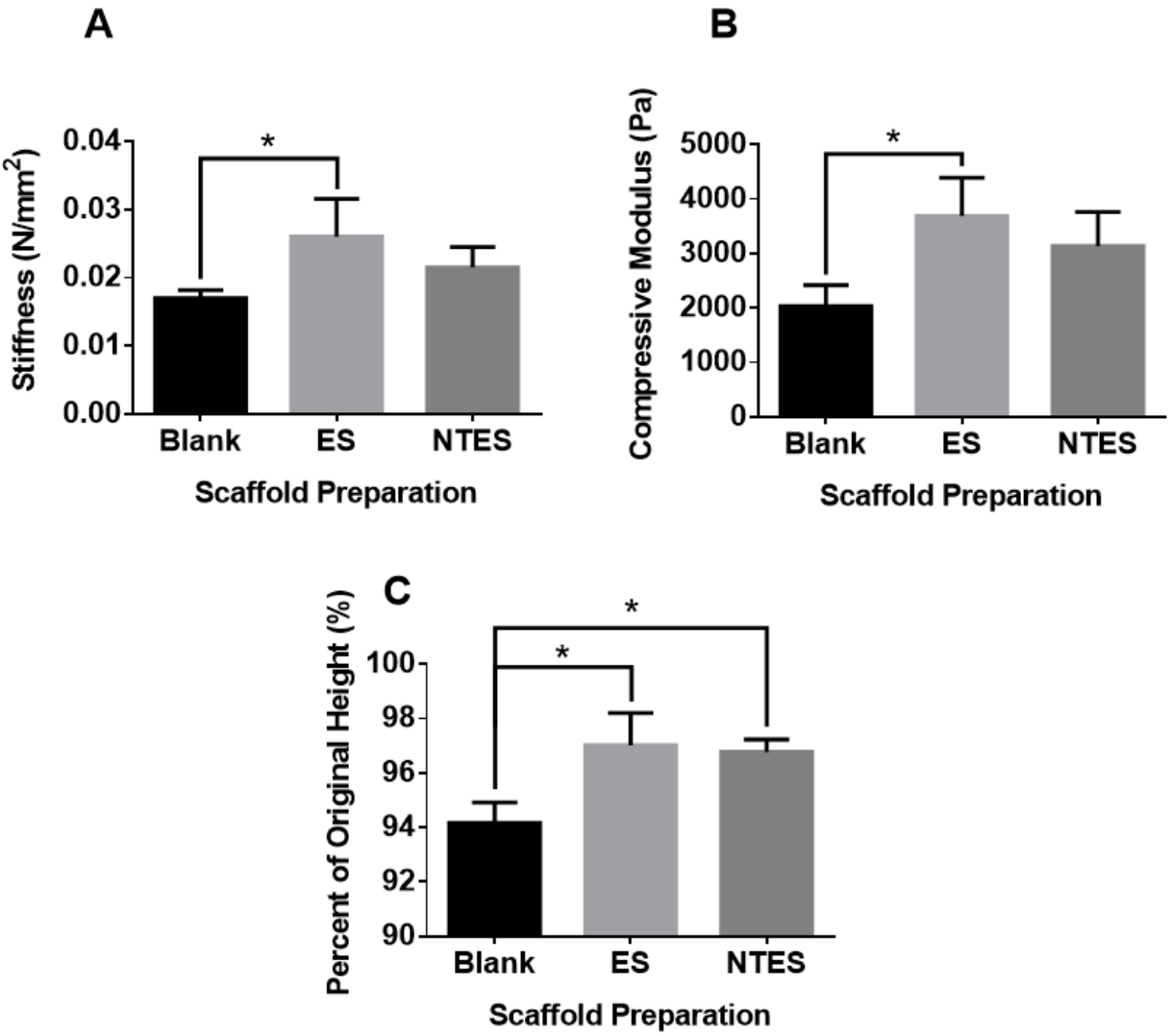

Figure 16. Mechanical properties of scaffolds: (A) Stiffness; (B) Compressive modulus (CM); and (C) Scaffold height after compressive tests. Data are presented as means ± standard deviation of three independent experiments, each performed in duplicates. Statistical analysis was performed using a one-way analysis of variance followed by Tukey post-hoc tests. An asterisk (*) indicates a significant difference with $p<0.05$.

4.2.6 Hydrolytic Degradation:

Scaffolds stored in a desiccator appeared to be stable for long periods of time (months). Scaffold resistance to hydrolytic degradation in aqueous solution was evaluated over 21 days to determine potential differences in the scaffold susceptibility to breakdown, as well as to evaluate their suitability for long-term cell culture (Figure 17A).

Changes in optical density were assumed to reflect a loss of scaffold microstructure due to hydrolysis. No significant change in optical density was observed during 21 days for the scaffolds with either ES or NTES particles. On the other hand, the optical density significantly decreased for the scaffolds without particles after 14 and 21 days (49 ± 31% and 41 ± 18%, respectively), compared to their values at day 0 (p<0.001 in both cases).

The volume of each scaffold at day 0 and day 21 was also measured as another marker of scaffold degradation. Results at day 21 showed that the scaffolds with ES or NTES particles retained a significantly higher percentage of their initial volume, compared to the scaffolds without particles (86 ± 4% and 76 ± 8% for the scaffolds with ES and NTES particles, respectively, vs. 26 ± 10% for the scaffolds without particles; p<0.001 in both cases).

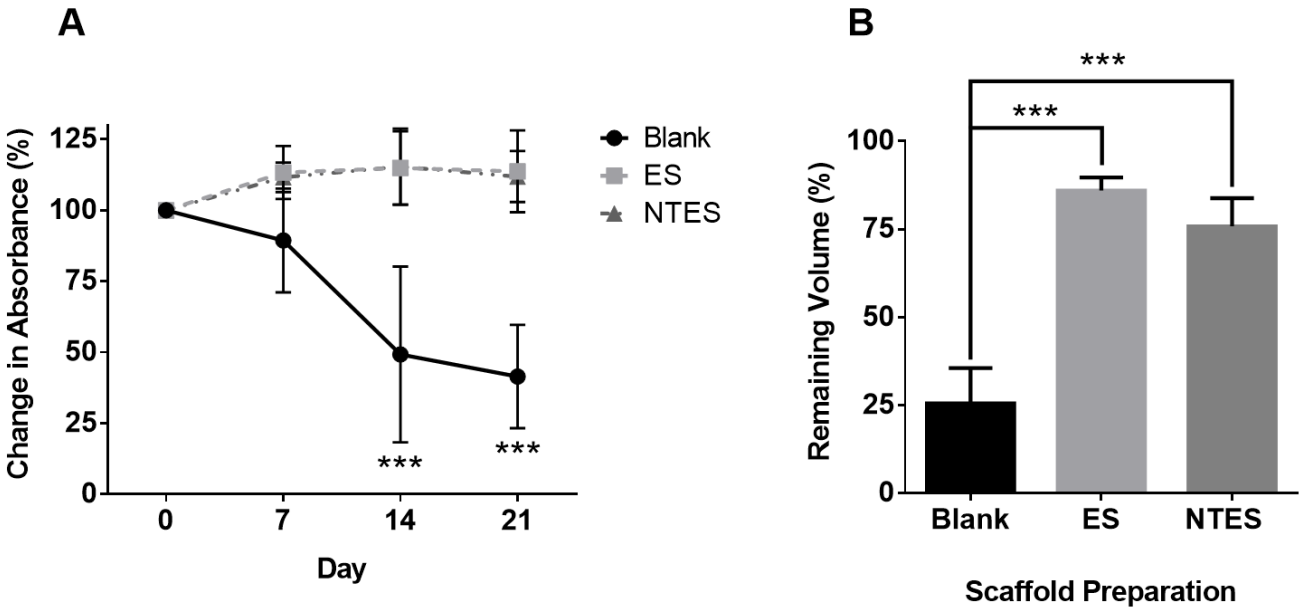

Figure 17. Degradation of scaffolds under cell culture conditions in phosphate buffered saline: (A) Change in the absorbance of the scaffolds (at 590 nm); (B) Change in the total scaffold volume over 21 days. Data are presented as means ± standard deviations of three independently prepared scaffolds of each type. Statistical analysis was performed using a two-way ANOVA followed by Tukey post-hoc tests (A) and a one-way ANOVA followed by Tukey post-hoc tests (B). A triple asterisk (***) indicates a significant difference with $p<0.001$.

4.2.7 Particle Distribution:

The distribution of ES or NTES particles within the scaffolds was evaluated by μCT imaging (Figure 18). As described in Materials and Methods (Section 3.3.5), an integrated density value reflecting the homogeneity of particle distribution was calculated. Scaffolds without particles were used as control. Results showed that the differential integrated density values were more scattered for the scaffolds with ES particles than for the scaffolds with NTES particles (63.5 A.U. [interquartile range: 31.3 – 95.6] vs. 54.5 A.U. [interquartile range: 45.37 – 63.5], respectively). However, the difference was not statistically significant. The lower values with the scaffolds with NTES particles suggest that these scaffolds had a consistently more homogeneous particle distribution than the scaffolds with ES particles. Note that a scaffold with perfectly homogeneous distribution of particles would display an integrated density value of zero.

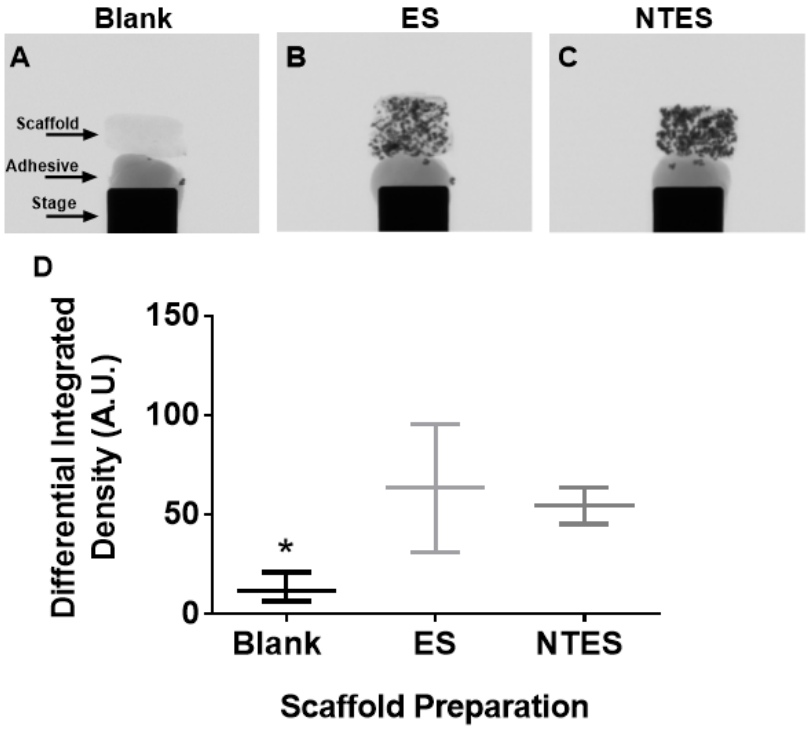

Figure 18. Micro-computed tomography (µCT) analysis of the particle distribution within the scaffolds. µCT analysis was performed on scaffolds without particles (A) and scaffolds with eggshell (ES) or nanotextured eggshell (NTES) particles (B and C, respectively) using the SkyScan 1174 µCT instrument. Integrated density values for the top and bottom halves of each scaffold image per rotation was acquired through a custom ImageJ macro. These upper and lower halves were subtracted from each other, pooled, and compared for each scaffold type (D). Data are presented as box and whisker plots with median (horizontal line), interquartile range (top and bottom of boxes), and minimum/maximum range (tails) of the median of 264 measurements acquired from three independent scaffolds for each experiment, for each scaffold type. Statistical analysis was performed using Kruskal-Wallis followed by Dunn's post-hoc with a Benjamini-Hochberg correction for multiple comparisons. An asterisk (*) indicated a significant difference with $p<0.05$.

Table 2. Physicochemical properties of the prepared scaffolds. Summary table for the physicochemical characterization of the three scaffold types, as well as the reported values for cancellous bone (from Cowin & Telega, 2003).

Properties	Scaffold Type			
	Blank	*ES*	*NTES*	*Cancellous Bone*
Porosity (%)	59 ± 5	81 ± 4	89 ± 5	70 - 80
Median Pore Size (μm)	99 [IQR: 74 – 135]	94 [IQR: 75 – 112]	113 [IQR: 88 – 140]	100 - 500
Stiffness (N/mm)	0.017 ± 0.001	0.026 ± 0.006	0.022 ± 0.003	Not Reported
Compressive Modulus (kPa)	2.03 ± 0.39	3.69 ± 0.70	3.14 ± 0.62	3,000
Remaining Scaffold Volume After 21 Days (%)	75 ± 10	14 ± 4	24 ± 8	N/A

4.3 Scaffold Cytocompatibility:

Potential scaffold cytotoxicity in cell culture was initially evaluated using murine RAW264.7 bone marrow macrophages in the scaffolds containing NTES particles (Appendix 1). A significant increase in cell number was observed by day 7 (207 ± 19% compared to day 0) (p=0.002). Initial assessment with these cells were performed to verify the sterility of scaffolds in cell culture after ethanol sterilization, as well as to optimize the cell seeding method. Adding multiple low volumes of highly concentrated cells was a superior approach to obtain deeper and better distributed cell seeding, rather than using larger volumes of a lower concentration of cell suspension. In addition, gentle handling of the loaded scaffolds during medium changes

was essential in order to prevent cell loss from the inside the scaffold. This optimal seeding method is described in Materials and Methods (Sections 3.4.2 – 3.4.3).

4.3.1 Retention of Mesenchymal Stem Cells in Scaffolds:

MSC retention in the scaffolds at day 0 after seeding was measured using the AlamarBlue® assay (Figure 19). Results showed that the inclusion of either ES or NTES particles into the scaffolds significantly increased the cell retention in the scaffolds (53 ± 23% and 57 ± 16% for scaffolds with ES and NTES particles, respectively, vs. 17 ± 10% for scaffolds without particles; $p<0.001$ in both cases).

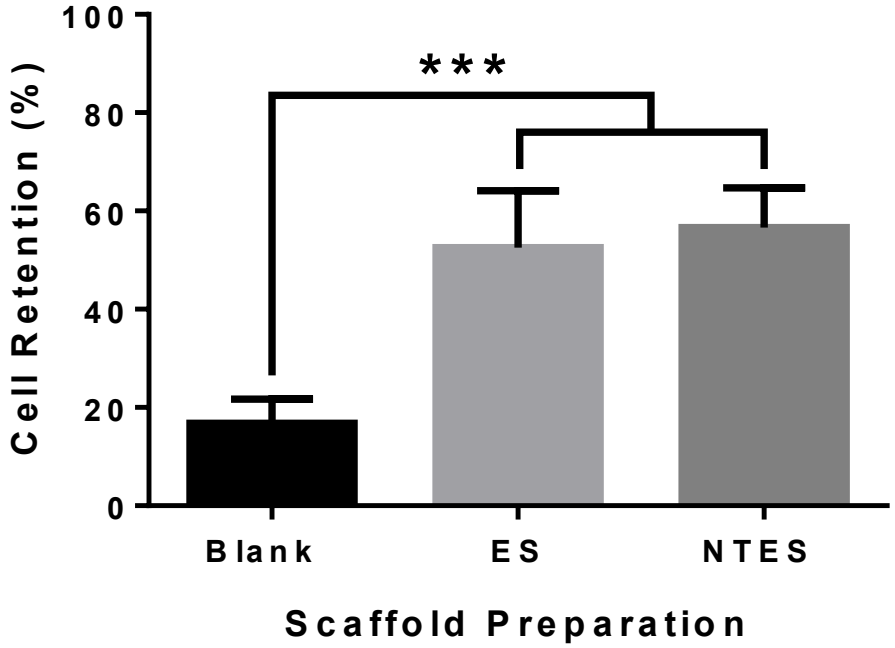

Figure 19. Mesenchymal stem cell retention in scaffolds. Scaffolds were incubated in medium containing 10% AlamarBlue®. Fluorescence measurements were made at excitation / emission wavelengths of 530nm / 590nm, and compared to a standard curve to determine cell number. Cell retention was calculated as a ratio between the experimentally determined number of cells and the number of cells originally seeded into the scaffold. Data are presented as means ± standard error of the means of 4 experiments (each performed with a different cell lot number). Statistical analysis was performed using a mixed linear model followed by Tukey post-hoc tests with a single-step adjustment. A triple asterisk (***) indicates a significant difference compared to both other scaffold types with $p<0.001$.

4.3.2 Cell Viability in Scaffolds:

MSC viability was evaluated every 7 days over the 21-day culture period (Figure 20). For all time points following day 0, the scaffolds with ES or NTES particles had a significantly higher percentage of viable cells than the scaffolds without particles ($p<0.05$ in all cases). While a decrease in cell viability was observed overtime in the scaffolds with either ES or NTES particles, the decrease was not statistically significant with the exception of day 14 and day 21 for the scaffolds with NTES particles ($p=0.005$ and $p=0.022$, respectively, relative to day 0). On the other hand, cell viability in the scaffolds without particles significantly decreased at each time point.

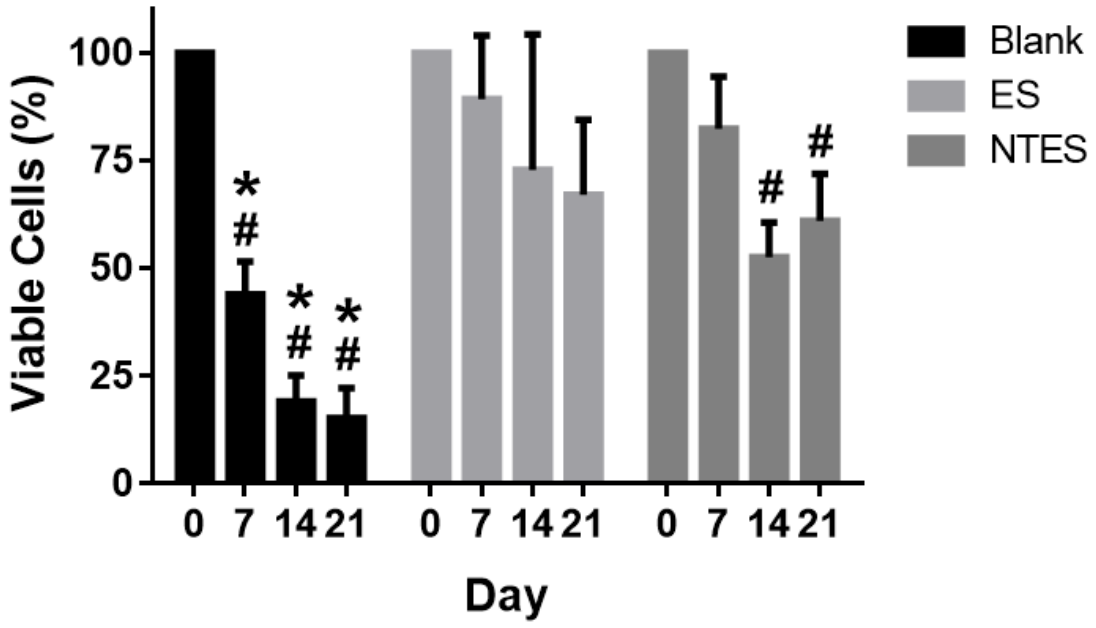

Figure 20. Mesenchymal stem cell viability in scaffolds. Scaffolds seeded with mesenchymal stem cells (MSCs) were incubated for 21 days in cell culture conditions (37°C, 5% CO_2, 95% humidity). At each time point, cell viability was evaluated using AlamarBlue® (Section 3.5.2). Fluorescence intensity (excitation/emission of 530 nm/590 nm) was compared to a standard curve to determine the number of live cells in the scaffold. For each scaffold, the percentage of viability at each time point was calculated based on the day 0 value. Data are presented as means ± standard error of the means of 4 experiments (each performed with a different cell lot number and in triplicates). Statistical analysis was performed using a mixed linear model followed by Tukey post-hoc tests with a single-step adjustment. An asterisk (*) indicates a significant difference (p<0.05) compared to all other scaffold types. A number sign (#) indicates a significant difference (p<0.05) compared to the same scaffold at day 0.

4.4 Osteogenic Differentiation of Mesenchymal Stem Cells in Scaffolds:

4.4.1 Alkaline Phosphatase (ALP) Activity:

Levels of Intracellular ALP activity in all types of scaffolds were measured over 21 days to evaluate early osteogenic differentiation (Figure 21). Results showed a time-dependent increase in ALP activity in the scaffolds with either ES or NTES particles, up to 558% at day 21 in the scaffolds with ES particles, and up to 540% at day 14 in the scaffolds with NTES particles (p=0.006 and p=0.002, respectively, relative to day 0). ALP activity in the scaffolds without particles did not significantly increase at any time point.

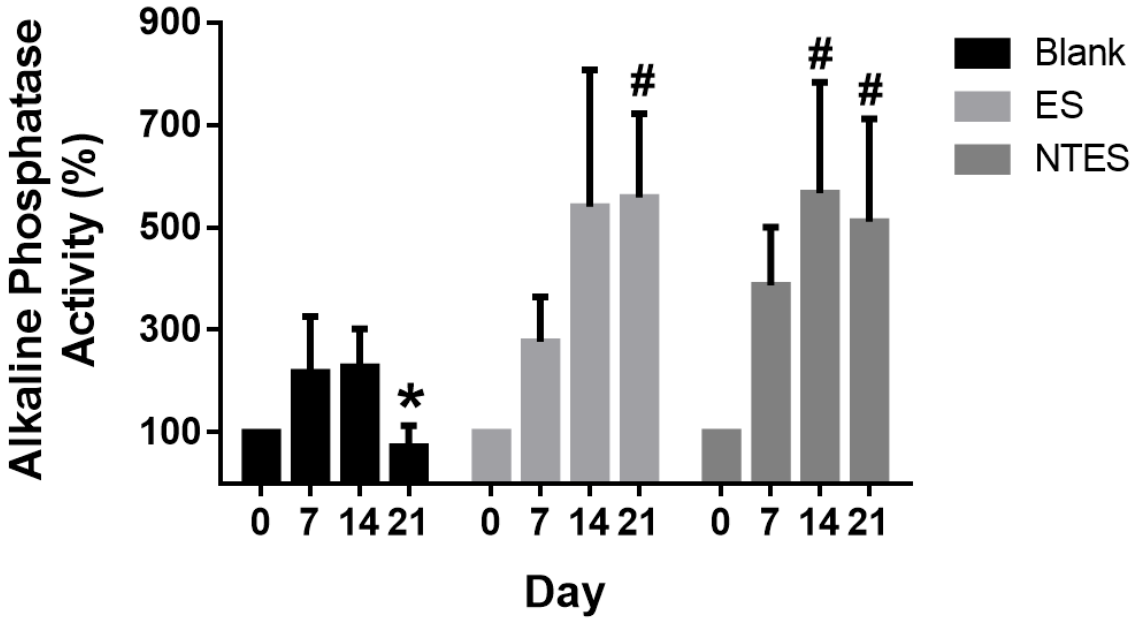

Figure 21. Alkaline phosphatase (ALP) activity in mesenchymal stem cells in scaffolds. An aliquot of mesenchymal stem cell protein lysate at each time point was incubated in a 96-well plate with 5 mM $MgCl_2$, 100 mM diethanolamine, and 2mM pNPP. Absorbance (at 405 nm) was compared to a previously determined alkaline phosphatase (ALP) activity standard curve. Results were expressed as percentages, relative to day 0. Data are presented as means ± standard error of the means of 4 experiments (each performed with a different cell lot number). Statistical analysis was performed using a mixed linear model followed by Tukey post-hoc tests with a single-step adjustment. An asterisk (*) indicates a significant difference (p<0.05) compared to all other scaffold types. A number sign (#) indicates a significant difference (p<0.05) compared to the same scaffold at day 0.

4.4.2 Synthesis of Osteogenic Proteins by Mesenchymal Stem Cells:

The levels of two osteogenic proteins, RUNX2 and OPN, in the scaffolds with either ES or NTES particles were semi-quantified over 21 days (Figure 22), to evaluate a later stage of MSC osteogenic differentiation. This analysis was not performed with scaffolds without particles, due to the extremely low number of cells in these scaffolds at each time point (as seen in Figure 20). Although not statistically significant, an increase in both RUNX2 and OPN levels was observed over time in the scaffolds with ES particles. A similar increase in both protein levels was observed in the scaffolds with NTES scaffolds and was significant at day 21 for RUNX2 (p=0.022, relative to day 0).

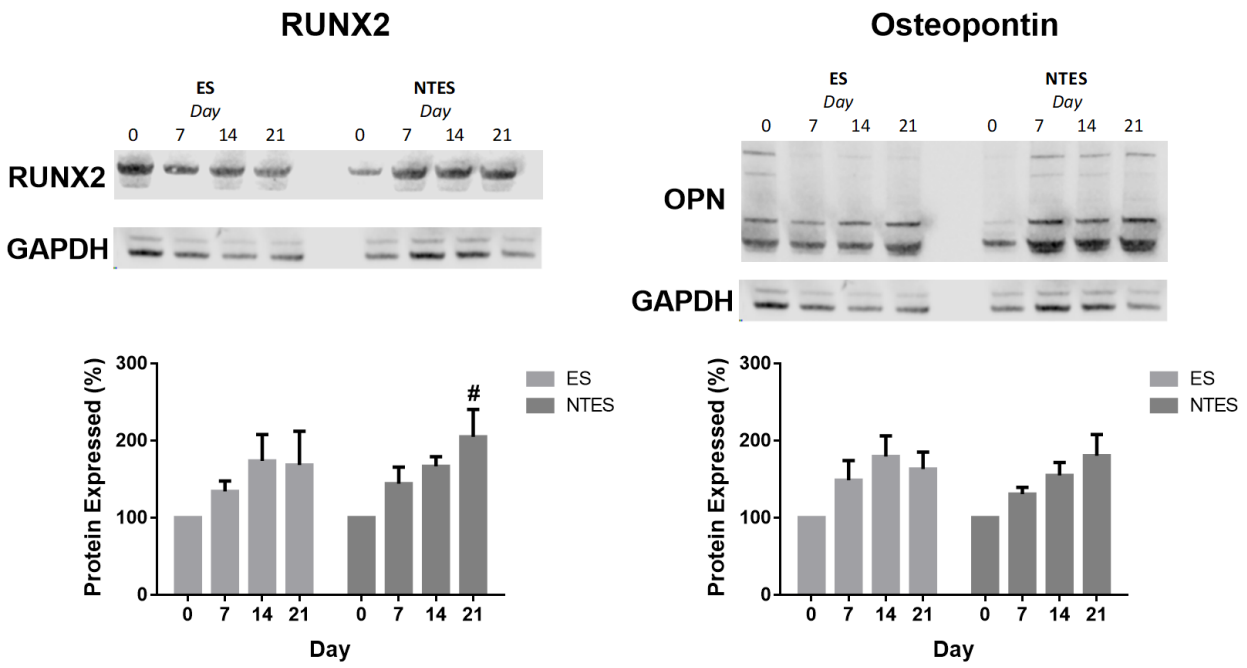

Figure 22. Western blot analysis of osteogenic markers of mesenchymal stem cells (MSCs) in scaffolds. An aliquot of MSC protein lysate at each time point was concentrated by trichloroacetic acid (TCA) precipitation, separated via sodium dodecyl sulfate – polyacrylamide gel electrophoresis (SDS-PAGE), and transferred to a polyvinylidene fluoride (PVDF) membrane. Western blotting was sequentially performed for RUNX2, osteopontin (OPN), and glyceraldehyde phosphate dehydrogenase (GAPDH). The levels of RUNX2 and OPN were normalized to GAPDH, and then expressed as a percentage of their level at day 0. Data are presented as means ± standard error of the means of 4 experiments (each performed with a different cell lot number and in triplicates). Statistical analysis was performed using a mixed linear model followed by Tukey post-hoc tests with a single-step adjustment. A number sign (#) indicates a significant difference (p<0.05) compared to the same scaffold at day 0.

4.4.3 Morphological Changes in Mesenchymal Stem Cells in Scaffolds:

Changes in MSC cytoskeleton and viability during the 21-day incubation period were evaluated using live-cell confocal microscopy (Figure 23). Confocal images of all scaffolds were taken on day 0 and day 21. Scaffolds with either ES or NTES particles depicted a high number of cells, at both day 0 (Figure 23B and C) and day 21 (Figure 23E and F). In addition, cells displayed an elongated and stretched morphology by day 21 (Figure 24). On the other hand, MSCs in the blank scaffolds (scaffolds without particles) were much rounder than those in the scaffolds with either ES or NTES particles. There was also very little change in either the cell morphology or number between days 0 and 21 (Figure 23A and D), and the overall cell number was low.

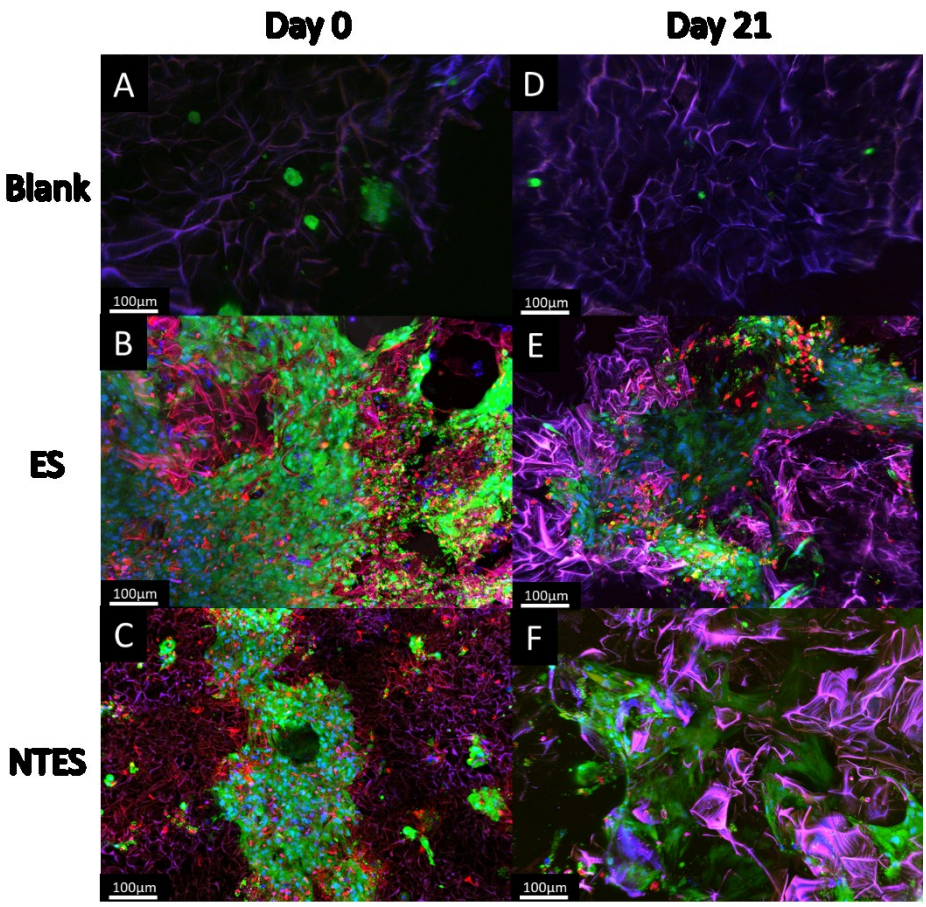

Figure 23. Mesenchymal stem cell morphology in scaffolds. Representative images of MSCs at day 0 and day 21 in the blank scaffolds (scaffolds without particles) (A, D), in the scaffolds with ES particles (B, E), and in the scaffolds with NTES particles (C, F). The scaffolds were incubated for 20 min at 37°C/5% CO_2 in Dulbecco's phosphate buffered saline (PBS) containing 2 µM calcein-AM, 4 µM ethidium homodimer-1, and 160 µM of Hoechst 33342. At the end of the incubation, the scaffolds were washed with 37°C PBS and mounted on glass slides with a 1 mm spaced coverslip. Images were acquired using a confocal microscope (LSM 880) and processed using Imaris image analysis software. In viable MSCs, the cytoplasm is green and the nucleus is blue, while non-viable MSCs are red. The pink/purple background is due to autofluorescence of the scaffold constituents.

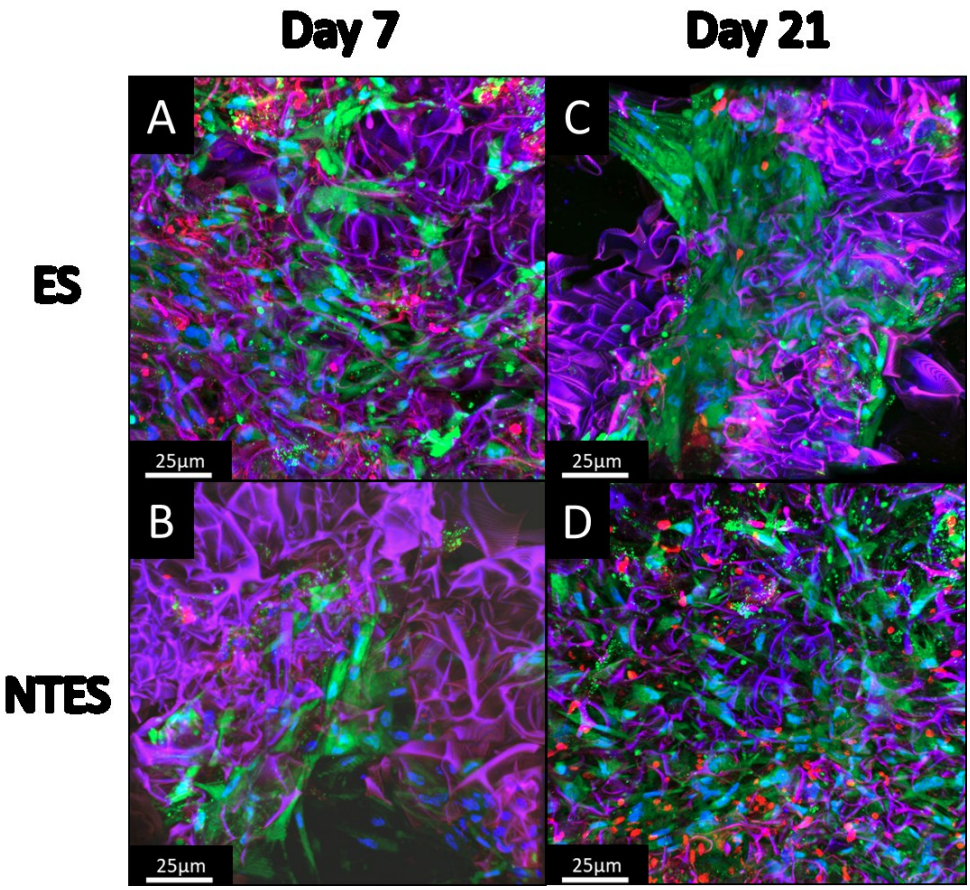

Figure 24. Mesenchymal stem cell morphology in scaffolds (higher magnification). Representative images of MSCs at day 0 and day 21 in the blank scaffolds (A, D), the scaffolds with ES particles (B, E), and the scaffolds with NTES scaffolds (C, F). The scaffolds were incubated for 20 min at 37°C/5% CO_2 in Dulbecco's phosphate buffered saline (PBS) containing 2 µM calcein-AM, 4 µM ethidium homodimer-1, and 160 µM of Hoechst 33342. Following the incubation, the scaffolds were washed with 37°C PBS and mounted on glass slides with a 1 mm spaced coverslip. Images were acquired using a confocal microscope (LSM 880) and processed using Imaris image analysis software. In viable MSCs, the cytoplasm is green and the nucleus is blue, while non-viable MSCs are red. The pink/purple background is due to autofluorescence of the scaffold constituents.

5.0 Discussion:

5.1 Preparation of Scaffolds and Particle-induced Changes in Scaffold Physicochemical Properties:

This research was performed in two steps. The first part was to create and characterize the ES and NTES particles. This was performed to establish the standard morphology and elemental composition of the particles, and to identify changes in these characteristics due to the nanotexturing treatment. The second part was to design, prepare, and characterize the scaffolds, with and without particles, in order to assess their suitability for bone regeneration. A variety of changes in particle properties were observed after acid treatment. Moreover, the inclusion of particles in the scaffolds led to significant improvements in the scaffold characteristics. The evaluation of these features and changes was critical in order to predict the suitability of the hydrogel scaffolds with particles to promote osteogenic differentiation.

5.1.1 Changes in Eggshell Particle Properties Due to Nanotexturing:

ES particles were sieved to filter those in the 229 μm – 381 μm size range, followed by treatment with PA to induce surface nanotexture. This acid treatment of the ES particles to produce NTES particles led to a rough and disorganized surface texture at the submicron scale (nanotexturing effect). SEM, EDS and FTIR analyses revealed cuboidal crystals on the surface of NTES particles that were interpreted as calcium phosphate deposits. These deposits likely resulted from a chemical reaction between ES (~94% $CaCO_3$) and PA, leading to the formation of insoluble $Ca_3(PO_4)_2$ via the reaction $3CaCO_3 + 2H_3PO_4 \rightarrow Ca_3(PO4)_2 + 3CO_2 + 3H_2O$. In agreement with this interpretation, FTIR analysis of NTES particles detected phosphate bond

peaks at 500 cm^{-1}, 1000 cm^{-1}, and 1600 cm^{-1}. In addition, ES contains occluded matrix proteins and their exposure on the particle surface after etching was suggested by FTIR peaks between 2800 cm^{-1} and 3500 cm^{-1}, which correspond to the peptide bond that was only observed after acid treatment. Overall, the nanotexturing treatment with PA created a surface nanotexture, with the exposure of calcium phosphate deposits and occluded matrix proteins.

With regards to their potential use as a bone regeneration biomaterial, both ES and NTES particles are predicted to exhibit osteogenic properties. Calcium carbonate affects the adhesion properties of MSCs and may induce osteogenesis (Li et al., 2018; Neunzehn et al., 2015). The NTES particles would have three additional distinct osteogenic features. Surface nanotexture facilitates MSC adherence (Boyan et al., 2016) and induces osteogenic differentiation via stimulation of cytoskeletal disorganization (Dalby et al., 2007; Roberts et al., 2016). In addition, calcium phosphate deposits are well known to stimulate osteogenic induction (Li et al., 2017; Müller et al., 2008). Finally, the proteins exposed on the NTES particle surface likely include collagens and OPN expression (among > 500 other ES matrix proteins (Chien et al., 2008)), which have been shown to induce osteogenesis in MSCs (Chen et al., 2014; Singh et al., 2018).

5.1.2 Optimization of Scaffold Preparation Method:

Optimal physicochemical properties of the hydrogel scaffolds for bone regeneration were considered when selecting the polymers and the preparation methods. Biomimeticism is important in biomaterials, so the ideal scaffold would be mechanically as strong as cancellous bone with a high compressibility, while still possessing a high porosity and appropriate pore

sizes in the range of 100 to 500 µm. Some of the most popular polymers for bone regeneration scaffolds include collagen, hyaluronic acid, and PLGA (Shi et al., 2016). A number of preparation methods were tested, as described in the next paragraph. A variety of different polymers (PLGA, chitosan, and alginate) were initially evaluated for scaffold creation. Chitosan has excellent biocompatibility with success in bone regeneration applications, as well as a tailorable pore size and porosity (Parisi et al., 2018). Alginate also possesses these properties, while producing a mechanically stronger final material (Zmora et al., 2002). Therefore, the combination of both chitosan and alginate was considered to have the potential to generate a composite hydrogel with enhanced physicochemical properties.

Scaffolds were initially prepared using 2% chitosan (no alginate) and the three different preparation methods (freeze-drying, gelation, and porogen leeching). However, each preparation method led to the scaffold collapse during the drying phase. While keeping the scaffolds in a frozen state prevented collapse, the freeze-gelation method continued to produce scaffolds that would often collapse during drying, and therefore, this method was abandoned. When evaluating scaffolds made of 2% chitosan and ES particles, the porogen leeching method often produced scaffolds that were mechanically very weak and degraded rapidly in PBS. Overall, the freeze-drying method led to the most promising results (Table 2). Due to their opposite charges in solution, chitosan (+) and alginate (-) are expected to crosslink when present in combination; however, the increased viscosity made it harder to homogeneously distribute the particles, with corroborate a previous study from Lawrie et al. (2007). The optimal method appeared to necessitate distributing homogeneously the particles (ES or NTES) in the AS first, adding the chitosan and mixing again, and finally adding the glutaraldehyde.

Ultimately, the 2% chitosan – 2% alginate co-polymer was chosen to prepare the scaffolds (either without particles [blank], or with ES or NTES particles) for all subsequent experiments conducted during this Master's project.

5.1.3. Effects of Particle Inclusion on Chitosan-Alginate Co-Polymer Scaffold Microstructure and Physicochemical Properties:

SEM analysis of the scaffolds showed that the inclusion of particles (either ES or NTES) led to a much more unorganized structure, with an increase in porosity. In addition, the stiffness, CM and scaffold stability increased in the presence of the particles.

The improvements in the scaffold microstructure (for the purpose of bone regeneration) due to inclusion of particles may be partly explained by the method of scaffold preparation: directional freezing, ice crystal growth and lyophilization. In the absence of particles, the directional growth of ice crystals is uninterrupted, creating a very organized porous structure. On the other hand, when particles are present in the co-polymer suspension, the ice crystals are unable to penetrate the solid particles, and must terminate or grow around the particles, which creates a disordered porous structure (Pawelec et al., 2015). The growth of ice crystals around particles may also cause merging of adjacent ice crystals to create larger crystals, which generates larger pores (O'Brien et al., 2004). Therefore, disruptions in the direction of ice crystal growth by ES or NTES particles lead to an increase in the scaffold porosity and a modified pore size distribution. The increase in stiffness and CM of the scaffolds with ES or NTES particles (Table 2) could be due to the solid particles acting as a reinforcement of the polymeric matrix (Torres-Sanchez et al., 2017). The physicochemical properties of the scaffolds

with ES and NTES particles were quite similar (Table 2) except for a significant increase in the median pore size of the NTES particle scaffolds.

The increases in particle homogeneity and pore size in the scaffolds with NTES particles, in comparison to the scaffolds with ES particles (Table 2), is likely explained by chemical interactions that occur between the particles and the co-polymers when the sol-gel is created. Indeed, an ancillary experiment showed that the ES particles consistently sank to the bottom of the AS before mixing, such that when chitosan and glutaraldehyde were added to induce gelation, the particles were more heterogeneously distributed (data not shown). On the other hand, the addition of NTES particles consistently caused the alginate to become more viscous, allowing a more homogeneous distribution of the particles before the addition of the chitosan and glutaraldehyde (data not shown). This increased viscosity, which keeps the particles in suspension during the freezing step, may have come from an increase in H-bonding between the exposed matrix proteins and the polymers (Lin et al., 2005) and/or an increase in calcium phosphate-induced gelation due to ionic bonding (Alves Cardoso et al., 2014).

Finally, the greater resistance to hydrolytic degradation in PBS solution of the scaffolds with either ES or NTES particles, in comparison to the scaffolds without particles (Figure 17), was likely due to the scaffolds with particles having increased bonding capabilities with either ES or NTES particles, whereas these bonds would not be available in the scaffolds without particles. With fewer or weaker chemical bonds holding together the scaffold without particles, the material would be more susceptible to hydrolysis (Ren et al., 2005).

5.1.4 Implications of Scaffold and Particle Features on Bone Regeneration Capabilities:

The goal of the material design process was to obtain scaffolds with a pore size and porosity similar to those of cancellous bone. These two properties are critical for MSC growth, nutrient diffusion, and waste removal. Cancellous bone has an average porosity of 70% – 80% and a median pore size of 100µm - 500µm, depending on the bone (Cowin & Telega, 2003). The scaffolds with ES or NTES particles depicted a porosity of 81 ± 4% and 89 ± 5%, respectively, and a median pore size of 94 µm [interquartile range: 75 µm –112 µm] and 113 µm [interquartile range: 88 µm – 140 µm], respectively. These values suggest that both scaffolds types (with ES or NTES particles) are suitable as a bone regeneration material, in contrast to the scaffolds without particles, which had a similar pore size but a porosity of only 59 ± 5%.

Mechanical testing showed that the scaffolds with particles had slightly larger CM than the scaffolds without particles (3.69 ± 0.70 kPa and 3.14 ± 0.62 kPa for the scaffolds with ES and NTES particles, respectively, vs. 2.03 ± 0.39 kPa for scaffolds without particles), but the difference was only significant between the scaffolds with ES particles and the scaffolds without particles, and the CM remained much lower than that of cancellous bone (approximately 3000 kPa [Chen & McKittrick, 2011; Currey et al., 2007]). The scaffolds containing ES or NTES particles, however, did show resistance to microstructure damage after compressing the scaffolds to a zero-nominal thickness while under a light load. Therefore, while the material may not be appropriate for load-bearing applications, it may be suitable for non-load bearing applications (e.g., fractures in hand or wrist). In addition, it has been reported that chitosan and alginate scaffolds with low mechanical strength can be appropriate for bone regeneration despite their low mechanical strength, particularly when a mineral component (nano-HA or

nano-bioactive glass) is dispersed throughout the scaffold (Thein-Han & Misra, 2009; Srinivasan et al., 2012). In fact, materials with a CM as low as 1.5 kPa have been observed to support osteogenic differentiation (Winkler et al., 2018).

Overall, the scaffolds containing particles possessed more favorable physicochemical properties than the scaffolds without particles. In addition, the inclusion of ES or NTES particles into the scaffolds could provide a site for MSC-mediated remodeling of the ES calcium carbonate into calcium phosphate, which has been seen with ES in some studies (Baliga et al., 1998; Uraz et al., 2013), while the surrounding scaffolding should improve cell viability and cell interaction with ES particles. Results also showed that the scaffolds with NTES particles possessed more osteogenic-promoting factors than the ES counter-part, as well as a greater median pore size. They also have calcium phosphate and exposed matrix proteins on the particle surface (collagens, OPN), both of which are strong differentiating signals for MSCs (Li et al., 2017; Lukasova et al., 2017). One of the objectives of this Master's thesis was to evaluate MSC differentiation in both types of scaffolds in order to detect possible differences in the osteogenic potential of scaffolds with ES or NTES particles.

5.2 Mesenchymal Stem Cell Growth and Viability in Scaffolds:

With the scaffolds and particle characteristics well defined, the next step was to examine cellular growth and viability in the scaffolds, since MSCs must adhere to scaffolds and remain viable during the lengthy process of osteogenic differentiation. Initial cytotoxicity tests were performed with RAW264.7 macrophages (see Appendix 1). The RAW264.7 macrophages

demonstrated a proliferative response in the scaffolds with particles after 7 days in culture. Cytotoxicity evaluations with the blank scaffolds were not performed, since chitosan and alginate polymer scaffolds are well-known to be non-cytotoxic (Rodrigues et al., 2012; Sun & Tan, 2013). Following these promising results, osteogenic differentiation in the scaffolds was evaluated over 21 days using commercially available MSC lots from four different human donors. Cells from these four different lots were evaluated to account for differences in age, sex, race, and other genetic factors (Phinney et al., 1999; Stolzing et al., 2008).

5.2.1 Optimization of Cell Culture Conditions in Scaffolds:

The cell microenvironment in the cancellous region of bone is similar to normal physiological conditions (37^{o}C, pH 7.4, with low CO_2 / high O_2). However, two mechanical forces act on the cells in this tissue: the shear force from blood flowing through the vasculature (Etheridge et al., 2016), and the compressive force from weight bearing exerted upon the bone (Michalopoulos et al., 2012). Ideally, a biomaterial should be evaluated *in vitro* under conditions that mimic the site of implantation. *In vitro*, shear and dynamic compressive forces can be mimicked in a perfusion bioreactor (e.g., the CartiGen C9-X from Tissue Growth Technologies), where cells can experience similar mechanical forces to those that induce *in vivo* osteogenic differentiation of MSCs (Tran et al., 2011). Unfortunately, after spending a significant amount of time to master the programming and fine-tuning of appropriate aseptic techniques using the CartiGen C9X bioreactor, a number of insurmountable technical issues were encountered. In particular, particles of a few hundred microns in size constantly re-appeared after complete cleaning of the bioreactor, even in the absence of cells and scaffolds. In spite of rebuilding certain plastic parts of the bioreactor using 316-stainless steel, the particles, presumably

derived from breakdown/degradation of some internal component(s), were repeatedly observed. Due to time and financial constraints, the use of this perfusion bioreactor was abandoned for the purpose of this project.

Instead, a static culture method was used, in which the media was supplemented with low-dose of differentiation constituents, in order to promote a low osteogenic differentiation and minimize the effects of the medium on osteogenesis. Cell culture inserts were also used in 24-well plates, to partly overcome nutrient diffusion limitations in thick (>1 mm) materials (Gaspar et al., 2012).

5.2.2 Cellular Retention:

Scaffolds with ES or NTES particles both demonstrated a higher retention of the seeded MSCs compared to the scaffolds without particles; consistent results were obtained with the four lots of MSCs. This higher cell retention suggests cell adhesion inside the scaffolds, and is likely due to two factors inherent to the particle scaffolds. The first is the increase of roughness of the pore wall surfaces due to the presence of either ES or NTES particles. This increase in roughness is due to changes in ice crystal growth patterns in the presence of particles and it has been well documented that MSCs adhere better to rough surfaces than to smooth ones (Tillotson et al., 2016). The second is the higher percentage of porosity in the scaffolds with particles, which may have allowed greater MSC penetration into the scaffolds during seeding.

One hypothesis was that nanotexturing of the NTES particles would increase cell adhesion; however, this was not observed. It is possible that the number of particles within the scaffold was not high enough to have a large number of cells in direct contact with a particle

during seeding (the polymer portion of the scaffold presents more surface area than the particles).

5.2.3 Cellular Proliferation:

The number of cells present in the scaffolds was measured every 7 days, over a 21-day period. The scaffolds without particles demonstrated a consistent, significant decrease in viable cell numbers. On the other hand, the scaffolds with ES or NTES particles exhibited a non-significant decrease in cell number over the 21-day period, with the exception of a minor, but statistically significant, decrease at day 14 for the scaffold with NTES particles. This improvement in the scaffold ability to maintain large numbers of viable cells was likely due to the greater porosity of the scaffolds with particles in comparison to the scaffolds without particles, since porosity is critical for the diffusion of nutrients and waste metabolites. It is not entirely clear if the loss of cells in the scaffolds without particles was due to cell death (caused by a lack of nutrient diffusion or inefficient waste removal) or due to poor adhesion of the cells because of unsatisfactory conditions within those scaffolds. However, high levels of cellular debris were observed with the blank scaffolds during the medium changes, which was not observed with the scaffolds with either type of particles. There were no significant differences in the number of viable cells between scaffolds with ES or NTES particles at each time point. This demonstrates that nanotexture did not have any effect on cell viability, and confirms that pore size and porosity are the main factors affecting cellular viability (Murphy & O'Brien, 2010).

5.2.4 Importance of Cellular Adhesion and Proliferation for Bone Regeneration:

The observed increases in MSC retention and viability led to the hypothesis that scaffolds with either type of particles would be a superior bone regeneration material than the scaffolds without particles, for two reasons. Cellular adhesion is critical for an implantable biomaterial, since the recruitment of cells *in vivo* and their retention in the scaffold are key factors (Khalili & Ahmad, 2015). Additionally, the first step in MSC differentiation into osteoblasts is adhesion; indeed, MSCs are unable to differentiate unless their pseudopodia are attached to a surface (Wang & Chen, 2013). With respect to the viable cell number over time, a greater number of osteoblast-differentiated MSCs in these scaffolds would lead to greater secretion of new bone mineral. Therefore, it is critical for a biomaterial to sustain the viability of the cells by facilitating proper nutrient diffusion and by promoting cell adherence.

5.3 Mesenchymal Stem Cell Differentiation in Scaffolds:

Osteogenic differentiation of MSCs seeded into the different scaffolds was evaluated by monitoring three distinct properties: increased ALP activity, increases in the levels of osteogenic proteins RUNX2 and OPN, and changes in MSC morphology.

5.3.1 Alkaline Phosphatase Activity of Mesenchymal Stem Cells:

ALP is one of the earliest markers of osteogenic differentiation, and has very low activity in undifferentiated MSCs (Prins et al., 2014). Extractable ALP activity of MSCs seeded into the different scaffold types was evaluated every 7 days for 21 days. In most studies, ALP activities

are normalized to the total protein levels. However, in the present study, cells were lysed directly in the scaffolds, which led to the extraction of proteins from the FBS in the culture, thereby affecting the protein concentration of the sample. To overcome this issue, ALP activity was normalized to the number of cells in the scaffolds, determined by AlamarBlue®.

ALP activity in the scaffolds without particles did not increase over 21 days, suggesting that osteogenic differentiation did not occur. On the other hand, the time-dependent increase in ALP activity was observed in the scaffolds with ES or NTES particles, suggesting that osteogenic differentiation was occurring. The poor adhesion observed in the scaffolds without particles, as well as the cell death or detachment would account for the lack of increase in ALP activity in these scaffolds. Adhesion is a necessary step for differentiation to occur, and cells that are stressed due to lack of nutrients will not differentiate. However, the scaffolds with ES or NTES particles were able to sufficiently support the viability of MSCs, and a continual increase in ALP activity was observed. Once again, no significant differences were observed between the two scaffolds with particles, but ALP activity increased earlier in the scaffolds with NTES particles (day 14) than in the scaffolds with ES particles (day 21).

5.3.2 Levels of Osteogenic Proteins in Mesenchymal Stem Cells:

Levels of the osteogenic proteins RUNX2 and OPN were measured in the cell lysates from scaffolds with ES and NTES particles. Western blot analyses were not performed on cell lysates from scaffolds without particles due to the extremely low number of cells and the high levels of FBS in the lysate. Dilute protein lysates were concentrated through TCA precipitation. Initially, the use of a total protein stain was considered to quantify the protein amount for

Western blotting; however, the FBS present in the lysate skewed the protein determinations. Therefore, a constant volume of lysate was loaded and samples were normalized to GAPDH immunoreactivity. GAPDH is a housekeeping enzyme whose levels do not change during osteogenic differentiation (Quiroz et al., 2010).

RUNX2 synthesis is an early marker for osteogenic differentiation, while OPN levels increase during middle to late stage differentiation (Wagner et al., 2010; Zhang et al., 2011). Results showed that RUNX2 levels tend to increase with time in the scaffolds with either ES or NTES particles. This same trend was observed for OPN. However, the increase was not statistically significant with the exception of RUNX2 at day 21 in the scaffolds with NTES particles. Nevertheless, together with the increases in ALP activity observed in the scaffolds with either particles, these results suggest that osteogenic differentiation was occurring. The synthesis of OPN also suggests that the cells had progressed to become nearly mature osteoblasts (Wagner et al., 2010). Again, no significant differences in the levels of either proteins were observed between the scaffolds with the two types of particles, despite the significant increase of RUNX2 at day 21 compared to day 0 in the scaffolds with NTES particles.

5.3.3 Changes in Mesenchymal Stem Cell Morphology:

Confocal microscopy was used to qualitatively assess the degree of MSC differentiation. Indeed, MSCs differentiating into osteoblasts become more cuboidal (Rodríguez et al., 2004; Yourek et al., 2007). Results showed that MSCs in the scaffolds without particles remained very spherical from day 0 to day 21, indicating that the cells did not differentiate or interact strongly with the scaffold. This shape may also indicate that the MSC pseudopodia were not extended

for adhesion to the scaffold surfaces. Indeed, surface-adhered but undifferentiated MSCs have a fibroblast-like (thin and elongated) morphology (Yourek et al., 2007). While there was no change in the number of dead cells observed, it is likely that the washing steps used prior to imaging would have removed dead and non-adherent cells. The extremely low cell density observed in the images of scaffolds without particles correlated with the low number of viable cells observed in Figure 20.

Cells in the scaffolds with ES or NTES particles at day 0 had a regular fibroblast-like morphology that is a characteristic of adhered, undifferentiated MSCs. Cell density, similar to the results of cell retention and viability (Figures 19 and 20, respectively), was also very high compared to the scaffolds without particles, and very few dead cells were observed. After 21 days in culture, the MSCs in the scaffolds of either type of particles exhibited a cuboidal shape, which confirms that the cells were undergoing differentiation. Interestingly, cells further away from the particles appeared to have a more elongated morphology, which suggests that they were not differentiated. It may also indicate cell-to-cell communication between differentiated MSCs (Etheridge et al., 2016). Indeed, it is possible that when MSCs adhere to either ES or NTES particles, start differentiating, and then transduce a differentiating signal to nearby MSCs that are further away from particles, leading to the stretching appearance of remote cells.

5.3.4 Overall Differentiation Analysis:

Multiple parameters were used to determine if osteogenic differentiation was occurring in the MSCs seeded in each type of scaffolds. However, since differentiation is such a complex process, the results must be taken as a whole rather than examined individually. The scaffolds

without particles clearly demonstrated that very few cells were retained, and that osteogenic differentiation did not occur. Although the protein levels of RUNX2 and OPN in blank scaffolds were not evaluated, the lack of changes in ALP activity in conjunction with the observed cell morphology were consistent.

The scaffolds with either ES or NTES particles, however, exhibited increasing levels of ALP activity, morphological changes, and a small, although not statistically significant, increase in the levels of RUNX2 and OPN. The ALP activity in both scaffold types exhibited a plateau at day 14, which is when ALP peaks have been shown to be correlated to MSCs approaching late stage of differentiation (when mineralization begins to occur) (Beck et al., 2000; Hanna et al., 2018). It is also at this time point that cells started to become more cuboidal. Therefore, the scaffolds with either type of particles were found to facilitate osteogenic differentiation of MSCs.

Overall, the results of this thesis showed that the scaffolds with either type of particles facilitated osteogenic differentiation. However, no difference was observed between the scaffolds with ES or NTES particles. This may be due to the fact that the concentration of particles within the scaffolds may not have been high enough to be able to detect differences between the effects of ES and NTES particles. Indeed, while it is possible that MSCs adherent to NTES particles were more differentiated than MSCs on ES particles, the particle effects on cell differentiation may have been minimized because of the low concentration of particles in the scaffolds, leading to non-significant differences between the scaffolds with the two types of particles. The particle concentration was however optimized to maximize their number without sacrificing scaffold porosity and pore size.

An important aspect of this research was that experiments were performed with cells from four different human donors (individual results are detailed in Appendix 3). Results showed some variability in the appearance of osteogenic markers, due in part to donor-to-donor differences, as discussed earlier. However, a consistent trend was observed in all measurements with MSCs from each individual donor, as well as in the pooled data (Figures 19-22).

6.0 Conclusions and Future Directions:

ES and novel NTES particles were generated from chicken ES, and then incorporated into chitosan-alginate co-polymer scaffolds. The characterization of ES and NTES particles showed that PA-nanotexturing treatment induced both a surface nanotexture and deposits of calcium phosphate on the NTES particle surface. The presence of either ES or NTES particles improved the scaffold physicochemical properties in all aspects related to the intended bone regeneration applications. The inclusion of either ES or NTES particles also improved MSC retention, and thereby likely adhesion, to the scaffolds, and increased the percentage of MSC viability in the scaffolds over a 21-day cell culture. Finally, the inclusion of either ES or NTES particles induced osteogenic differentiation of MSCs, assessed by ALP activity, levels of osteogenic proteins RUNX2 and OPN, and changes in MSC morphology over time. Scaffolds without particles did not show any of the characteristic features of osteogenic differentiation. Finally, no significant differences in any of the physicochemical, material properties or cellular comparisons were observed between the scaffolds with either ES or NTES particles.

A logical future direction for this research project would be to evaluate these novel scaffolds in an animal model. The scaffolds with either ES or NTES particles were successful in facilitating osteogenesis in culture, but the cell culture system is a much simpler system than a living organism. The benefit of the animal model would be to confirm that bone regeneration is actually facilitated by the scaffolds containing ES or NTES particles, in a living system with multiple cell types and different growth factors. It is also possible that the animal model tests would reveal differences between scaffolds containing ES or NTES particles. The first line of investigation could be the assessment of cytotoxicity, inflammation, neovascularization, and

potential ectopic mineralization following subcutaneous implantation of the scaffolds. A bone defect animal model (e.g., rat calvarial defect) would then be required to evaluate bone regeneration. Other experiments may include analyzing the effects of a larger number of particles in the scaffolds. This may however require the use of a different polymeric scaffold, since the particle concentration was optimized with the hydrogel composite used in the present work to maintain a proper pore size and porosity. Finally, experiments using a perfused system (bioreactor) under dynamic compression and with regular culture medium (as opposed to low-dose osteogenic culture medium) would allow better perfusion of the scaffolds and may reveal particle-specific effects by eliminating the confounding factors due to the use of an osteogenic culture medium.

7.0 Appendices:

7.1 Appendix 1:

Cytotoxic effects of the scaffolds were initially evaluated using RAW264.7 bone marrow macrophages. These cells were also used to optimize the cell seeding and culturing protocols prior to using the MSCs. The macrophages were cultured up to the third passage in 75 cm^2 flasks (Corning) with Dulbecco's modified eagle medium (DMEM; Gibco) supplemented with 10% FBS, and grown to approximately 85% confluency. Confluent cells were detached from the flask using 0.25% trypsin-EDTA (Life Technologies). The trypsin-EDTA was inactivated with the addition of fresh DMEM /10% FBS.

At the third passage. macrophages were resuspended in fresh DMEM/10% FBS at 8334 cells/µl, so that a total of 250,000 cells would be seeded in each scaffold after pipetting 2.5 µl of cell suspension 6 times on each scaffold. Specifically, 2.5 µl of macrophage suspension were first pipetted onto the scaffolds in two random spots, followed by a 30-min incubation. All incubations occurred under cell culture conditions. After repeating this seeding step three times, the scaffolds were incubated for 1 h, flipped 180^o, and the entire procedure was repeated on this other side. Finally, the scaffolds were incubated for 1.5h after the addition of a few drops of DMEM/10% FBS, were placed in a 48-well plate (Corning), covered gently with DMEM/10% FBS, and incubated overnight under cell culture conditions. Following the overnight incubation, scaffolds were transferred to a new 48-well plate (Corning) and approximately 1 ml of DMEM/10% FBS was added to each well containing the scaffolds. The macrophage-loaded scaffolds were cultured for a period of 7 days, with media changes every other day.

The retention of macrophages in the different scaffolds was evaluated using the AlamarBlue® assay. Scaffolds at day 0 were washed thoroughly with DMEM/10% FBS (37°C) to dislodge any poorly adherent or dead cells. Scaffolds were then incubated for 3h under cell culture conditions in DMEM/10% FBS supplemented with 10% AlamarBlue® reagent (ThermoFisher Scientific). At the end of the incubation, a 100 µl aliquot was added to a 96-well plate (Corning) and fluorescence was determined at an excitation/emission wavelength of 530 nm/590 nm (BioTek Eon, BioTek). The number of cells in the scaffolds was then determined using a standard curve generated with known numbers of macrophages.

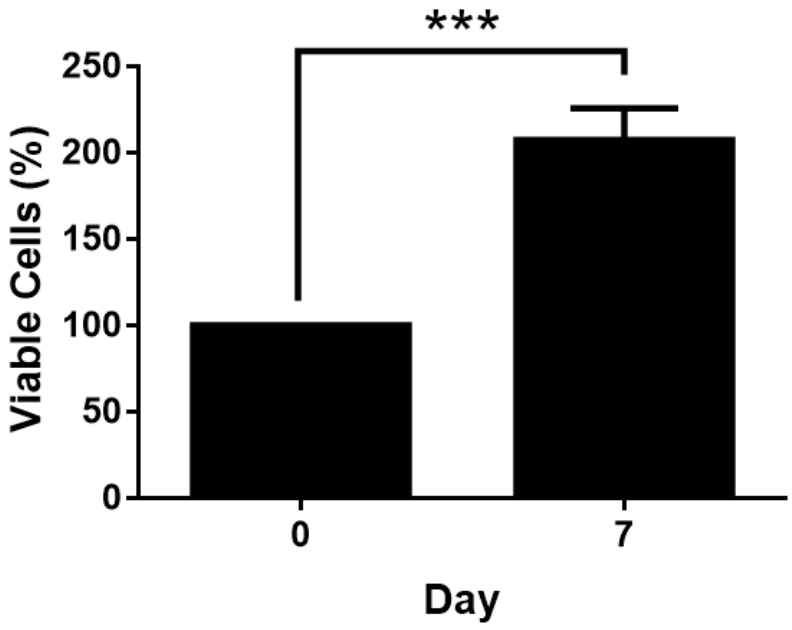

Figure A1. Proliferation of RAW 264.7 bone marrow macrophages in nanotextured eggshell scaffolds. Scaffolds seeded with RAW 264.7 bone marrow macrophages were grown for 7 days in cell culture conditions (37°C, 5% CO_2, 95% humidity). The scaffold was incubated with Dulbecco's Modified Eagle Medium supplemented with 10% fetal bovine serum with 10% AlamarBlue® for 3 h under cell culture conditions. Fluorescence intensity (excitation/emission of 530 nm/590 nm) was compared to a standard curve to determine the number of live cells in the scaffolds. Data are presented as means ± standard deviation of 3 scaffolds. Statistical analysis was performed using a Student's t-test. An asterisk (*) indicates a significant difference of (p<0.05).

7.2 Appendix 2:

Lot #1

ATCC® Number:	PCS-500-012™
Lot Number:	64430737
Name:	Bone Marrow-Derived Mesenchymal Stem Cells; Normal, Human
Species:	Human (*Homo sapiens*)
Manufacture Date:	10AUG2016
Fill Volume:	1 mL
Passage Number:	1
Donor Tissue Source:	Fresh bone marrow
Donor Gender:	Female
Donor Age:	34 years
Donor Race:	Caucasian

Lot #2

ATCC® Number:	PCS-500-012™
Lot Number:	70011721
Name:	Bone Marrow-Derived Mesenchymal Stem Cells; Normal, Human
Species:	Human (*Homo sapiens*)
Manufacture Date:	08JAN2018
Fill Volume:	1.1 mL
Passage Number:	2
Donor Tissue Source:	Bone Marrow
Donor Gender:	Male
Donor Age:	21 years
Donor Race:	Asian/Vietnamese

Lot #3

ATCC® Number:	PCS-500-012™
Lot Number:	70011720
Name:	Bone Marrow-Derived Mesenchymal Stem Cells; Normal, Human
Species:	Human (*Homo sapiens*)
Manufacture Date:	02JAN2018
Fill Volume:	1.1 mL
Passage Number:	2
Donor Tissue Source:	Bone Marrow
Donor Gender:	Male
Donor Age:	24 years
Donor Race:	White

Lot #4

On Fri, Jul 27, 2018 at 4:23 PM, Rosemary Hill (Technical) <Rosemary.Hill@cedarlanelabs.com> wrote:

> Hi again Nick,
>
> I asked a few of our suppliers about lot availability for their bone marrow mesenchymal stem cells, I am still waiting to hear back from some of them, but I did find one option for you so far, from Cell Engineering Technologies:
>
> Cedarlane cat# HMSC.BM-500 Human Bone Marrow Derived Mesenchymal Stem Cells (Size: 500,000 cells) $694 (only one lot available, from a 25-year-old Caucasian male donor)

Figure A2. Mesenchymal stem cell donor information experimental lots. Information regarding donor race, gender, and age for each of the 4 different mesenchymal stem cell lots used for the experiments.

7.3 Appendix 3:

The following graphs are the results of the cell retention, viability, and analysis of osteogenic markers for each MSC donor that was used throughout this research (results from pooled lots are presented in the results section of this thesis).

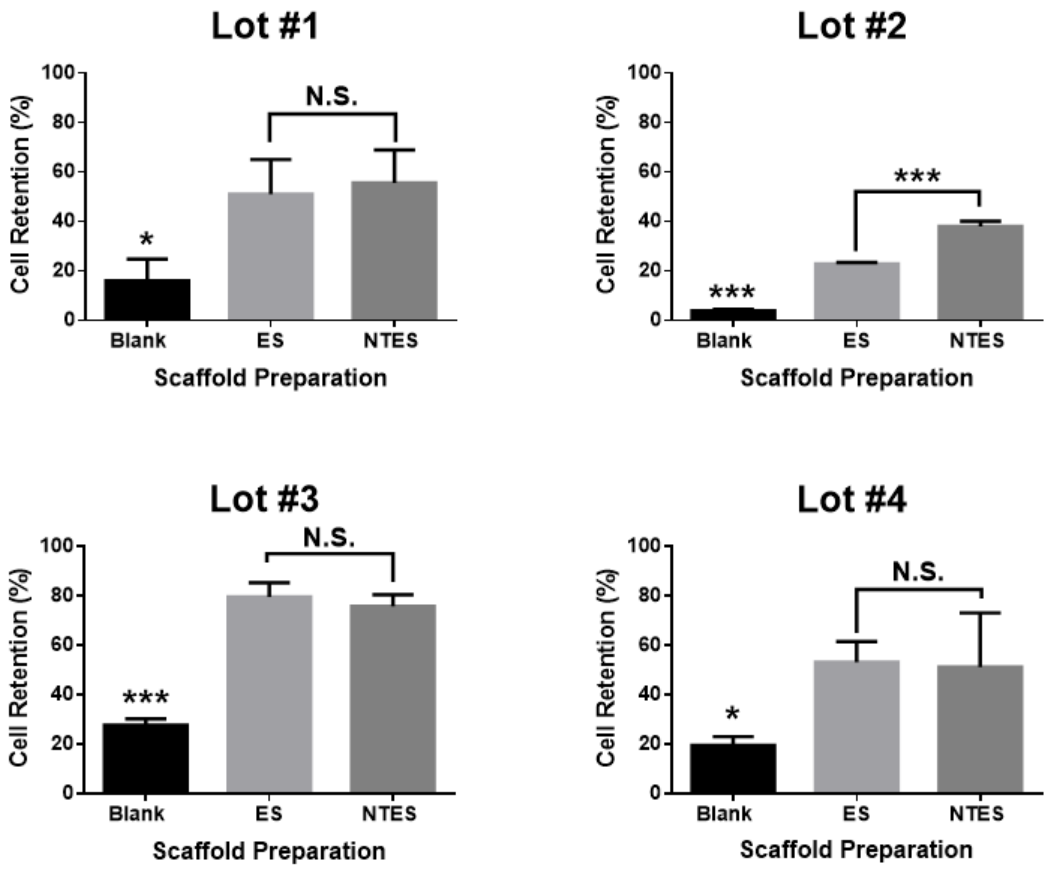

Figure A3. Individual donor results of mesenchymal stem cell retention in scaffolds. Scaffolds were incubated in medium containing 10% AlamarBlue®. Fluorescence measurements were made at excitation / emission wavelengths of 530 nm / 590 nm, and compared to a standard curve to determine cell number. Cell retention was calculated as a ratio between the experimentally determined number of cells and the number of cells originally seeded into the scaffold. Data are presented as means ± standard deviation of 3 scaffolds. Statistical analysis was performed using a one-way analysis of variance (ANOVA) followed by Tukey post-hoc tests. An asterisk (*) and a triple asterisk (***) indicate a significant difference compared to the other scaffold types with $p<0.05$ and $p<0.001$, respectively.

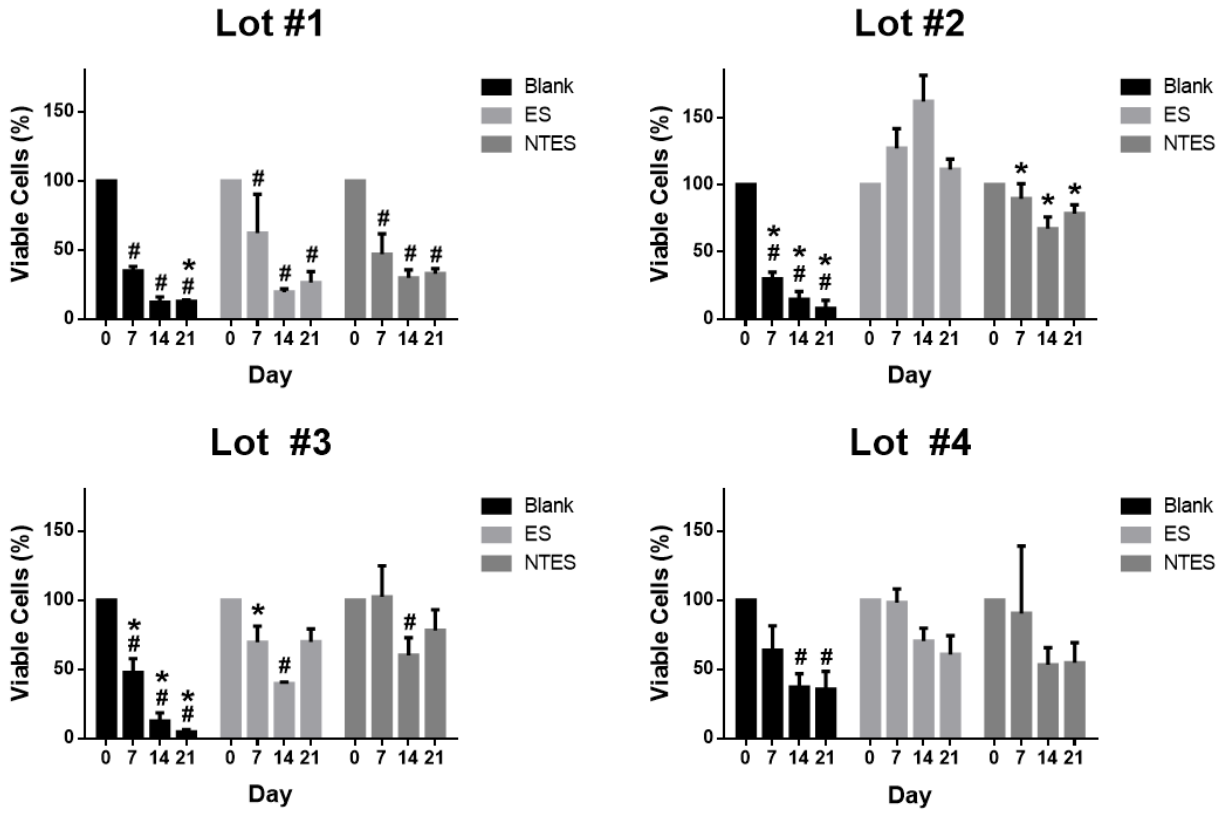

Figure A4. Individual donor results of mesenchymal stem cell viability over time in scaffolds.

Scaffolds seeded with mesenchymal stem cells (MSCs) were grown for 21 days in cell culture conditions (37°C, 5% CO_2, 95% humidity). At each time point, cell viability was evaluated using AlamarBlue®. Fluorescence intensity (excitation/emission of 530 nm/590 nm) was compared to a standard curve to determine the number of live cells in the scaffold. For each scaffold, the percentage of viability at each time point was calculated based on the day 0 value. Data are presented as means ± standard deviation of 3 scaffolds. Statistical analysis was performed using a one-way analysis of variance (ANOVA) followed by Tukey post-hoc tests. An asterisk (*) indicates a significant difference compared to the other scaffold types with $p<0.05$.

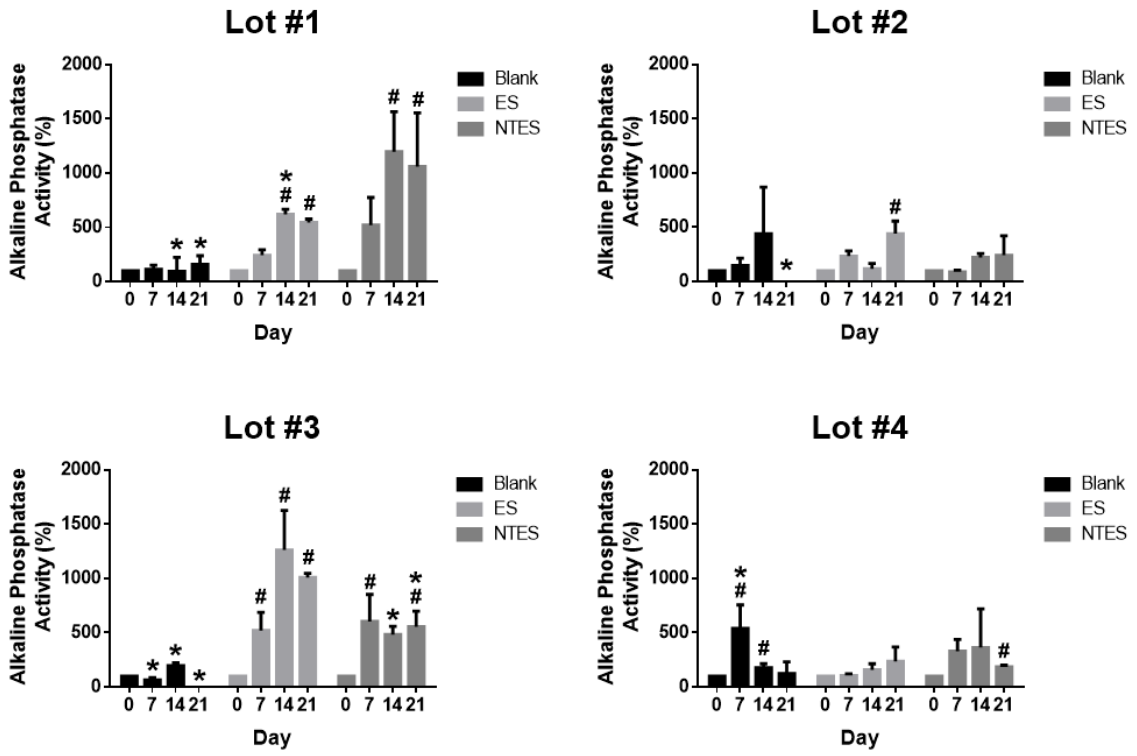

Figure A5. Individual donor results of alkaline phosphatase activity of mesenchymal stem in scaffolds. An aliquot of mesenchymal stem cell protein lysate at each time point was incubated in a 96-well plate with 5 mM $MgCl_2$, 100 mM diethanolamine, and 2 mM pNPP. Absorbance (405 nm) was compared to a previously determined alkaline phosphatase (ALP) activity standard curve. Results were expressed as percentages, relative to day 0. Data are presented as means ± standard deviation of 3 scaffolds. Statistical analysis was performed using a one-way analysis of variance (ANOVA) followed by Tukey post-hoc tests. An asterisk (*) indicates a significant difference compared to the other scaffold types with $p<0.05$.

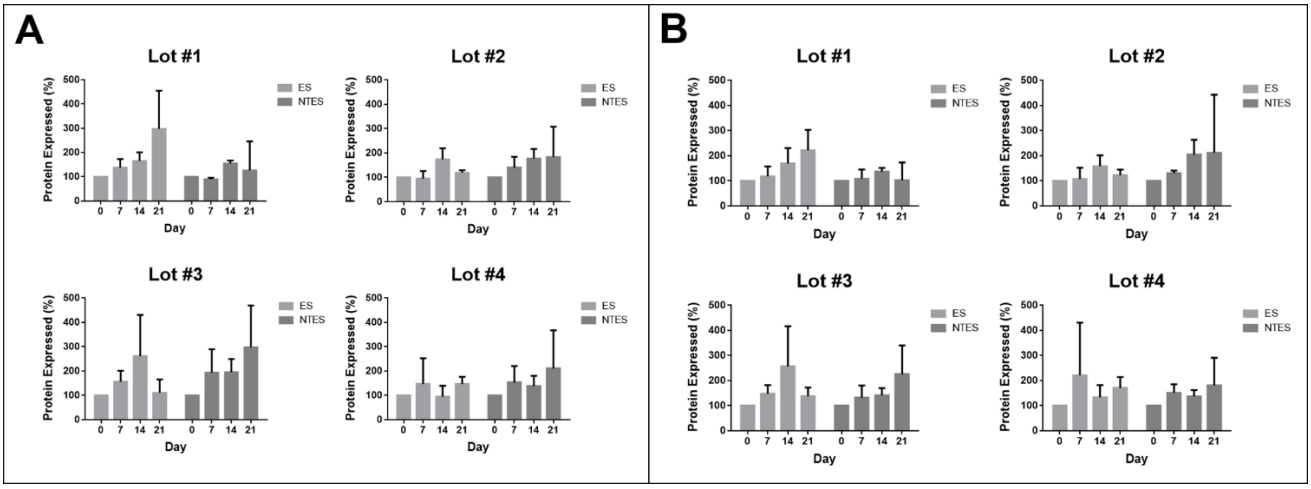

Figure A6. Individual donor results of Western blot analysis of osteogenic markers of mesenchymal stem cells (MSCs) in scaffolds. An aliquot of MSC protein lysate at each time point was concentrated by TCA precipitation, separated via SDS-PAGE, and transferred to PVDF membrane. Western blotting was sequentially performed for RUNX2, osteopontin (OPN), and GAPDH. Levels of RUNX2 and OPN were normalized to GAPDH, and then expressed as a percentage of the level at day 0. Data are presented as means ± standard deviation of 3 scaffolds. Statistical analysis was performed using a one-way analysis of variance (ANOVA) followed by Tukey post-hoc tests. An asterisk (*) indicates a significant difference compared to the other scaffold types with $p<0.05$.

8.0 References:

Akbarzadeh Baghban, A., Dehghani, A., Ghanavati, F., Zayeri, F., & Ghanavati, F. (2009). Comparing alveolar bone regeneration using Bio-Oss and autogenous bone grafts in humans: a systematic review and meta-analysis. *Iranian Endodontic Journal*, *4*(4), 125–130.

Alves Cardoso, D., Van Den Beucken, J. J. J. P., Both, L. L. H., Bender, J., Jansen, J. A., & Leeuwenburgh, S. C. G. (2014). Gelation and biocompatibility of injectable alginate-calcium phosphate gels for bone regeneration. *Journal of Biomedical Materials Research - Part A*, *102*(3), 808–817. https://doi.org/10.1002/jbm.a.34754

Amini, A. R., Laurencin, C. T., & Nukavarapu, S. P. (2012). Bone tissue engineering: recent advances and challenges. *Critical Reviews in Biomedical Engineering*, *40*(5), 363–408. https://doi.org/10.1615/CritRevBiomedEng.v40.i5.10

Anseth, K. S., Bowman, C. N., & Brannon-Peppas, L. (1996). Mechanical properties of hydrogels and their experimental determination. *Biomaterials*, *17*(17), 1647–1657. https://doi.org/10.1016/0142-9612(96)87644-7

Aro, H. T., & Aho, A. J. (1993). Clinical use of bone allografts. *Annals of Medicine*. https://doi.org/10.3109/07853899309147303

Asghar, W., Kim, Y. T., Ilyas, A., Sankaran, J., Wan, Y., & Iqbal, S. M. (2012). Synthesis of nano-textured biocompatible scaffolds from chicken eggshells. *Nanotechnology*, *23*(47). https://doi.org/10.1088/0957-4484/23/47/475601

Baino, F., Hamzehlou, S., & Kargozar, S. (2018). Bioactive glasses: Where are we and where are we going? *Journal of Functional Biomaterials*, *9*(1). https://doi.org/10.3390/jfb9010025

Baliga, M., Davies, P., & Dupoirieux, L. (1998). [Powdered eggshell in the repair of cystic cavities of the jaw. Preliminary study]. *Revue de Stomatologie et de Chirurgie Maxillo-Faciale*, *99 Suppl 1*, 86–88. Retrieved from http://www.ncbi.nlm.nih.gov/pubmed/9697237

Bartnikowski, M., Bartnikowski, N. J., Woodruff, M. A., Schrobback, K., & Klein, T. J. (2015). Protective effects of reactive functional groups on chondrocytes in photocrosslinkable hydrogel systems. *Acta Biomaterialia*. https://doi.org/10.1016/j.actbio.2015.08.038

Bas, O., De-Juan-Pardo, E. M., Meinert, C., D'Angella, D., Baldwin, J. G., Bray, L. J., … Hutmacher, D. W. (2017). Biofabricated soft network composites for cartilage tissue engineering. *Biofabrication*, *9*(2). https://doi.org/10.1088/1758-5090/aa6b15

Beck, G. R., Zerler, B., & Moran, E. (2000). Phosphate is a specific signal for induction of osteopontin gene expression. *Proceedings of the National Academy of Sciences*, *97*(15), 8352–8357. https://doi.org/10.1073/pnas.140021997

Bi, X., & Liang, A. (2016). In Situ-Forming Cross-linking Hydrogel Systems: Chemistry and Biomedical Applications. In *Emerging Concepts in Analysis and Applications of Hydrogels* (Vol. 86, pp. 541–547). InTech. https://doi.org/10.5772/63954

Boyan, B. D., Cheng, A., Olivares-Navarrete, R., & Schwartz, Z. (2016). Implant Surface Design Regulates Mesenchymal Stem Cell Differentiation and Maturation. *Advances in Dental Research*, *28*(1), 10–17. https://doi.org/10.1177/0022034515624444

Boyan, B.D., Cheng, A., Olivares-Navarrete, R., & Schwartz, Z. (2016). Implant Surface Design Regulates Mesenchymal Stem Cell Differentiation and Maturation. *Advances in Dental Research*, *28*(1), 10–17. https://doi.org/10.1177/0022034515624444

Boyan, Barbara D., Hummert, T. W., Dean, D. D., & Schwartz, Z. (1996). Role of material surfaces in regulating bone and cartilage cell response. *Biomaterials*. https://doi.org/10.1016/0142-9612(96)85758-9

Buck, D. W., & Dumanian, G. A. (2012a). Bone Biology and Physiology. *Plastic and Reconstructive Surgery*, *129*(6), 1314–1320. https://doi.org/10.1097/PRS.0b013e31824eca94

Buck, D. W., & Dumanian, G. a. (2012b). Bone biology and physiology: Part I. The fundamentals. *Plastic and Reconstructive Surgery*, *129*(6), 1314–1320. https://doi.org/10.1097/PRS.0b013e31824eca94

Cacciotti, I. (2016). Cationic and anionic substitutions in hydroxyapatite. In *Handbook of Bioceramics and Biocomposites*. https://doi.org/10.1007/978-3-319-12460-5_7

Campana, V., Milano, G., Pagano, E., Barba, M., Cicione, C., Salonna, G., … Logroscino, G. (2014a). Bone substitutes in orthopaedic surgery: from basic science to clinical practice. *Journal of Materials Science: Materials in Medicine*, *25*(10), 2445–2461. https://doi.org/10.1007/s10856-014-5240-2

Campana, V., Milano, G., Pagano, E., Barba, M., Cicione, C., Salonna, G., … Logroscino, G. (2014b). Bone substitutes in orthopaedic surgery: from basic science to clinical practice. *Journal of Materials Science: Materials in Medicine*, *25*(10), 2445–2461. https://doi.org/10.1007/s10856-014-5240-2

Chai, Q., Jiao, Y., & Yu, X. (2017). Hydrogels for Biomedical Applications: Their Characteristics and the Mechanisms behind Them. *Gels*, *3*(1), 6. https://doi.org/10.3390/gels3010006

Chen, P. Y., & McKittrick, J. (2011). Compressive mechanical properties of demineralized and deproteinized cancellous bone. *Journal of the Mechanical Behavior of Biomedical Materials*, *4*(7), 961–973. https://doi.org/10.1016/j.jmbbm.2011.02.006

Chen, Q., Shou, P., Zheng, C., Jiang, M., Cao, G., Yang, Q., … Shi, Y. (2016). Fate decision of mesenchymal stem cells: Adipocytes or osteoblasts? *Cell Death and Differentiation*, *23*(7), 1128–1139. https://doi.org/10.1038/cdd.2015.168

Chen, Qing, Shou, P., Zhang, L., Xu, C., Zheng, C., Han, Y., … Shi, Y. (2014). An Osteopontin-Integrin Interaction Plays a Critical Role in Directing Adipogenesis and Osteogenesis by Mesenchymal Stem Cells. *STEM CELLS*, *32*(2), 327–337. https://doi.org/10.1002/stem.1567

Chien, Y. C., Hincke, M. T., & McKee, M. D. (2008). Avian eggshell structure and osteopontin. *Cells Tissues Organs*, *189*(1–4), 38–43. https://doi.org/10.1159/000151374

Christman, K. L. (2019). Biomaterials for tissue repair. *Science*, *363*(6425), 340–342. https://doi.org/10.1126/science.aar2955

Coates, J. (2006). Interpretation of Infrared Spectra, A Practical Approach. In *Encyclopedia of Analytical Chemistry*. https://doi.org/10.1002/9780470027318.a5606

Combes, C., & Rey, C. (2010). Bioceramics. In *Ceramic Materials: Processes, Properties and Applications* (pp. 493–521). London, UK: ISTE. https://doi.org/10.1002/9780470612415.ch12

Cooper, M. T., & Kaeding, C. (2010). Comparison of the hospital cost of autograft versus allograft soft-tissue anterior cruciate ligament reconstructions. *Arthroscopy - Journal of Arthroscopic and Related Surgery*. https://doi.org/10.1016/j.arthro.2010.04.004

Cowin, S., & Telega, J. (2003). Bone Mechanics Handbook, 2nd Edition. -. *Applied Mechanics Reviews*, *56*(4), B61. https://doi.org/10.1115/1.1579463

Currey, J. D., Pitchford, J. W., & Baxter, P. D. (2007). Variability of the mechanical properties of bone, and its evolutionary consequences. *Journal of the Royal Society Interface*, *4*(12), 127–135. https://doi.org/10.1098/rsif.2006.0166

Dadhich, P., Das, B., Pal, P., Srivas, P. K., Dutta, J., Ray, S., & Dhara, S. (2016). A Simple Approach for an Eggshell-Based 3D-Printed Osteoinductive Multiphasic Calcium Phosphate Scaffold. *ACS Applied Materials and Interfaces*, *8*(19), 11910–11924. https://doi.org/10.1021/acsami.5b11981

Dalby, M. J., Gadegaard, N., Tare, R., Andar, A., Riehle, M. O., Herzyk, P., … Oreffo, R. O. C. (2007). The control of human mesenchymal cell differentiation using nanoscale symmetry and disorder. *Nature Materials*, *6*(12), 997–1003. https://doi.org/10.1038/nmat2013

Davidenko, N., Schuster, C. F., Bax, D. V., Raynal, N., Farndale, R. W., Best, S. M., & Cameron, R. E. (2015). Control of crosslinking for tailoring collagen-based scaffolds stability and mechanics. *Acta Biomaterialia*, *25*, 131–142. https://doi.org/10.1016/j.actbio.2015.07.034

Dehghani, F., & Annabi, N. (2011). Engineering porous scaffolds using gas-based techniques. *Current Opinion in Biotechnology*, *22*(5), 661–666. https://doi.org/10.1016/j.copbio.2011.04.005

Demirel, M., & Aksakal, B. (2016). The synthesis of eggshell-derived nano- and microscale hydroxyapatite bioceramic bone grafts. *Journal of Sol-Gel Science and Technology*. https://doi.org/10.1007/s10971-015-3915-x

Dimarino, A. M., Caplan, A. I., & Bonfield, T. L. (2013). Mesenchymal stem cells in tissue repair. *Frontiers in Immunology*, *4*(September), 201. https://doi.org/10.3389/fimmu.2013.00201

Dupoirieux, L, Pourquier, D., & Souyris, F. (1995). Powdered eggshell: a pilot study on a new bone substitute for use in maxillofacial surgery. *Journal of Cranio-Maxillo-Facial Surgery : Official Publication of the European Association for Cranio-Maxillo-Facial Surgery*, *23*, 187–194. https://doi.org/10.1016/S1010-5182(05)80009-5

Dupoirieux, Laurent, Neves, M., & Pourquier, D. (2000). Comparison of pericranium and eggshell as space fillers used in combination with guided bone regeneration: An experimental study. *Journal of Oral and Maxillofacial Surgery*, *58*(1), 40–46. https://doi.org/10.1016/S0278-2391(00)80013-0

Duval, K., Grover, H., Han, L.-H., Mou, Y., Pegoraro, A. F., Fredberg, J., & Chen, Z. (2017). Modeling Physiological Events in 2D vs. 3D Cell Culture. *Physiology*, *32*(4), 266–277. https://doi.org/10.1152/physiol.00036.2016

Eiselt, P., Yeh, J., Latvala, R. K., Shea, L. D., & Mooney, D. J. (2000). Porous carriers for biomedical applications based on alginate hydrogels. *Biomaterials*. https://doi.org/10.1016/S0142-9612(00)00033-8

Elashoff, D., Grogan, T., & Tetradis, S. (2014). Bone Healing in a Marginal Mandibular Defect, *123*(5), 1149–1155. https://doi.org/10.1002/lary.23782.BMP-2

Engelberg, I., & Kohn, J. (1991). Physico-mechanical properties of degradable polymers used in medical applications: A comparative study. *Biomaterials*, *12*(3), 292–304. https://doi.org/10.1016/0142-9612(91)90037-B

Epure, V., Griffon, M., Pollet, E., & Avérous, L. (2011). Structure and properties of glycerol-plasticized chitosan obtained by mechanical kneading. *Carbohydrate Polymers*. https://doi.org/10.1016/j.carbpol.2010.09.003

Etheridge, L., Mason, R. A., Saleh, F., & Genever, P. (2016). Cell-cell signaling pathways that regulate mesenchymal stromal cell differentiation. In *The Biology and Therapeutic Application of Mesenchymal Cells* (Vol. The Biolog, pp. 91–103). Hoboken, NJ, USA: John Wiley & Sons, Inc. https://doi.org/10.1002/9781118907474.ch9

Fatherazi, S., Matsa-Dunn, D., Foster, B. L., Rutherford, R. B., Somerman, M. J., & Presland, R. B. (2009). Phosphate regulates osteopontin gene transcription. *Journal of Dental Research*. https://doi.org/10.1177/0022034508328072

Fiume, E., Barberi, J., Verné, E., & Baino, F. (2018). Bioactive Glasses: From Parent 45S5 Composition to Scaffold-Assisted Tissue-Healing Therapies. *Journal of Functional Biomaterials*, *9*(1), 24. https://doi.org/10.3390/jfb9010024

Gaspar, D. A., Gomide, V., & Monteiro, F. J. (2012). The role of perfusion bioreactors in bone tissue engineering. *Biomatter*, *2*(4), 167–175. https://doi.org/10.4161/biom.22170

Gogolides, E., Constantoudis, V., Patsis, G. P., & Tserepi, A. (2006). A review of line edge roughness and surface nanotexture resulting from patterning processes. *Microelectronic Engineering*, *83*(4-9 SPEC. ISS.), 1067–1072. https://doi.org/10.1016/j.mee.2006.01.162

Goldberg, V. M. (1992). Natural History of Autografts and Allografts. In *Bone Implant Grafting*. https://doi.org/10.1007/978-1-4471-1934-0_2

Golub, E. E., & Boesze-Battaglia, K. (2007). The role of alkaline phosphatase in mineralization. *Current Opinion in Orthopaedics*, *18*(5), 444–448. https://doi.org/10.1097/BCO.0b013e3282630851

Gong, J. P., Katsuyama, Y., Kurokawa, T., & Osada, Y. (2003). Double-network hydrogels with extremely high mechanical strength. *Advanced Materials*, *15*(14), 1155–1158. https://doi.org/10.1002/adma.200304907

Hakkarainen, M., & Albertsson, A. C. (2008). Degradation products of aliphatic and aliphatic-aromatic polyesters. *Advances in Polymer Science*. https://doi.org/10.1007/12_2007_128

Hanna, H., Mir, L. M., & Andre, F. M. (2018). In vitro osteoblastic differentiation of mesenchymal stem cells generates cell layers with distinct properties. *Stem Cell Research & Therapy*, *9*(1), 203. https://doi.org/10.1186/s13287-018-0942-x

Hilborne, L. H. (1998). Examining amended reports in surgical pathology. *Archives of Pathology & Laboratory Medicine*, *122*(4), 301–302.

Hincke, M. T., Chien, Y.-C., Gerstenfeld, L. C., & McKee, M. D. (2008). Colloidal-gold Immunocytochemical Localization of Osteopontin in Avian Eggshell Gland and Eggshell. *Journal of Histochemistry & Cytochemistry*, *56*(5), 467–476. https://doi.org/10.1369/jhc.2008.950576

Hincke, M. T., Gautron, J., Tsang, C. P. W., McKee, M. D., & Nys, Y. (1999). Molecular Cloning and Ultrastructural Localization of the Core Protein of an Eggshell Matrix Proteoglycan, Ovocleidin-116. *Journal of Biological Chemistry*, *274*(46), 32915–32923. https://doi.org/10.1074/jbc.274.46.32915

Hincke, M. T., Nys, Y., Gautron, J., Mann, K., Rodriguez-Navarro, A. B., & McKee, M. D. (2012). The eggshell: structure, composition and mineralization. *Frontiers in Bioscience (Landmark Edition)*, *17*(1), 1266–1280. https://doi.org/10.2741/3985

Ho, M. H., Kuo, P. Y., Hsieh, H. J., Hsien, T. Y., Hou, L. T., Lai, J. Y., & Wang, D. M. (2004). Preparation of porous scaffolds by using freeze-extraction and freeze-gelation methods. *Biomaterials*, *25*(1), 129–138. https://doi.org/10.1016/S0142-9612(03)00483-6

Holback, H., Yeo, Y., & Park, K. (2011). Hydrogel swelling behavior and its biomedical applications. In *Biomedical Hydrogels* (pp. 3–24). Elsevier. https://doi.org/10.1533/9780857091383.1.3

Hsieh, C. Y., Tsai, S. P., Ho, M. H., Wang, D. M., Liu, C. E., Hsieh, C. H., … Hsieh, H. J. (2007). Analysis of freeze-gelation and cross-linking processes for preparing porous chitosan scaffolds. *Carbohydrate Polymers*. https://doi.org/10.1016/j.carbpol.2006.05.002

Infante, A., & Rodríguez, C. I. (2018). Osteogenesis and aging: lessons from mesenchymal stem cells. *Stem Cell Research & Therapy*, *9*(1), 244. https://doi.org/10.1186/s13287-018-0995-x

Invitrogen Molecular Probes. (2005). LIVE/DEAD Viability/Cytotoxicity Kit for mammalian cells. *Product Information, Catalog Number: MP 03224*, 1–7. Retrieved from https://tools.lifetechnologies.com/content/sfs/manuals/mp03224.pdf

Islam, M., Motasim Bellah, M., Sajid, A., Raziul Hasan, M., Kim, Y. T., & Iqbal, S. M. (2015). Effects of Nanotexture on Electrical Profiling of Single Tumor Cell and Detection of Cancer from Blood in Microfluidic Channels. *Scientific Reports*, *5*(September), 1–9. https://doi.org/10.1038/srep13031

Ivanova, E. P., Bazaka, K., & Crawford, R. J. (2014). Metallic biomaterials: types and advanced applications. *New Functional Biomaterials for Medicine and Healthcare*, 121–147. https://doi.org/10.1533/9781782422662.121

Jastrzbski, W., Sitarz, M., Rokita, M., & Bułat, K. (2011). Infrared spectroscopy of different phosphates structures. *Spectrochimica Acta - Part A: Molecular and Biomolecular Spectroscopy*, *79*(4), 722–727. https://doi.org/10.1016/j.saa.2010.08.044

Jones, J. R., Brauer, D. S., Hupa, L., & Greenspan, D. C. (2016). Bioglass and Bioactive Glasses and Their Impact on Healthcare. *International Journal of Applied Glass Science*, *7*(4), 423–434. https://doi.org/10.1111/ijag.12252

Karageorgiou, V., & Kaplan, D. (2005). Porosity of 3D biomaterial scaffolds and osteogenesis. *Biomaterials*, *26*(27), 5474–5491. https://doi.org/10.1016/j.biomaterials.2005.02.002

Kattimani, V., Lingamaneni, K. P., Chakravarthi, P. S., Kumar, T. S. S., & Siddharthan, A. (2016). Eggshell-Derived Hydroxyapatite. *Journal of Craniofacial Surgery*, *27*(1), 112–117. https://doi.org/10.1097/SCS.0000000000002288

Kenny, S. M., & Buggy, M. (2003). Bone cements and fillers: a review. *Journal of Materials Science. Materials in Medicine*, *14*(11), 923–938. Retrieved from http://www.ncbi.nlm.nih.gov/pubmed/15348504

Khalili, A., & Ahmad, M. (2015). A Review of Cell Adhesion Studies for Biomedical and Biological Applications. *International Journal of Molecular Sciences*, *16*(8), 18149–18184. https://doi.org/10.3390/ijms160818149

Khang, D., Choi, J., Im, Y. M., Kim, Y. J., Jang, J. H., Kang, S. S., … Park, J. W. (2012). Role of subnano-, nano- and submicron-surface features on osteoblast differentiation of bone marrow mesenchymal stem cells. *Biomaterials*, *33*(26), 5997–6007. https://doi.org/10.1016/j.biomaterials.2012.05.005

Kirkpatrick, J. S., Cornell, C. N., Hoang, B. H., Hsu, W., Watson, J. T., Watters, W. C., … Anderson, S. (2010). Bone void fillers. *Journal of the American Academy of Orthopaedic Surgeons*. https://doi.org/10.5435/00124635-201009000-00009

Komori, T. (2010). Regulation of osteoblast differentiation by runx2. *Advances in Experimental Medicine and Biology*, *658*, 43–49. https://doi.org/10.1007/978-1-4419-1050-9_5

Langenbach, F., & Handschel, J. (2013). Effects of dexamethasone, ascorbic acid and β-glycerophosphate on the osteogenic differentiation of stem cells in vitro. *Stem Cell Research and Therapy*, *4*(5), 1. https://doi.org/10.1186/scrt328

Lawrie, G., Keen, I., Drew, B., Chandler-Temple, A., Rintoul, L., Fredericks, P., & Grøndahl, L. (2007). Interactions between alginate and chitosan biopolymers characterized using FTIR and XPS. *Biomacromolecules*, *8*(8), 2533–2541. https://doi.org/10.1021/bm070014y

Leboy, P. S., Vaias, L., Uschmann, B., Golub, E., Adams, S. L., & Pacifici, M. (1989). Ascorbic acid induces alkaline phosphatase, type X collagen, and calcium deposition in cultured chick chondrocytes. *Journal of Biological Chemistry*. https://doi.org/VL - 264

Li, X., Yang, X., Liu, X., He, W., Huang, Q., Li, S., & Feng, Q. (2018). Calcium carbonate nanoparticles promote osteogenesis compared to adipogenesis in human bone-marrow mesenchymal stem cells. *Progress in Natural Science: Materials International*, *28*(5), 598–608. https://doi.org/10.1016/j.pnsc.2018.09.004

Li, Y., Jiang, T., Zheng, L., & Zhao, J. (2017). Osteogenic differentiation of mesenchymal stem cells (MSCs) induced by three calcium phosphate ceramic (CaP) powders: A comparative study. *Materials Science and Engineering C*, *80*, 296–300. https://doi.org/10.1016/j.msec.2017.05.145

Li, Z., & Zhang, M. (2005). Chitosan-alginate as scaffolding material for cartilage tissue engineering. *Journal of Biomedical Materials Research - Part A*, *75*(2), 485–493. https://doi.org/10.1002/jbm.a.30449

Liao, C. J., Chen, C. F., Chen, J. H., Chiang, S. F., Lin, Y. J., & Chang, K. Y. (2002). Fabrication of porous biodegradable polymer scaffolds using a solvent merging/particulate leaching method. *Journal of Biomedical Materials Research*, *59*(4), 676–681. https://doi.org/10.1002/jbm.10030

Lim, J. Y., & Donahue, H. J. (2007). Cell Sensing and Response to Micro- and Nanostructured Surfaces Produced by Chemical and Topographic Patterning. *Tissue Engineering*, *13*(8), 1879–1891. https://doi.org/10.1089/ten.2006.0154

Lin, Y. H., Liang, H. F., Chung, C. K., Chen, M. C., & Sung, H. W. (2005). Physically crosslinked alginate/N,O-carboxymethyl chitosan hydrogels with calcium for oral delivery of protein drugs. *Biomaterials*, *26*(14), 2105–2113. https://doi.org/10.1016/j.biomaterials.2004.06.011

Lukasova, V., Buzgo, M., Sovkova, V., Dankova, J., Rampichova, M., & Amler, E. (2017). Osteogenic differentiation of 3D cultured mesenchymal stem cells induced by bioactive peptides. *Cell Proliferation*, *50*(4), 1–12. https://doi.org/10.1111/cpr.12357

Luu, H. H., Song, W. X., Luo, X., Manning, D., Luo, J., Deng, Z. L., … He, T. C. (2007). Distinct roles of bone morphogenetic proteins in osteogenic differentiation of mesenchymal stem cells. *Journal of Orthopaedic Research*. https://doi.org/10.1002/jor.20359

Lyu, S. P., Schley, J., Loy, B., Lind, D., Hobot, C., Sparer, R., & Untereker, D. (2007). Kinetics and time-temperature equivalence of polymer degradation. *Biomacromolecules*. https://doi.org/10.1021/bm070313n

M., B., P., D., & L., D. (1998). Powdered eggshell in the repair of cystic cavities of the jaw. Preliminary study. *Revue de Stomatologie et de Chirurgie Maxillo-Faciale*, *99 Suppl 1*, 86–88.

Ma, G., Wang, Z., Chen, J., Yin, R., Chen, B., & Nie, J. (2014). Freeze-dried chitosan-sodium hyaluronate polyelectrolyte complex fibers as tissue engineering scaffolds. *New Journal of Chemistry*. https://doi.org/10.1039/c3nj00701d

Ma, Z., Gao, C., Gong, Y., & Shen, J. (2003). Paraffin spheres as porogen to fabricate poly(L-lactic acid) scaffolds with improved cytocompatibility for cartilage tissue engineering. *Journal of Biomedical Materials Research. Part B, Applied Biomaterials*, *67*(November), 610–617. https://doi.org/10.1002/jbm.b.10049

Makadia, H. K., & Siegel, S. J. (2011). Poly Lactic-co-Glycolic Acid (PLGA) as biodegradable controlled drug delivery carrier. *Polymers*. https://doi.org/10.3390/polym3031377

Mangano, C., Paino, F., d'Aquino, R., de Rosa, A., Iezzi, G., Piattelli, A., … Tirino, V. (2011). Human Dental Pulp Stem Cells hook into Biocoral scaffold forming an engineered biocomplex. *PLoS ONE*, *6*(4). https://doi.org/10.1371/journal.pone.0018721

Michalopoulos, E., Knight, R. L., Korossis, S., Kearney, J. N., Fisher, J., & Ingham, E. (2012). Development of Methods for Studying the Differentiation of Human Mesenchymal Stem Cells Under Cyclic Compressive Strain. *Tissue Engineering Part C: Methods*, *18*(4), 252–262. https://doi.org/10.1089/ten.tec.2011.0347

Motamedian, S. R. (2015). Smart scaffolds in bone tissue engineering: A systematic review of literature. *World Journal of Stem Cells*, *7*(3), 657. https://doi.org/10.4252/wjsc.v7.i3.657

Müller, P., Bulnheim, U., Diener, A., Lüthen, F., Teller, M., Klinkenberg, E. D., … Rychly, J. (2008). Calcium phosphate surfaces promote osteogenic differentiation of mesenchymal stem cells. *Journal of Cellular and Molecular Medicine*, *12*(1), 281–291. https://doi.org/10.1111/j.1582-4934.2007.00103.x

Müller, P., Langenbach, A., Kaminski, A., & Rychly, J. (2013). Modulating the Actin Cytoskeleton Affects Mechanically Induced Signal Transduction and Differentiation in Mesenchymal Stem Cells. *PLoS ONE*, *8*(7), 1–8. https://doi.org/10.1371/journal.pone.0071283

Murakami et al. (2007). Physicochemical study of calcium carbonate$_3$ from egg shells. *Ciência e Tecnologia de Alimentos*, *27*(3), 658–662. https://doi.org/10.1590/S0101-20612007000300035

Murphy, C. M., & O'Brien, F. J. (2010). Understanding the effect of mean pore size on cell activity in collagen-glycosaminoglycan scaffolds. *Cell Adhesion and Migration*, *4*(3), 377–381. https://doi.org/10.4161/cam.4.3.11747

Nakada, H., Numata, Y., Sakae, T., Okazaki, Y., Tanimoto, Y., Tamaki, H., … Z. LeGeros, R. (2008). Comparison of Bone Mineral Density and Area of Newly Formed Bone Around Ti-15%Zr-4%Nb-4%Ta Alloy and Ti-6%Al-4%V Alloy Implants. *Journal of Hard Tissue Biology*, *17*(3), 99–108. https://doi.org/10.2485/jhtb.17.99

Nakashima, K., Zhou, X., Kunkel, G., Zhang, Z., Deng, J. M., Behringer, R. R., & de Crombrugghe, B. (2002). The Novel Zinc Finger-Containing Transcription Factor Osterix Is Required for Osteoblast Differentiation and Bone Formation. *Cell*, *108*(1), 17–29. https://doi.org/10.1016/S0092-8674(01)00622-5

Neighbour, T. (2008). The Global Orthobiologics Market: Players, Products and Technologies Driving Change. *Epsicom Business Intelligence*, *2*.

Neunzehn, J., Szuwart, T., & Wiesmann, H.-P. (2015). Eggshells as natural calcium carbonate source in combination with hyaluronan as beneficial additives for bone graft materials, an in vitro study. *Head & Face Medicine*, *11*(1), 12. https://doi.org/10.1186/s13005-015-0070-0

Noda, M., & Denhardt, D. T. (2008). Chapter 18 - Osteopontin. *Principles of Bone Biology*. https://doi.org/http://dx.doi.org/10.1016/B978-0-12-373884-4.00037-9

Nokhodchi, A., & Tailor, A. (2004). In situ cross-linking of sodium alginate with calcium and aluminum ions to sustain the release of theophylline from polymeric matrices. *Farmaco*. https://doi.org/10.1016/j.farmac.2004.08.006

Nusselt, T., Hofmann, A., Wachtlin, D., Gorbulev, S., & Rommens, P. M. (2014). CERAMENT treatment of fracture defects (CERTiFy): Protocol for a prospective, multicenter, randomized study investigating the use of CERAMENT^{TM} BONE VOID FILLER in tibial plateau fractures. *Trials*, *15*(1), 1–11. https://doi.org/10.1186/1745-6215-15-75

Nys, Y., Gautron, J., Garcia-Ruiz, J. M., & Hincke, M. T. (2004). Avian eggshell mineralization: Biochemical and functional characterization of matrix proteins. *Comptes Rendus - Palevol*. https://doi.org/10.1016/j.crpv.2004.08.002

O'Brien, F. J., Harley, B. A., Yannas, I. V., & Gibson, L. (2004). Influence of freezing rate on pore structure in freeze-dried collagen-GAG scaffolds. *Biomaterials*, *25*(6), 1077–1086. https://doi.org/10.1016/S0142-9612(03)00630-6

Oppenheim, J., Segal, D., & Spitzer, D. (2002). Persistent Iliac Crest Donor Site Pain: Independent Outcome Assessment. *Neurosurgery*, *51*(3), 854–855. https://doi.org/10.1097/00006123-200209000-00060

Padmanabhan, S. K., Salvatore, L., Gervaso, F., Catalano, M., Taurino, A., Sannino, A., & Licciulli, A. (2015). Synthesis and Characterization of Collagen Scaffolds Reinforced by Eggshell Derived Hydroxyapatite for Tissue Engineering. *Journal of Nanoscience and Nanotechnology*, *15*(1), 504–509. https://doi.org/10.1166/jnn.2015.9489

Pangburn, S. H., Trescony, P. V., & Heller, J. (1982). Lysozyme degradation of partially deacetylated chitin, its films and hydrogels. *Biomaterials*. https://doi.org/10.1016/0142-9612(82)90043-6

Parisi, L., Toffoli, A., Ghiacci, G., & Macaluso, G. (2018). Tailoring the Interface of Biomaterials to Design Effective Scaffolds. *Journal of Functional Biomaterials*, *9*(3), 50. https://doi.org/10.3390/jfb9030050

Park, K.-H., Kim, M.-H., Park, S.-H., Lee, H. J., Kim, I. K., & Chung, H.-M. (2004). Synthesis of Arg–Gly–Asp (RGD) Sequence Conjugated Thermo-Reversible Gel via the PEG Spacer Arm as an Extracellular Matrix for a Pheochromocytoma Cell (PC12) Culture. *Bioscience, Biotechnology, and Biochemistry*, *68*(11), 2224–2229. https://doi.org/10.1271/bbb.68.2224

Pawelec, K. M., Husmann, A., Best, S. M., & Cameron, R. E. (2014). A design protocol for tailoring ice-templated scaffold structure. *Journal of the Royal Society Interface*. https://doi.org/10.1098/rsif.2013.0958

Pawelec, K. M., Husmann, A., Best, S. M., & Cameron, R. E. (2015). Altering crystal growth and annealing in ice-templated scaffolds. *Journal of Materials Science*, *50*(23), 7537–7543. https://doi.org/10.1007/s10853-015-9343-z

Peppas, N. A. (1997). Hydrogel and Drug Deliery. *Current Opinion in Colloid Interface Science*, (2), 531–537. https://doi.org/10.1016/S1359-0294(97)80103-3

Phinney, D. G., Kopen, G., Righter, W., Webster, S., Tremain, N., & Prockop, D. J. (1999). Donor variation in the growth properties and osteogenic potential of human marrow stromal cells. *Journal of Cellular Biochemistry*. https://doi.org/10.1002/(SICI)1097-4644(19991201)75:3<424::AID-JCB8>3.0.CO;2-8

Piattelli, A., Podda, G., & Scarano, A. (1997). Clinical and histological results in alveolar ridge enlargement using coralline calcium carbonate. *Biomaterials*, *18*(8), 623–627. https://doi.org/10.1016/S0142-9612(96)00158-5

Pikal, M. J., & Shah, S. (1990). The collapse temperature in freeze drying: Dependence on measurement methodology and rate of water removal from the glassy phase. *International Journal of Pharmaceutics*. https://doi.org/10.1016/0378-5173(90)90231-R

Polo-Corrales, L., Latorre-Esteves, M., & Ramirez-Vick, J. E. (2014). Scaffold Design for Bone Regeneration. *Journal of Nanoscience and Nanotechnology*. https://doi.org/10.1166/jnn.2014.9127

Prasad, K., Bazaka, O., Chua, M., Rochford, M., Fedrick, L., Spoor, J., … Bazaka, K. (2017). Metallic biomaterials: Current challenges and opportunities. *Materials*, *10*(8). https://doi.org/10.3390/ma10080884

Prins, H. J., Braat, A. K., Gawlitta, D., Dhert, W. J. A., Egan, D. A., Tijssen-Slump, E., … Martens, A. C. (2014). In vitro induction of alkaline phosphatase levels predicts in vivo bone forming capacity of human bone marrow stromal cells. *Stem Cell Research*. https://doi.org/10.1016/j.scr.2013.12.001

Quiroz, F. G., Posada, O. M., Gallego-Perez, D., Higuita-Castro, N., Sarassa, C., Hansford, D. J., … López, L. E. (2010). Housekeeping gene stability influences the quantification of osteogenic markers during stem cell differentiation to the osteogenic lineage. *Cytotechnology*. https://doi.org/10.1007/s10616-010-9265-1

Ramesh, S., Natasha, A. N., Tan, C. Y., Bang, L. T., Ramesh, S., Ching, C. Y., & Chandran, H. (2016). Direct conversion of eggshell to hydroxyapatite ceramic by a sintering method. *Ceramics International*. https://doi.org/10.1016/j.ceramint.2016.02.015

Ren, D., Yi, H., Wang, W., & Ma, X. (2005). The enzymatic degradation and swelling properties of chitosan matrices with different degrees of N-acetylation. *Carbohydrate Research*, *340*(15), 2403–2410. https://doi.org/10.1016/j.carres.2005.07.022

Riley, A., Sturrock, C. J., Mooney, S. J., & Luck, M. R. (2014). Quantification of eggshell microstructure using X-ray micro computed tomography. *British Poultry Science*, *55*(3), 311–320. https://doi.org/10.1080/00071668.2014.924093

Roberts, J. N., Sahoo, J. K., McNamara, L. E., Burgess, K. V., Yang, J., Alakpa, E. V., … Dalby, M. J. (2016). Dynamic Surfaces for the Study of Mesenchymal Stem Cell Growth through Adhesion Regulation. *ACS Nano*, *10*(7), 6667–6679. https://doi.org/10.1021/acsnano.6b01765

Rodrigues, S., Dionísio, M., López, C. R., & Grenha, A. (2012). Biocompatibility of Chitosan Carriers with Application in Drug Delivery. *Journal of Functional Biomaterials*, *3*(3), 615–641. https://doi.org/10.3390/jfb3030615

Rodríguez, J. P., González, M., Ríos, S., & Cambiazo, V. (2004). Cytoskeletal organization of human mesenchymal stem cells (MSC) changes during their osteogenic differentiation. *Journal of Cellular Biochemistry*. https://doi.org/10.1002/jcb.20234

Rowe, D. W. (2008). *Principles of Bone Biology*. *Principles of Bone Biology*. https://doi.org/10.1016/B978-0-12-373884-4.00008-2

Salloum, Z., Lehoux, E. A., Harper, M.-E., & Catelas, I. (2018). Effects of cobalt and chromium ions on oxidative stress and energy metabolism in macrophages in vitro. *Journal of Orthopaedic Research®*, 1–10. https://doi.org/10.1002/jor.24130

Sanyang, M. L., Sapuan, S. M., Jawaid, M., Ishak, M. R., & Sahari, J. (2016). Effect of plasticizer type and concentration on physical properties of biodegradable films based on sugar palm (arenga pinnata) starch for food packaging. *Journal of Food Science and Technology*, *53*(1), 326–336. https://doi.org/10.1007/s13197-015-2009-7

Sekine, W., & Haraguchi, Y. (2011). Thickness limitation and cell viability of multi-layered cell sheets and overcoming the diffusion limit by a porous-membrane culture insert. *Journal of Biochips & Tissue Chips*, *01*(01), 1–9. https://doi.org/10.4172/2153-0777.S1-007

Shen, X., Ruan, J., Zhou, Z., Zhang, H., & Zhou, Z. (2007). Fabrication of porous scaffolds using NaHCO3particulates as the porogen material. *Journal Wuhan University of Technology, Materials Science Edition*, *22*(2), 279–283. https://doi.org/10.1007/s11595-005-2279-4

Shi, C., Yuan, Z., Han, F., Zhu, C., & Li, B. (2016). Polymeric biomaterials for bone regeneration. *Annals of Joint*, *1*, 27–27. https://doi.org/10.21037/aoj.2016.11.02

Shum, L. C., White, N. S., Mills, B. N., de Mesy Bentley, K. L., & Eliseev, R. A. (2016). Energy Metabolism in Mesenchymal Stem Cells During Osteogenic Differentiation. *Stem Cells and Development*, *25*(2), 114–122. https://doi.org/10.1089/scd.2015.0193

Siddiqui, N., Asawa, S., Birru, B., Baadhe, R., & Rao, S. (2018). PCL-Based Composite Scaffold Matrices for Tissue Engineering Applications. *Molecular Biotechnology*, *60*(7), 506–532. https://doi.org/10.1007/s12033-018-0084-5

Silva, A. K. A., Richard, C., Bessodes, M., Scherman, D., & Merten, O. W. (2009). Growth factor delivery approaches in hydrogels. *Biomacromolecules*, *10*(1), 9–18. https://doi.org/10.1021/bm801103c

Singh, A., Gill, G., Kaur, H., Amhmed, M., & Jakhu, H. (2018). Role of osteopontin in bone remodeling and orthodontic tooth movement: a review. *Progress in Orthodontics*, *19*(1). https://doi.org/10.1186/s40510-018-0216-2

Smith, B. T., Santoro, M., Grosfeld, E. C., Shah, S. R., van den Beucken, J. J. J. P., Jansen, J. A., & Mikos., A. G. (2017). Incorporation of fast dissolving glucose porogens into an injectable calcium phosphate cement for bone tissue engineering. *Acta Biomaterialia*. https://doi.org/10.1016/j.actbio.2016.12.024

Srinivasan, S., Jayasree, R., Chennazhi, K. P., Nair, S. V., & Jayakumar, R. (2012). Biocompatible alginate/nano bioactive glass ceramic composite scaffolds for periodontal tissue regeneration. *Carbohydrate Polymers*, *87*(1), 274–283. https://doi.org/10.1016/j.carbpol.2011.07.058

Stolzing, A., Jones, E., McGonagle, D., & Scutt, A. (2008). Age-related changes in human bone marrow-derived mesenchymal stem cells: Consequences for cell therapies. *Mechanisms of Ageing and Development*, *129*(3), 163–173. https://doi.org/10.1016/j.mad.2007.12.002

Sun, J., & Tan, H. (2013). Alginate-based biomaterials for regenerative medicine applications. *Materials*, *6*(4), 1285–1309. https://doi.org/10.3390/ma6041285

Sun, Y., Qi, X., Sun, H., Zhao, H., & Li, Y. (2016). Understanding about How Different Foaming Gases Effect the Interfacial Array Behaviors of Surfactants and the Foam Properties. *Langmuir*, *32*(30), 7503–7511. https://doi.org/10.1021/acs.langmuir.6b02269

Thein-Han, W. W., & Misra, R. D. K. (2009). Biomimetic chitosan–nanohydroxyapatite composite scaffolds for bone tissue engineering. *Acta Biomaterialia*, *5*(4), 1182–1197. https://doi.org/10.1016/j.actbio.2008.11.025

Tillotson, M., Logan, N., & Brett, P. (2016). Osteogenic stem cell selection for repair and regeneration. *Bone Reports*, *5*, 22–32. https://doi.org/10.1016/j.bonr.2016.01.003

Tkalec, G., Knez, Ž., & Novak, Z. (2015). Formation of polysaccharide aerogels in ethanol. *RSC Advances*. https://doi.org/10.1039/c5ra14140k

Torres-Sanchez, C., Al Mushref, F. R. A., Norrito, M., Yendall, K., Liu, Y., & Conway, P. P. (2017). The effect of pore size and porosity on mechanical properties and biological response of porous titanium scaffolds. *Materials Science and Engineering C*, *77*, 219–228. https://doi.org/10.1016/j.msec.2017.03.249

Touaitahuata, H., Cres, G., de Rossi, S., Vives, V., & Blangy, A. (2014). The mineral dissolution function of osteoclasts is dispensable for hypertrophic cartilage degradation during long bone development and growth. *Developmental Biology*. https://doi.org/10.1016/j.ydbio.2014.06.020

Tozzi, G., De Mori, A., Oliveira, A., & Roldo, M. (2016). Composite hydrogels for bone regeneration. *Materials*. https://doi.org/10.3390/ma9040267

Tran, R. T., Naseri, E., Kolasnikov, A., Bai, X., & Yang, J. (2011). A new generation of sodium chloride porogen for tissue engineering. *Biotechnology and Applied Biochemistry*. https://doi.org/10.1002/bab.44

Tran, S. C., Cooley, A. J., & Elder, S. H. (2011). Effect of a mechanical stimulation bioreactor on tissue engineered, scaffold-free cartilage. *Biotechnology and Bioengineering*, *108*(6), 1421–1429. https://doi.org/10.1002/bit.23061

Tuchman, A., Brodke, D. S., Youssef, J. A., Meisel, H. J., Dettori, J. R., Park, J. B., … Wang, J. C. (2016). Iliac Crest Bone Graft versus Local Autograft or Allograft for Lumbar Spinal Fusion: A Systematic Review. *Global Spine Journal*, *6*(6), 592–606. https://doi.org/10.1055/s-0035-1570749

Uraz, A., Gultekin, S. E., Senguven, B., Karaduman, B., Sofuoglu, I. P., Pehlivan, S., … Eren, K. (2013). Histologic and histomorphometric assessment of eggshell-derived bone graft substitutes on bone healing in rats. *Journal of Clinical and Experimental Dentistry*, *5*(1). https://doi.org/10.4317/jced.50968

US Department of Health and Human Services. (2004). Bone health and osteoporosis: a report of the Surgeon General. *US Health and Human Services*, 437. https://doi.org/10.2165/00002018-200932030-00004

Van Tomme, S. R., Storm, G., & Hennink, W. E. (2008). In situ gelling hydrogels for pharmaceutical and biomedical applications. *International Journal of Pharmaceutics*. https://doi.org/10.1016/j.ijpharm.2008.01.057

Vieira, M. G. A., Da Silva, M. A., Dos Santos, L. O., & Beppu, M. M. (2011). Natural-based plasticizers and biopolymer films: A review. *European Polymer Journal*, *47*(3), 254–263. https://doi.org/10.1016/j.eurpolymj.2010.12.011

Wagner, E. R., He, B.-C., Chen, L., Zuo, G.-W., Zhang, W., Shi, Q., … Haydon, R. C. (2010). Therapeutic Implications of PPARγ in Human Osteosarcoma. *PPAR Research*, *2010*, 1–16. https://doi.org/10.1155/2010/956427

Wang, Y.-K., & Chen, C. S. (2013). Cell adhesion and mechanical stimulation in the regulation of mesenchymal stem cell differentiation. *Journal of Cellular and Molecular Medicine*, *17*(7), 823–832. https://doi.org/10.1111/jcmm.12061

Weinans, H., & Huiskes, R. I. K. (2015). The Relationship Between Stress Shielding and Bone Resorption Around Total Hip Stems and the Effects of Flexible Materials The Relationship Between Stress Shielding and Bone Resorption Around Total Hip Stems and the Effects of Flexible Materials. *Clinical Orthopaedics and Related Research*, (December), 124–134. https://doi.org/10.1097/00003086-199201000-00014

Winkler, T., Sass, F. A., Duda, G. N., & Schmidt-Bleek, K. (2018). A review of biomaterials in bone defect healing, remaining shortcomings and future opportunities for bone tissue engineering. *Bone & Joint Research*, *7*(3), 232–243. https://doi.org/10.1302/2046-3758.73.BJR-2017-0270.R1

Wong, R. S. H., Ashton, M., & Dodou, K. (2015). Effect of crosslinking agent concentration on the properties of unmedicated hydrogels. *Pharmaceutics*, *7*(3), 305–319. https://doi.org/10.3390/pharmaceutics7030305

Xu, H. H. K., Weir, M. D., Burguera, E. F., & Fraser, A. M. (2006). Injectable and macroporous calcium phosphate cement scaffold. *Biomaterials*, *27*(24), 4279–4287. https://doi.org/10.1016/j.biomaterials.2006.03.001

Xu, H., & Ren, D. (2015). Lysosomal Physiology. *Annual Review of Physiology*. https://doi.org/10.1146/annurev-physiol-021014-071649

Yoshimura, K., Toibana, A., & Nakahama, K. (1988). Human lysozyme: Sequencing of a cDNA, and expression and secretion by Saccharomyces cerevisiae. *Biochemical and Biophysical Research Communications*. https://doi.org/10.1016/0006-291X(88)90461-5

Yourek, G., Hussain, M. A., & Mao, J. J. (2007). Cytoskeletal Changes of Mesenchymal Stem Cells During Differentiation. *ASAIO Journal*, *53*(2), 219–228. https://doi.org/10.1097/MAT.0b013e31802deb2d

Yuan, X., Wei, Y., Villasante, A., Ng, J. J. D., Arkonac, D. E., Chao, P. hsiu G., & Vunjak-Novakovic, G. (2017). Stem cell delivery in tissue-specific hydrogel enabled meniscal repair in an orthotopic rat model. *Biomaterials*, *132*, 59–71. https://doi.org/10.1016/j.biomaterials.2017.04.004

Zhang, Y., Xie, R. -l., Croce, C. M., Stein, J. L., Lian, J. B., van Wijnen, A. J., & Stein, G. S. (2011). A program of microRNAs controls osteogenic lineage progression by targeting transcription factor Runx2. *Proceedings of the National Academy of Sciences*, *108*(24), 9863–9868. https://doi.org/10.1073/pnas.1018493108

Zhao, F., Yao, D., Guo, R., Deng, L., Dong, A., & Zhang, J. (2015). Composites of Polymer Hydrogels and Nanoparticulate Systems for Biomedical and Pharmaceutical Applications. *Nanomaterials*, *5*(4), 2054–2130. https://doi.org/10.3390/nano5042054

Zhao, X., Lui, Y. S., Choo, C. K. C., Sow, W. T., Huang, C. L., Ng, K. W., … Loo, J. S. C. (2015). Calcium phosphate coated Keratin-PCL scaffolds for potential bone tissue regeneration. *Materials Science and Engineering C*, *49*, 746–753. https://doi.org/10.1016/j.msec.2015.01.084

Zmora, S., Glicklis, R., & Cohen, S. (2002). Tailoring the pore architecture in 3-D alginate scaffolds by controlling the freezing regime during fabrication. *Biomaterials*, *23*(20), 4087–4094. https://doi.org/10.1016/S0142-9612(02)00146-1